



# LUND UNIVERSITY

## Synthesising colloidal molecules with tunable interactions from soft responsive microgel particles

Månsson, Linda

2019

*Document Version:*

Publisher's PDF, also known as Version of record

[Link to publication](#)

*Citation for published version (APA):*

Månsson, L. (2019). *Synthesising colloidal molecules with tunable interactions from soft responsive microgel particles*. Media-Tryck, Lund University, Sweden.

*Total number of authors:*

1

### General rights

Unless other specific re-use rights are stated the following general rights apply:

Copyright and moral rights for the publications made accessible in the public portal are retained by the authors and/or other copyright owners and it is a condition of accessing publications that users recognise and abide by the legal requirements associated with these rights.

- Users may download and print one copy of any publication from the public portal for the purpose of private study or research.
- You may not further distribute the material or use it for any profit-making activity or commercial gain
- You may freely distribute the URL identifying the publication in the public portal

Read more about Creative commons licenses: <https://creativecommons.org/licenses/>

### Take down policy

If you believe that this document breaches copyright please contact us providing details, and we will remove access to the work immediately and investigate your claim.

LUND UNIVERSITY

PO Box 117  
221 00 Lund  
+46 46-222 00 00

# Synthesising colloidal molecules with tunable interactions from soft responsive microgel particles

LINDA MÅNSSON | PHYSICAL CHEMISTRY | LUND UNIVERSITY





# Synthesising colloidal molecules with tunable interactions from soft responsive microgel particles

by

Linda Månsson



**LUND**  
UNIVERSITY

DOCTORAL DISSERTATION

by due permission of the Faculty of Science at Lund University.  
To be defended on the 3rd of May 2019 at 10:15, in lecture hall B at the Centre for  
Chemistry and Chemical Engineering at Lund University.

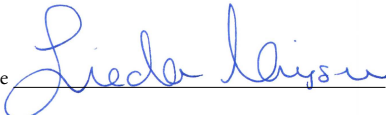
*Faculty opponent*

Prof. Matthias Karg

Heinrich Heine University Düsseldorf

|  |  |  |       |
|--|--|--|-------|
| Organization<br><b>LUND UNIVERSITY</b><br>Department of Chemistry<br>Box 124<br>SE-221 00 LUND<br>Sweden   |  | Document name<br><b>DOCTORAL DISSERTATION</b>                |       |
|  |  | Date of disputation<br><b>2019-05-03</b>                     |       |
|  |  | Sponsoring organization                                      |       |
| Author(s)<br><b>Linda Månsson</b>  |  |  |       |
| Title and subtitle<br><b>Synthesising colloidal molecules with tunable interactions from soft responsive microgel particles</b>  |  |  |       |
| Abstract<br><p>Colloidal self-assembly is an attractive bottom-up approach to new superstructures and materials with new properties. However, the typical spherical shape and isotropic interaction potential limit the repertoire of ordered structures that can be obtained from synthetic colloids. In order to expand the repertoire of structures, much effort has over the last decades been directed towards the preparation of colloids with anisotropic shapes and interactions and a more complex organisation. In an effort to replicate the concepts of valency and directionality that control the number, position and orientation of neighbours in molecular systems, the colloidal analogues have been prepared through controlled clustering of spherical colloids. However, as the lack of scientific publications in the field reveals, the typical charged hard sphere-nature of the constituent spheres - typically based on silica, polystyrene or poly(methyl methacrylate) - has made self-assembly of these so-called colloidal molecules difficult to control, resulting in jammed states where both translation and rotation are locked. The present thesis addresses this issue by reaching beyond classical electrostatic stabilisation, this by introducing poly(<i>N</i>-isopropylacrylamide) (PNIPAM) and poly(<i>N</i>-isopropylmethacrylamide) (PNIPMAM) microgel-based colloidal molecules that allow for both the strength and the range of the interactions, as well as the volume fraction, to be conveniently tuned with salt concentration, pH and temperature for a more successful assembly. This thesis foremost concerns design and development of methods for assembling microgels into colloidal molecules, and demonstration of the temperature-tunable interactions. Altogether, these results represent important steps towards assembly of novel superstructures and materials, and moreover, towards new colloidal model systems that capture the anisotropy of, for example, biological colloids such as proteins.</p> |  |  |       |
| Key words<br><b>microgels, polymers, colloids, colloidal synthesis, colloidal molecules, self-assembly, material science, confocal microscopy, light scattering</b>  |  |  |       |
| Classification system and/or index terms (if any)  |  |  |       |
| Supplementary bibliographical information  |  | Language<br><b>English</b>                                   |       |
| ISSN and key title   |  | ISBN<br>978-91-7422-620-1 (print)<br>978-91-7422-621-8 (pdf) |       |
| Recipient's notes  |  | Number of pages<br><b>225</b>                                | Price |
|  |  | Security classification                                      |       |

I, the undersigned, being the copyright owner of the abstract of the above-mentioned dissertation, hereby grant to all reference sources the permission to publish and disseminate the abstract of the above-mentioned dissertation.

Signature 

Date 2019-03-25

# Synthesising colloidal molecules with tunable interactions from soft responsive microgel particles

by

Linda Månsson



**LUND**  
UNIVERSITY

A doctoral thesis at a university in Sweden takes either the form of a single, cohesive research study (monograph) or a summary of research papers (compilation thesis), which the doctoral student has written alone or together with one or several other author(s).

In the latter case the thesis consists of two parts. An introductory text puts the research work into context and summarizes the main points of the papers. Then, the research publications themselves are reproduced, together with a description of the individual contributions of the authors. The research papers may either have been already published or are manuscripts at various stages (in press, submitted, or in draft).

**Cover illustration front:** LEGO® scientist in action.

Photo: Johan Fischer, @adrumdrum\_photography (Instagram).

**Cover illustration back:** Real scientist in action.

Photo: Johan Fischer, @adrumdrum\_photography (Instagram).

**Funding information:** The thesis work was financially supported by the European Research Council (ERC-339678-COMPASS), the Knut and Alice Wallenberg Foundation (Knut and Alice Wallenbergs Stiftelse) (KAW 2014.0052) and the Swedish Research Council (Vetenskapsrådet) (VR 2015-05426).

© Linda Månsson 2019

Faculty of Science at Lund University, Department of Chemistry

ISBN: 978-91-7422-620-1 (print)

ISBN: 978-91-7422-621-8 (pdf)

Printed in Sweden by Media-Tryck, Lund University, Lund 2019



Media-Tryck is an environmentally certified and ISO 14001:2015 certified provider of printed material. Read more about our environmental work at [www.mediatryck.lu.se](http://www.mediatryck.lu.se)

**MADE IN SWEDEN** 

*Begriper Du även detta, är Du i detta ämne lika förfaren som denna boks framstående författare. Var därmed nöjd, ty längre kan ingen människa komma.*

Axel Wallengren (o.k.s. Falstaff, fakir) i *En hvar sin egen professor* (1894)





# | Contents

|  |           |
|--|-----------|
| List of publications . . . . .   | iii       |
| Author contributions . . . . .   | iv        |
| Publications not included in the thesis . . . . .                            | v         |
| Acknowledgements . . . . .   | vii       |
| Populärvetenskaplig sammanfattning . . . . .                                 | ix        |
| <b>A Introductory chapters</b>   | <b>I</b>  |
| <b>1 Introduction</b>  | <b>3</b>  |
| 1.1 Colloids . . . . .   | 4         |
| 1.2 Colloidal self-assembly and new materials . . . . .                      | 5         |
| 1.3 Shaping colloids for self-assembly . . . . .                             | 6         |
| 1.4 Aim of the thesis . . . . .  | 7         |
| 1.5 Outline of the thesis . . . . .  | 9         |
| <b>2 Microgels</b>   | <b>11</b> |
| 2.1 Structure and softness . . . . .   | 12        |
| 2.2 Temperature-responsive behaviour . . . . .                               | 12        |
| 2.3 Microgels at oil-water interfaces . . . . .                              | 17        |
| 2.4 Microgels confined in shrinking droplets . . . . .                       | 20        |
| 2.5 Small clusters of oppositely charged microgels . . . . .                 | 22        |
| <b>3 Synthesis methods</b>   | <b>25</b> |
| 3.1 Microgel synthesis . . . . .   | 26        |
| 3.2 Microgel-microgel coupling . . . . .                                     | 29        |
| 3.3 Bowl-shaped polystyrene/microgel core-shell particle synthesis . . . . . | 32        |
| 3.4 PDMS oil droplet synthesis . . . . .                                     | 33        |

|          |   |     |
|----------|---|-----|
| <b>4</b> | <b>Experimental techniques</b>  | 37  |
| 4.1      | Light scattering . . . . .  | 38  |
| 4.2      | Confocal microscopy . . . . .   | 45  |
| 4.3      | Zetametry . . . . .   | 48  |
| 4.4      | Nuclear magnetic resonance (NMR) spectroscopy . . . . .   | 51  |
| 4.5      | Sedimentation methods . . . . .   | 54  |
| 4.6      | Microfluidics . . . . .   | 56  |
| <b>5</b> | <b>Summary of main results</b>  | 65  |
| 5.1      | Short recapitulation: The knowledge gap and the solution . . . . .  | 66  |
| 5.2      | Microgels - ideal building blocks . . . . .   | 67  |
| 5.3      | Some general remarks on the preparation of colloidal molecules . . . . .  | 67  |
| 5.4      | Interfacial tension-driven anchoring to small emulsion oil droplets . . . . .   | 68  |
| 5.5      | Evaporation-induced assembly from W/O emulsions . . . . .   | 79  |
| 5.6      | Electrostatic attraction-driven assembly of oppositely charged microgels . . . . .  | 84  |
| <b>6</b> | <b>Conclusions and outlook</b>  | 89  |
| <b>B</b> | <b>Scientific publications</b>  | 109 |
|          | Paper I: A new route towards colloidal molecules with externally tunable interaction sites . . . . .                                  | III |
|          | Paper II: A microgel-Pickering emulsion route to colloidal molecules with temperature-tunable interaction sites . . . . .             | 137 |
|          | Paper III: Colloidal molecules with temperature-tunable directional interactions prepared using droplet-based microfluidics . . . . . | 161 |
|          | Paper IV: Preparation of colloidal molecules with temperature-tunable interactions from oppositely charged microgel spheres . . . . . | 185 |

## List of publications

This thesis is based on the following publications, referred to by their Roman numerals:

- I **A new route towards colloidal molecules with externally tunable interaction sites**  
L. K. Månsson, J. N. Immink, A. M. Mihut, P. Schurtenberger, J. J. Crassous  
*Faraday discussions*, 2015, 181: 49-69
  
- II **A microgel-Pickering emulsion route to colloidal molecules with temperature-tunable interaction sites**  
L. K. Månsson, F. Peng, J. J. Crassous, P. Schurtenberger  
*Manuscript in preparation for submission*
  
- III **Colloidal molecules with temperature-tunable directional interactions prepared using droplet-based microfluidics**  
F. Peng\*, L. K. Månsson\*, S. H. Holm, S. Ghosh, G. Carlström, J. J. Crassous, P. Schurtenberger, J. O. Tegenfeldt  
*Manuscript in preparation for submission*
  
- IV **Preparation of colloidal molecules with temperature-tunable interactions from oppositely charged microgel spheres**  
L. K. Månsson, T. de Wild, F. Peng, S. H. Holm, J. O. Tegenfeldt, P. Schurtenberger  
*Manuscript in preparation for submission*

\* These authors contributed equally.

The publications are appended at the end of the thesis.

## **Author contributions**

### **Paper I: A new route towards colloidal molecules with externally tunable interaction sites**

PS and JJC designed the study with my input. I synthesised and characterised the microgel systems together with JNJ, under the supervision of AMM and JJC. I did the experimental work and data treatment on oil droplets and microgel-decorated oil droplets with support from JJC and AMM. JJC developed the model for contact angle estimation. Overall, PS supervised the study. I wrote the manuscript with input from the co-authors.

### **Paper II: A microgel-Pickering emulsion route to colloidal molecules with temperature-tunable interaction sites**

PS and I designed the study with input from JJC. Except for the isolation of colloidal molecules that was performed by FP, I did all the experimental work and data analysis under supervision of PS. I wrote the manuscript with input from the co-authors.

### **Paper III: Colloidal molecules with temperature-tunable directional interactions prepared using droplet-based microfluidics**

PS and JOT designed the study with input from the co-authors. I synthesised and characterised the microgel systems. GC performed the NMR experiments. FP and SHH designed and produced the microfluidic devices. FP, SHH and SG prepared and isolated the colloidal molecules. PS and JOT jointly supervised the study, with input from JJC. FP, SHH and I wrote the manuscript with input from the co-authors.

### **Paper IV: Preparation of colloidal molecules with temperature-tunable interactions from oppositely charged microgel spheres**

PS and I designed the study. I was responsible for synthesis and characterisation of the microgel systems. I did the experimental work on cluster synthesis and characterisation together with TdW. SHH designed the DLD device. FP produced the DLD device and did the DLD sorting. PS supervised the study, with input from JOT on the DLD sorting. I wrote the main part of the manuscript, with input from the co-authors.

## Publications not included in the thesis

The following publications are not included in this thesis:

- i **Anisotropic responsive microgels with tunable shape and interactions**  
J. J. Crassous, A. M. Mihut, L. K. Månsson, P. Schurtenberger  
*Nanoscale*, 2015, 7: 15971-15982
  
- ii **Sphere-tubule superstructures through supramolecular and supracolloidal assembly pathways**  
J. Cautela, V. Lattanzi, L. K. Månsson, L. Galantini, L., J. J. Crassous  
*Small*, 2018, 14: 1803215
  
- iii **Assembling responsive microgels at responsive lipid membranes**  
M. Wang, A. M. Mihut, E. Rieloff, A. P. Dabkowska, L. K. Månsson, J. N. Immink, E. Sparr, J. J. Crassous  
*Proceedings of the National Academy of Sciences*, 2019, 116: 5442-5450



## Acknowledgements

*Peter.* Thank you for valuable support and guidance during my PhD years. I am so grateful for you introducing me to the world of physical chemistry and colloids, while, at the same time, moulding the research project so to fit my interest for wet-lab and synthesis chemistry. Thank you for always listening to and considering my ideas and input - I cannot remember you ever saying no a suggestion of mine. Finally, thank you for investing both time and resources in my education and encouraging me to take courses, go to research schools and take part in conferences.

*Jérôme and Ulf.* I was fortunate to have two co-supervisors who were interested and engaged in my work. Thank you, *Jérôme*, for a never-ending stream of research ideas, and for many interesting discussions over the years. *Ulf*, through your ‘Hur går det med forskningen?’ I felt like you always had my back.

*Past and present members of the Schurtenberger group.* Thanks to all members of the Schurtenberger group, past and present, with whom I had the pleasure not only to discuss science but who also became great friends. Special thanks to my ‘PhD siblings’, *Maxime, Jasper, Feifei* and *Sofi*. I loved sharing this experience with you!

*The microfluidics group: Feifei, Somnath, Alfredo, Peter, Stefan and Jonas.* This collaboration was a beautiful marriage between microgels and microfluidics. It was a pleasure working with you all!

*Emil and Tijn.* I was lucky to supervise the undergraduate thesis projects of two excellent students who contributed to my research projects. Thanks for your hard work!

*Office 2OP 81-84: Maxime, Brijitta, Janne-Mieke, Erik, Adriana and Priti.* Thanks to the great scientists with whom I had the honour to share an office. Special thanks to *Maxime* who was there from day one, through thick and thin. You are the best (and such a brilliant teacher of Dutch curse words)!

*Helena, Maria S. and the Christophers (H. and W.).* Thank you for tackling essentially all practical problems. You truly are the core of the well-oiled machinery called Physical Chemistry!

*Göran.* Thanks for always managing to squeeze my NMR experiments into the tight schedule.

*All of my colleagues at Physical Chemistry.* Thanks to everyone at Physical Chemistry. You contributed to a great work environment and made coffee and lunch breaks very fun. Special thanks to those of you who joined my classes at the gym (*Maxime, Maria V., Polina, Janne-Mieke, Julien, Marc* and others).



*Chris B.* Thanks to my faithful pen pal *Chris* at *engineeringwafer.com*. As much as I have enjoyed receiving your e-mails over the years, I have no interest in buying your silicon wafers. Nonetheless, I hope that we can stay in touch and that you keep filling up my spam folder.

*Family and friends.* My greatest fan club, your support has been invaluable.

Finally, thanks to *everyone* who helped me proofread this book. A special shout-out to *Tommy G.*, *Maxime* and *Jasper* - this book (and yours) would not look as appealing if it was not for the many kilometres of code that we shared over the past months. I have the 2.40 pm walking group - *Tommy G.*, *Axel*, *Johan L.*, *Jasper*, *João*, *Paolo* and others - to thank for fresh air, sunlight and good company during the intense writing period, and office 1KL 108-111 - *Polina*, *Maria V.* and *Alexis* - for providing a comfortable sofa for late night in-between-experiments naps. Also, I would not have survived the last couple of weeks if it was not for you, *Feifei*, ensuring that I had access to lot of Chinese snacks and steamed buns when I needed it the most.

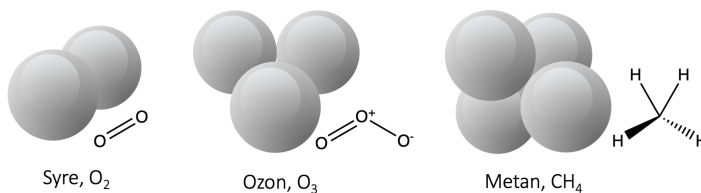
Last but not least, many thanks to *Johan F.* (@adrumdrum\_photography) for shooting the cover photos for this book and to *Paula* at *Media-Tryck* for help and good advice regarding formatting and printing.

## Populärvetenskaplig sammanfattning

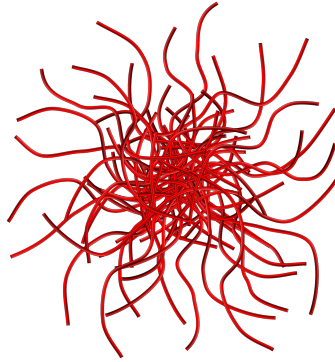
Kolloider, partiklar i storleksordningen en nanometer till en mikrometer, är inom materialvetenskapen attraktiva byggstenar vid konstruktion av olika material eftersom de spontant organiserar sig i periodiska strukturer. Till skillnad från biologiska kolloider såsom proteiner, röda blodkroppar, bakterier och virus, är de syntetiska kolloider som man har tillgång till inom materialvetenskapen i regel sfäriska, vilket tyvärr begränsar sätten på vilka de organiserar sig till endast en handfull enkla, tätpackade strukturer. Hur dessa strukturer är uppbyggda kan man enkelt föreställa sig om man drar paralleller till hur en frukthandlare staplar apelsiner: i en stabil stapel krävs det att apelsinerna tätpackats på ett sådant vis att varje apelsin omges av sex apelsingrannar i planet och tre i vardera plan ovan och under. Det är vidare så att ett materials egenskaper i stor utsträckning bestäms av just kolloidernas organisation: ju mer avancerad strukturen är, desto mer avancerade är i regel materialets egenskaper. Eftersom det idag råder stor efterfrågan på material med allt mer sofistikerade egenskaper - till exempel mekaniska, elektroniska och, kanske framförallt, fotoniska sådana - så krävs det att vi utvecklar strategier för att påverka kolloidernas organisation. Det känns ganska naturligt att formen är det attribut hos kolloiderna som är mest rättframt att manipulera i detta syfte. Jämför bara hur en frukthandlare staplar apelsiner, bananer och päron.

En strategi för att erhålla icke-sfäriska kolloider är att använda sig av sfäriska kolloider som byggstenar för små kluster. Klustren, som förväntas organisera sig på mer avancerade vis än sfärer, kan sedan användas som en andra generationens byggstenar för ett nytt material. Vid tillverkningen av dessa kluster har man försökt efterlikna formen hos molekyler, som är mycket mer komplexa när det kommer till organisation än sfäriska kolloider (och apelsiner). Ett kluster bestående av två sfärer liknar exempelvis en syremolekyl, ett kluster av tre en ozonmolekyl och ett kluster av fyra en metanmolekyl (Fig. 1). Dessa molekylliknande kluster går ofta under benämningen kolloidala molekyler.

Trots att det i den vetenskapliga litteraturen finns flera exempel på kolloidala molekyler så har man inte, med dessa som byggstenar, med någon framgång lyckats skapa de pe-



Figur 1: Exempel på kolloidala molekyler - från vänster till höger: syreliknande, ozonliknande, och metanliknande -samt motsvarande så kallade Nattaprojektioner som visar hur de olika atomslagen är bundna till varandra i tre dimensioner.



Figur 2: En mikrogelkolloid.

riodiska strukturer som är målet. Istället bildas oönskade, oregelbundna aggregat eller amorfa strukturer då de kolloidala molekylerna organiserar sig. Detta problem är relaterat till de kolloidala molekylernas komplexa form och svårigheten att kontrollera de interaktioner, den dragningskraft, som råder dem emellan. Sådana interaktioner kan vara antingen attraktiva eller repulsiva till sin natur, beroende på om kolloiderna dras till varandra eller stöter bort varandra.

Genom denna avhandling lägger vi fram mikrogelbaserade kolloidala molekyler som en lösning på detta problem. Mikrogeler är sfäriska, vattensvullna polymerkolloider (Fig. 2) med sådana egenskaper att naturen - huruvida attraktion eller repulsion dominerar - och styrkan i deras interaktioner, samt avstånden på vilka dessa verkar, enkelt och bekvämt kan styras med hjälp av temperaturen. Genom att konstruera kolloidala molekyler från mikrogeler kan interaktionerna styras via temperaturen också på denna nivå. Förmågan att kontrollera interaktionerna då de kolloidala molekylerna organiserar sig menar vi kommer att spela en avgörande roll för framgången med vilken nya material skapas i framtiden.

I denna bok beskrivs tre olika metoder som vi utvecklat för att framställa mikrogelbaserade kolloidala molekyler, och vi visar att interaktionerna mellan dessa kolloidala molekyler verkligen kan styras med hjälp av temperaturen. Eftersom varje ingående mikrogel i en kolloidal molekyl kan betraktas som en interaktionspunkt med förmågan att interagera med motsvarande punkter hos omgivande kolloidala molekyler, utgör den forskning som presenteras i denna bok ett viktigt steg mot att i framtiden kunna kontrollera antalet grannar, samt dess positioner, i en periodisk struktur, vilket är ett sedan länge eftersträvat mål inom materialvetenskapen.

## Part A

# Introductory chapters



*#IAmAScientistBecause there aren't many careers where 'insatiable curiosity' is a pro and not a con.*

- @MelissaClousez on Twitter

# I | Introduction

## Contents

|     |   |   |
|-----|---|---|
| 1.1 | Colloids . . . . .                                  | 4 |
| 1.2 | Colloidal self-assembly and new materials . . . . . | 5 |
| 1.3 | Shaping colloids for self-assembly . . . . .        | 6 |
| 1.4 | Aim of the thesis . . . . .                         | 7 |
| 1.5 | Outline of the thesis . . . . .                     | 9 |

To set the stage and to spark some curiosity about the reminding chapters of this thesis, this chapter aims at introducing the world of colloids with emphasis on their great potential as building blocks for new materials. In this context, the term 'colloidal molecules' is introduced and examples of methods for their preparation are listed. The knowledge gap that this thesis addresses is then identified and the aim of the thesis is presented. Lastly, the outline of the thesis is given.

## 1.1 Colloids

Colloidal particles, or simply colloids, are objects with at least one dimension in the order of 1 to 1,000 nm, dispersed in a continuous medium<sup>1-5</sup>. Colloidal systems are ubiquitous in Nature and in our daily life, with fog (water droplets dispersed in air), smoke (soot particles dispersed in air), milk (fat droplets dispersed in aqueous medium), paint (pigment particles dispersed in liquid medium) and blood (blood cells dispersed in aqueous medium) being just a few examples.

As colloids are much larger than atoms and molecules, yet much smaller than objects that can be resolved by the naked eye, the colloidal domain falls between the microscopic and macroscopic worlds. On the one hand, colloids are small enough to undergo endless and uncorrelated motion due to bombardment by molecules in the dispersion medium<sup>2-5</sup>. This so-called Brownian motion prevents the colloids from sedimenting under the influence of gravity - thus ensuring similar behaviour as for atoms and molecules - and allows them to explore the dispersion medium and enjoy the available entropy. On the other hand, as the length and time scales are shifted by several orders of magnitude compared to atoms and molecules, colloids are large enough and move sufficiently slow in order to be monitored and tracked through direct visualisation by, for example, optical microscopy, in situ and in real time.

A remarkable phenomenon exhibited by colloids is their ability to self-organise, without human intervention, into ordered structures as their number density increases, driven (for simple hard colloids) by a gain in free volume entropy that more than compensates for a loss of translational entropy<sup>2-5</sup>. This transition, from a long-ranged disordered - fluid - to a long-ranged ordered - crystal - state, is an example of a phase transition, and the phase behaviour of colloids also encompasses, for instance, glasses, and plastic and liquid crystals. Interestingly, the phase behaviour of (monodisperse, spherical) colloids is highly reminiscent of that of atoms and molecules. For this reason, colloids are often regarded as 'big atoms'<sup>6</sup> and constitute perfect playgrounds - owing to their large size and ease of study, but also to their (relatively) simple, easily tunable and highly variable inter-particle interaction potentials - to unravel many fundamental issues at the atomic and molecular level, such as the aforementioned phase behaviour and phase transitions and the corresponding underlying kinetic pathways, that are otherwise not easily accessible<sup>7-22</sup>.

## 1.2 Colloidal self-assembly and new materials

Colloids are not just proxies for atoms and molecules but due their spontaneous self-organisation - or self-assembly<sup>23</sup> - they constitute highly promising building blocks for the bottom-up preparation of superstructures, from clusters to entire materials, with useful properties<sup>24-26</sup>. This approach is known as colloidal LEGO<sup>27</sup>. As brick-by-brick assembly is both very time and resource-consuming, it is easy to see why self-assembly is a more appealing strategy for material synthesis and is one that Nature has employed for billions of years to assemble complex structures - take the constituents of cellular machinery, for example - at all scales<sup>23</sup>. The introduction of various motifs of Nature's self-assembly to the material science lab is however still in its infancy.

As building blocks, in addition to their ability to self-assemble, colloids have another merit in that the range and strength of their interactions - which naturally affect their organisation - can be tailored and varied greatly and quite easily, from steeply repulsive to deeply attractive, through physical or chemical alterations or by changing the dispersion medium<sup>18,28</sup>. In molecular systems, on the other hand, the interactions are dictated by the identity of the constituent atoms and the directionality of the molecular orbitals, which does not allow for any adjustments.

Yet another advantage of using colloids as building blocks is that their size is in the same range as the wavelength of visible light. This feature provides interesting optical properties, as illustrated by, for example, the structural color displayed by two- and three dimensional close-packed colloidal crystals due to Bragg diffraction. Nature provides several examples of such structural coloration. A natural opal, for instance, is iridescent because its constituent silica colloids are assembled into a three-dimensionally ordered array with a lattice constant comparable to the wavelength of visible light.<sup>29,30</sup> Other examples include beetle wing-cases, butterfly wings and bird feathers<sup>31-36</sup>.

Beyond simple close-packed crystals, much effort is directed towards the preparation of more sparsely populated, open and sophisticated ones, with applications in, for example, the area of photonics<sup>37-42</sup>. A photonic crystal is a structure in which the periodic arrangement of the building blocks prohibits the propagation of light of energy within a certain range, the band gap, much like a semiconductor influences the propagation of electrons. If the dielectric constant contrast is large enough, the material displays a complete photonic band gap that operates omnidirectionally and allows for full control of light in all three dimensions of space<sup>43</sup>. Applications are, for example, fibres, displays and switches.



## 1.3 Shaping colloids for self-assembly

### 1.3.1 Shape governs organisation

The periodic structures obtained from colloidal self-assembly is a reflection of the information encoded in the constituent building blocks - shape, surface properties, charge, polarisability, magnetic dipole and mass - that govern the inter-particle interactions. Consider, to begin with, the simple hard spheres that due to a fully symmetrical interaction potential only self-assemble, at sufficiently high volume fraction, into dense crystal structures of very simple symmetry, such as face-centred cubic (FCC), hexagonal close-packed (HCP) and body-centred cubic (BCC). As the world is demanding increasingly sophisticated materials, self-assembly with a higher level of structural complexity is required. This can be achieved using colloids encoded with information that provides directional (and specific) interactions, which is most easily accomplished through geometrical (shape) and/or compositional (surface) alterations. This thesis is (foremost) concerned with the former.

It is quite intuitive that shape controls, first of all, the organisation of colloids through tangible effects on their close-packing; a fruiterer cannot stack (colloidal-sized) bananas or pears in the same way as he stacks oranges. Second, the concept of shape at the colloidal length scale reaches far beyond the geometry of an object's surface, and extends also to the shape of the interaction field. It is therefore not surprising that colloids of (sufficiently) different shapes - say, spheres and rods - self-assemble into different crystal structures. With these realisations, the introduction of novel shapes to allow for access to new crystal structures and materials has become an area of great endeavour<sup>26,44-50</sup>. However, we are only beginning to unravel - with the help from theory and computer simulations - such shape-structure relationships<sup>51-54</sup> and we still have limited knowledge about which shapes that are desirable to produce a stipulated assembly.

Whereas in a perfect world colloids of any shape can be prepared, the majority of synthetic colloids, for surface energy minimisation reasons, are spherical and fully isotropic with respect to the interactions. Even though major advances in colloidal synthesis have provided us with several (however still quite simple) shapes beyond the sphere - such as rods<sup>55-60</sup>, spindels<sup>61-63</sup>, mushroom caps and bowls<sup>64-69</sup>, cubes<sup>70,71</sup>, dumbbells<sup>72-74</sup>, peanuts<sup>75,76</sup>, ice cream cones<sup>77</sup> and snowmen<sup>78</sup> - precise control of particle shape is still very challenging. As an alternative to direct synthesis methods, an approach involving controlled clustering of colloidal spheres has been developed. Seeking inspiration from atoms and molecules, in an effort to replicate the valency and directionality arising from the presence of anisotropic orbitals, the spheres are assembled in such a way so as to make the resulting small, discrete clusters resemble space-filling molecule models.

These clusters, collectively referred to as ‘colloidal molecules’<sup>79,80</sup>, have recently gained much attention from the material science community, as theory and simulations have predicted the self-assembly of colloids with a tetrahedral arrangement of attractive interaction sites into a diamond lattice with photonic properties<sup>81–84</sup>. In addition, due to their resemblance with molecules, colloidal molecules hold great promise as realistic model systems capable of closely mimicking molecular self-assembly and phase behaviour.

### 1.3.2 Preparing colloidal molecules

In the preparation of colloidal molecules, besides good yield, high monodispersity is naturally desired. Here, monodispersity refers to a distinct cluster configuration (shape) and a given number of spherical particles in each cluster. However, preparing clusters with a well-defined shape is difficult because the interactions between spherical building blocks are non-directional. As a consequence, colloidal spheres typically form aggregates with a very broad size distribution and no well-defined shape when dispersed in a liquid medium. To overcome this problem, the spherical building blocks need to have some built-in property or functionality that can be exploited to direct their assembly, such as a surface with single-stranded DNA-coated<sup>85</sup>, magnetic<sup>86</sup> or hydrophobic<sup>87</sup> patches. Alternatively, the assembly method itself needs to impose a certain organisation on the spheres. For example, minimisation of the second moment of mass distribution yielded a set of well-defined clusters from polystyrene (PS) spheres suspended in shrinking emulsion droplets<sup>88</sup>. The use of surfaces patterned with arrays of particle-capturing holes is another example, where the dimensions of the holes relative to that of the particles determine the valency and geometry of the resulting clusters<sup>89</sup>. These examples constitute just a small part of the plethora of methods that have been reported for the preparation of colloidal molecules<sup>80</sup>. Other mechanisms for driving the controlled assembly include, for instance, coalescence of soft, liquid protrusions or shells<sup>90,91</sup>, electrostatic attraction between oppositely charged spheres<sup>92</sup> and depletion-induced assembly of spherical<sup>93</sup>, shape-complementary<sup>67,94</sup>, and smooth-rough colloids<sup>95,96</sup>. In addition to controlled clustering, a number of direct synthesis routes have been reported. These include, for example, polymerisation of liquid protrusions<sup>97–100</sup> and nodule formation in seeded emulsion polymerisation<sup>101–103</sup>.

## 1.4 Aim of the thesis

It is quite intuitive that the substitution of spheres for anisotropic particles puts greater demands on self-assembly, as there is a larger probability of kinetic trapping of particle

positions and orientations (a colloidal-sized banana cannot move around as freely among its neighbours as an orange does). This is reflected in the fact that, whereas several different methods for the preparation of colloidal molecules have been published in literature, reports on their self-assembly have been extremely scarce, with a single notable exception<sup>104</sup>. This is likely due to difficulties with controlling and tuning the charged hard sphere-like inter-particle interactions during assembly, set by the identity of the spherical constituents that are typically based on silica, PS or poly(methyl methacrylate) (PMMA). For a successful assembly, the attractive and repulsive interactions need to be balanced so to allow for reversibility in ‘bond formation’. Only then do the building blocks have the ability to adjust their positions relative to one another and to find their optimum positions in the assembling, periodic structure. In practice, this means that we need to furnish colloids with tunable interactions - in terms of both range and strength - that reach beyond classical electrostatic stabilisation.

The most straightforward way of preparing colloidal molecules with tunable inter-particle interactions is naturally to pick building blocks with such properties. In the present thesis, this is realised using soft, crosslinked polymer colloids, so-called microgels<sup>105,106</sup>, with properties such that the range and strength of the interactions - together with particle size, volume fraction, softness and charge density - can be conveniently manipulated almost at will using temperature as an external stimulus. The temperature-responsive behaviour stems from the corresponding polymer - in our case poly(*N*-isopropylacrylamide) (PNIPAM)<sup>107,108</sup> or poly(*N*-isopropylmethacrylamide) (PNIPMAM) - displaying a lower critical solution temperature (LCST) below which the interactions with water are favourable and above which they are not<sup>109</sup>. This is manifested in a transition from a solvated coil to a collapsed globule. For the corresponding microgels<sup>110–112</sup>, the LCST translates into a so-called volume phase transition (VPT) characterised by a change from a soft repulsive state below the threshold temperature, where the particle is highly water-swollen and stabilised by dangling polymer chains, to a short-range attractive state (in the case of sufficient charge screening) above the threshold temperature, where the water-content is less, the particle more compact and hard sphere-like, and the steric stabilisation is lost. As both the inter-particle interactions and the volume fraction are tunable with temperature, the use of microgels allow for external control of phase behaviour, which enables, for example, crystal annealing, which is successfully used in molecular systems. To these intriguing particle properties, add the fact that microgels are cheap and easy to make, as highly monodisperse systems, with standard, up-scalable bulk synthesis protocols that can be modified to affect particle properties such as size, charge, softness and functionality.

The primary aim of this thesis is to implement the use of microgels as building blocks for low-valency colloidal molecules with temperature-tunable directional interactions, where each microgel can be considered a well-defined interaction site. This naturally

starts with synthesis and characterisation of the required microgels and continues with design and development of methods for their assembly. We have primarily relied on three methods for the preparation of colloidal molecules, fundamentally different in the sense that the driving force for microgel assembly differs in the three cases. In brief, the assembly strategy involves, in the first method, adsorption of surface active microgels to the interface of small emulsion oil droplets (Section 5.4). In the second method, microgels confined in water emulsion droplets are forced to form clusters as the water evaporates (Section 5.5). Finally, electrostatic attraction between oppositely charged microgels drives assembly in the third method (Section 5.6). Following generation of colloidal molecules by means of the aforementioned methods, the next steps are, first, isolation (purification) of the target colloidal molecules, and, second, demonstration of their temperature-tunable interactions.

In a greater perspective, the work presented in this thesis is part of a strive towards one of the long-desired goals of the colloidal domain: to get control over the valency and directionality of colloids and thereby over the number and position of neighbours in a periodic structure. The preparation of colloids with valence and directional interactions can, first of all, help to expand the range of colloidal crystals and thereby open a world of exciting applications of which a full three-dimensional photonic band gap material<sup>37,39–42</sup> is just one example. Second, these colloids can provide a useful model for understanding molecular phase transitions such as crystallisation, but also a model to give insight into interactions between colloids with complex anisotropic shapes and interactions, proteins and other bio-macromolecules being one example.

## 1.5 Outline of the thesis

The work presented in this book represents an arc of experimental work carried out over four years and focuses on the development of methods for the preparation of colloidal molecules with valence and temperature-tunable directional interactions through controlled assembly of temperature-responsive microgel colloids.

In **Chapter 2**, the unique properties of individual microgel particles and of microgel suspensions are described.

In **Chapter 3**, the particle synthesis methods are introduced.

In **Chapter 4**, introductions to the main experimental techniques are given.

In **Chapter 5**, the main results of the research papers are summarised.

In **Chapter 6**, concluding remarks and outlook are provided.

Happy reading!



*#IAmAScientistBecause I did not want to wear a business suit to work every day.*  
- @RLybrand629 on Twitter

## 2 | Microgels

### Contents

|     |  |    |
|-----|--|----|
| 2.1 | Structure and softness . . . . .                         | 12 |
| 2.2 | Temperature-responsive behaviour . . . . .               | 12 |
| 2.3 | Microgels at oil-water interfaces . . . . .              | 17 |
| 2.4 | Microgels confined in shrinking droplets . . . . .       | 20 |
| 2.5 | Small clusters of oppositely charged microgels . . . . . | 22 |

As microgels play a central role in this thesis, it is only fair that an entire chapter is devoted to them. Whereas the term ‘microgel’<sup>105</sup> is used to describe any intramolecularly crosslinked macromolecule<sup>106</sup>, this thesis exclusively concerns colloidal microgels based on the polymers PNIPAM<sup>110</sup> and PNIPMAM<sup>111,112</sup>. Whereas more in-depth reviews can be found elsewhere<sup>113–115</sup>, the aim of this chapter is to briefly introduce the most important properties and behaviours of these intriguing, soft, responsive colloids. The most well-known of their characteristics is their LCST-related VPT<sup>109,116</sup>, based on which they have earned a classification as ‘smart’ materials with applications as emulsion stabilisers<sup>117</sup>, in drug delivery<sup>118</sup>, biosensors<sup>119</sup> and microlenses<sup>120</sup>.

## 2.1 Structure and softness

PNIPAM and PNIPMAM (Fig. 2.1) microgels are conveniently prepared as well-defined, spherical particles of narrow size distribution by free radical precipitation polymerisation (Section 3.1) of the corresponding monomers, *N*-isopropylacrylamide (NIPAM) and *N*-isopropylmethacrylamide (NIPMAM), with the bi-functional comonomer *N,N'*-methylenebisacrylamide (BIS) typically used as crosslinker<sup>110–112</sup>. A microgel particle is schematically depicted in Fig. 2.2 and displays (in the swollen state, below the VPT) a dense core-fuzzy shell-type structure with a gradually decaying polymer density towards the periphery<sup>121–124</sup> due to the faster polymerisation kinetics of BIS compared to the main monomers<sup>111,125</sup>. The presence of the soft shell allows for particle deformation and inter-particle interpenetration beyond particle-particle contact<sup>126,127</sup>, as different from the situation with hard spheres whose interaction potential goes to infinity at contact. Interpenetration is however limited, as it causes an increase in osmotic pressure that results in a net repulsive force (Section 2.2.3).

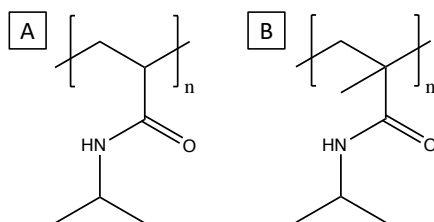


Figure 2.1: Chemical structure of the polymers (A) PNIPAM and (B) PNIPMAM.

## 2.2 Temperature-responsive behaviour

### 2.2.1 Water content and softness

The PNIP(M)AM polymer chains that constitute the polymer network are water-soluble, and the entire network is swollen by water to an extent governed by the state of osmotic pressure equilibrium. In the state of maximum (equilibrium) swelling, the water content is typically about 90%, but varies with temperature. The temperature effect stems from the LCST<sup>109</sup> of (linear) PNIPAM and PNIPMAM, at which the polymer undergo a coil-to-globule transition<sup>107</sup>. The LCST has its origin in a transition from good to bad solvent behaviour, characterised by polymer-polymer interactions becoming more favourable than polymer-water ones. The LCST translates into a so-called volume phase transition temperature (VPTT)<sup>116</sup> for the corresponding microgels, 32 and 45 °C for PNIPAM and PNIPMAM, respectively. At the VPTT,

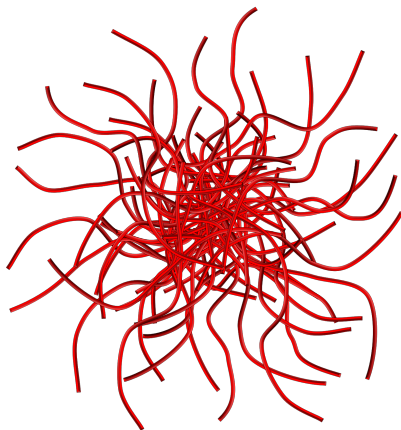


Figure 2.2: Cartoon of a PNIP(M)AM microgel particle with a dense core-fuzzy shell structure.

on a molecular level, the local environment around the polymer changes due to an entropically favoured release of hydrogen-bonded and structured water<sup>107</sup>, while, on the macromolecular level, the microgel particles respond by reducing their water content (to about 70%) - as is reflected by an increase in suspension opaqueness - and shrink. Hereby, the soft particle nature present below the VPTT transitions into a dense, (charged) hard sphere-like one above the VPTT. Microgels can thus behave as either soft or hard colloidal systems, depending on the conditions, offering the advantage of both in one particle.

### 2.2.2 Size, volume fraction and phase behaviour

At the VPTT, not only the degree of swelling - accessible from dynamic light scattering (DLS) measurements (Section 4.1) of the hydrodynamic radius  $R_H^{110}$  (Fig. 2.3A) - the water content and the particle morphology changes, but a number of other properties does too. First, deswelling is accompanied by an increase in surface charge density reflected by the electrophoretic mobility  $\mu$  (Fig. 2.3B)<sup>128,129</sup>. Typically, however, a significant difference between the VPTT and the electrokinetic transition temperature (ETT) is observed. This is believed to be due to electrostatic repulsion between polymer chains in the shell region that effectively serves to increase the VPTT of those chains.

As the particle size decreases across the VPTT, the volume fraction  $\phi$  that the particles occupy in suspension necessarily reduces. Like the typical colloid, (rigid to intermediately soft) microgels display a  $\phi$ -dependent fluid-crystal-glass phase behaviour, but the unique feature of microgel suspensions is that temperature can be used to go from one phase to another, in situ, by changing  $\phi$  while maintaining a constant number density



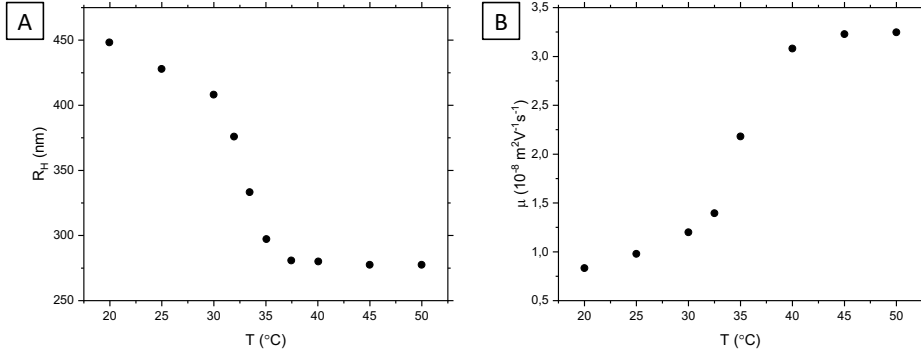


Figure 2.3: The particle de-swelling that occurs on crossing the VPTT is evident from (A) a decrease in  $R_H$  measured by DLS, and (B) an increase of  $|\mu|$  measured by zetametry. The measurements were performed on positively charged PNIPAM microgels.

(Fig. 2.4). This fact, in combination with the soft particle nature that allows for interpenetration, deformation and compression, leads to a rich phase behaviour, especially in the crystal and glass regimes<sup>131–141</sup>.

### 2.2.3 Inter-particle interactions

#### Below the VPTT

Besides providing a convenient way of tuning  $\phi$ , temperature constitutes a powerful tool with which the inter-particle interactions can be manipulated<sup>142</sup>. Below the VPTT, a combination of steric and electrostatic interactions make up the long-range, soft repulsive potential responsible for maintaining the stability of the suspension<sup>110,131,143</sup>. As touched upon above, the steric contribution originates from an increase in osmotic pressure that emerges when the fuzzy shells of neighbouring microgels start to interpenetrate. The repulsion can, in the dilute fluid regime, be well described by a simple Hertzian potential:

$$U_{Hertzian}(r) = \begin{cases} \epsilon \left(1 - \frac{r}{2R}\right)^{1/2} & r \leq 2R \\ 0 & r > 2R \end{cases} \quad (2.1)$$

where the microgels are modelled as completely penetrable spheres and where the magnitude of the potential is set by the elasticity of the polymer network<sup>144–147</sup>. In Eq. 2.1,  $r$  is the particle-particle separation,  $R$  the particle radius and  $\epsilon$  a dimensionless pre-factor determining the magnitude of the soft repulsion, which correlates with the elastic properties of the material. In the more concentrated regimes where interpenetration is more

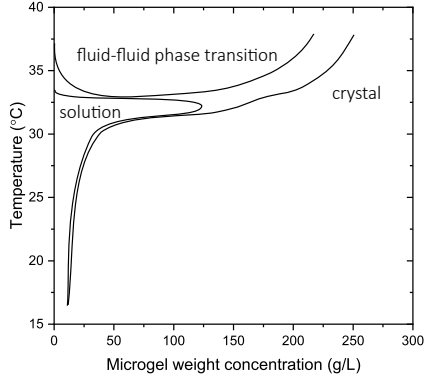


Figure 2.4: The phase diagram of neutral PNIPAM microgels suspended in water, determined from thermodynamic perturbation theory with an empirical correction of temperature. The figure is adapted from reference <sup>130</sup>. For the phase diagram of ionic microgels, please refer to reference <sup>131</sup>.

extensive, however the simple Hertzian model breaks down as full interpenetration is not possible - two microgels cannot occupy the exact same space. In this regime, a multi-Hertzian that ascribes a different elasticity to shell-shell, core-shell and core-core interactions has been shown to better capture the structural and dynamical features of the system <sup>148</sup>.

The electrostatic stabilisation, in turn, has its origin in charges emanating from ionic initiator fragments covalently bound to the polymer network. The electrostatic interactions are typically written as a DLVO<sup>149</sup>-derived Yukawa (screened Coulomb) potential:

$$U_{Yukawa}(r) = \frac{Z_{eff}^2 e^2}{4\pi\epsilon_0\epsilon_r} \left[ \frac{\exp(\kappa R)}{1 + \kappa R} \right]^2 \frac{\exp(-\kappa r)}{r} \quad (2.2)$$

with  $Z_{eff}$  the effective particle charge,  $e$  the elementary charge,  $\epsilon_0$  the vacuum dielectric permittivity,  $\epsilon_r$  the dielectric constant of the medium and  $\kappa^{-1}$  the so-called inverse Debye screening length.  $\kappa^{-1}$  measures the distance over which the repulsion is canceled by the screening effect of electrolytes and is expressed as:

$$\kappa^{-1} = \sqrt{\frac{\epsilon_0\epsilon_r k_B T}{\sum (z_i e)^2 c_i}} \quad (2.3)$$

where  $k_B$  is the Boltzmann constant,  $T$  the temperature,  $z_i$  the valency of ion  $i$  and  $c_i$  its concentration. For  $10^{-1}$  M 1:1 monovalent salt,  $\kappa^{-1}$  is about 0.96 nm, and increases with decreasing ionic strength to 96 nm at  $10^{-5}$  M (considered deionised). More elaborate models than the Yukawa account for the interpenetration of macroions<sup>147</sup>, but will not be discussed here.

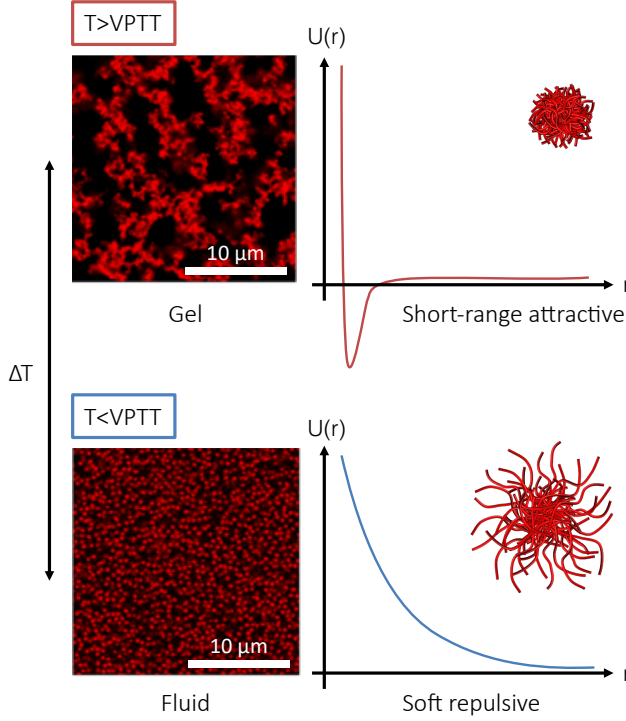


Figure 2.5: On crossing the VPTT, the inter-particle interaction potential changes from long-ranged soft repulsive (below the VPTT) to short-range attractive (above the VPTT), and (in case of sufficient electrostatic screening) a volume-spanning network structure forms. The confocal micrographs show a 3.0 wt% PNIPAM-co-AAc microgel suspension at (bottom) 20 and (top) 40 °C (top), respectively, at 100 mM KCl and 1 mM HCl.

## Above the VPTT

Above the VPTT, on the other hand, the dangling polymer ends responsible for steric stabilisation collapses and so the repulsive steric contribution to the inter-particle potential vanishes. At the same time, as the particle polymer density is considerably higher above the VPTT than below, a short-range attraction appears due to van der Waals forces, the sum of the attractive interactions originating from fluctuating dipole-dipole interactions. The van der Waals potential can be written as:

$$U_{vdW}(r) = -\frac{A_H}{6r} \left( \frac{R^2}{2R} \right) \quad (2.4)$$

with  $A_H$  the Hamaker constant that comprises the dielectric constants of the particles and the solvent and reflects the polarisability of the electron cloud. The van der Waals attraction, in case of insufficient electrostatic repulsion (low degree of ionisation and/or high ionic strength), effectively causes the microgel particles to reversibly flocculate<sup>150</sup> and form a volume-spanning gel network (Fig. 2.5). In this way, an interplay between

electrostatic repulsion tuned by salt concentration, and attractive van der Waals interactions controlled by temperature, constitutes a powerful tool with which the inter-particle interactions can be tuned, all the way from long-range, soft repulsive to short-range attractive. Due to the ease with which this tuning can be done, microgels have been useful model objects for investigation of phase behaviour as a function of the nature and range of the interactions<sup>130,140,141,145,146,151–156</sup>.

#### 2.2.4 Chain flexibility and the position of the VPTT

Despite the fact that the chemical structure of the repeat units of the polymer chain only differs by a single methyl group in the  $\alpha$ -position (Fig. 2.1), the VPTT of PNIPMAM (45 °C) is 13 °C higher than that of PNIPAM (32 °C). This stems from the extra methyl group of PNIPMAM posing a steric hindrance to the intra-molecular amide-amide hydrogen bonds that favours deswelling<sup>157</sup>. Intra-amide bonds are thus less energetically favoured for PNIPMAM and its deswelling therefore requires participation of a larger number of polymer chain segments in a cooperative manner.

Depending on the application, one can pick the polymer with the most suitable VPTT. Moreover, the fact that the two VPTTs are so well separated makes binary mixtures interesting objects of study, and phenomena such as sequential gelation have been observed<sup>158–160</sup>. In addition, the ability to tune the relative particle size with temperature has facilitated the preparation of binary crystals, this since below the VPTT of PNIPMAM, the size of PNIPAM microgels can be tuned without significantly altering the size of PNIPMAM ones. Finally, in binary clusters, such as colloidal molecules, the difference in VPTT should allow for induction of attractive ‘inter-cluster’ interactions between the PNIPAM microgels whereas the PNIPMAM ones remain repulsive. This is reminiscent of ‘patchy’ interactions displayed by, for example, proteins and other biomacromolecules.

### 2.3 Microgels at oil-water interfaces

In Paper I and Paper II (Section 5.4), the strong tendency of PNIP(M)AM microgels to adsorb to oil-water interfaces is exploited for the assembly of a small number of microgels around micron-sized oil-in-water (O/W) emulsion droplets. The aim of the following paragraphs is therefore to give a brief introduction to the most important aspects of microgel adsorption to oil-water interfaces. Output in this research area has been steadily growing, especially since the discovery that microgels can serve as responsive stabilisers for emulsions that can be broken on demand by affecting the viscoelastic properties of the interface through a change in temperature and/or pH<sup>161–167</sup>.

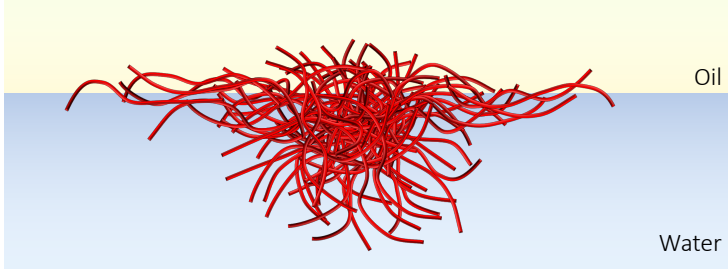


Figure 2.6: Cartoon showing the ‘fried egg-like’ conformation adopted by microgels at an oil-water interface. Due to their hydrophilic nature, adsorbed microgels mainly reside in the water phase with only a small protrusion into the oil phase.

### 2.3.1 Microgel conformation and localisation

The propensity of PNIPAM microgels to spontaneously adsorb to oil-water interfaces stems from the surface activity of linear PNIPAM<sup>168,169</sup>, in turn related to the amphiphilic nature of the polymer chain. Due to the polymer-colloid duality of microgels<sup>139</sup> this adsorption share features with that of both rigid particles and linear polymers<sup>170</sup>. Common for all three of them is that the driving force for adsorption has its origin in a lowering of the oil-water interfacial tension  $\gamma$  and, as a consequence, a lowering of the total energy of the system. Unlike rigid particles, however, both linear polymers and microgels, due to their inherent softness, have the ability to adopt their conformation at the interface<sup>171,172</sup>. It is nowadays well established that microgels strongly deform and adopt a flattened or ‘fried egg-like’ conformation on adsorption, with a larger diameter compared to in the bulk, and that microgel-microgel interpenetration is extensive<sup>166,173–175</sup>. Through this flattening, energetically unfavourable oil-water contacts are efficiently replaced by less unfavourable polymer-oil and polymer-water ones. The extent of flattening is governed by a balance between the free energy gain of covering a large interfacial area and the energy cost associated with elastic deformation of the polymer network.

Since microgels are hydrophilic and therefore more soluble in water than in oil, the majority of an adsorbed particle resides in the water phase with only a small portion immersed into the oil phase, as schematically depicted in Fig. 2.6. How much of a rigid particle that resides in the water phase is typically quantified by the contact angle  $\theta$  (Fig. 2.7), which, in case of microgels, cannot be very well estimated due to the aforementioned flattening.  $\theta$  determines, together with the interfacial tension  $\gamma$  and the particle radius  $R$ , the desorption energy  $E_d$ , for rigid particles at a flat interface expressed by:

$$E_d = \gamma\pi R^2(1 - |\cos \theta|)^2 \quad (2.5)$$

For  $\gamma$  not close to 0 or 180°,  $E_d$  reaches easily thousands of  $k_B T$  already for particles of a

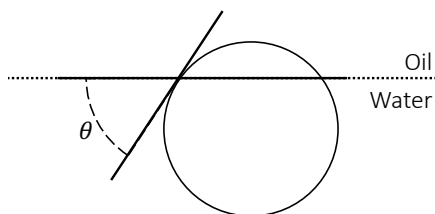


Figure 2.7: The position of a rigid particle in an oil-water interface determines the contact angle  $\theta$ .

few tens of nanometers, making adsorption essentially irreversible. Compared to rigid particles, microgels show an even stronger adsorption due to their ability to deform and make additional contacts with the interface<sup>171</sup>.

### 2.3.2 Inter-particle interactions

Inter-particle interactions between particles adsorbed to an interface is fundamentally different from those between particles in suspension. As in suspension, the effective interaction potential in the 2D interfacial plane is a superposition of the repulsive and attractive interactions. The interactions in play are quite well understood for spherical, rigid particles at a flat interface, and include electrostatic and capillary interactions<sup>170</sup>. In principle, van der Waals interactions can play a role as well, but these short-range interactions are usually negligibly small (especially true for highly water-swollen microgels) due to the repulsive interactions preventing the particles from coming close to each other. The situation becomes more complex in case the interface is no longer flat or the curvature is no longer negligible<sup>176,177</sup>. Moreover, for soft particles such as microgels, the additional degrees of freedom associated with deformation and polymer chain excursions in the interface make the interaction potential even more difficult to estimate, as revealed by the astonishing lack of literature in the area. For now, we can only observe the effects of the complex interactions present in microgel-laden interfaces, for instance through the microgels' organisation<sup>166,173</sup>.

Whereas the electrostatic inter-particle interactions in bulk can generally be well described by DLVO theory<sup>149</sup>, the situation is more complex at an interface<sup>170</sup>. Most importantly, whereas the part of the particle that resides in the water phase remains charged, the part immersed into the oil phase is to a large extent neutralised. Analogous to adsorption to an air-water interface<sup>178,179</sup>, this results in an asymmetric double layer and an overall interaction that is dependent on several parameters such as the relative immersion depth into the two phases, the dielectric constant of, and counter-ion concentration in, the two phases, and the degree of charge screening in the water phase.

Capillary inter-particle interactions, in turn, occur due to deformations of the inter-

face, and these interactions can be either repulsive or attractive depending on the local curvature<sup>170,180</sup>. On the macroscopic scale, where the gravitational pull is sufficient for deformations to occur, the aggregation phenomenon is known as the ‘Cheerios effect’<sup>181</sup>. For micrometer-sized colloids, however, the gravitational force is too small to produce a significant interfacial deformation, so capillary forces are negligible. However, deformations can be created due to surface roughness or chemical inhomogeneity. For this reason, capillary attractions are typically stronger for soft particles that are inherently extremely rough and heterogeneous.

## 2.4 Microgels confined in shrinking droplets

In Paper III (Section 5.5), exploited is a process by which microgels confined in monodisperse water-in-oil (W/O) emulsion droplets form small clusters as the water evaporates. As such geometric confinement-induced clustering of microgels has not previously been reported in literature, this section will instead briefly review the work done on solid spheres; hence the title of this section is a little misleading. Whereas clustering of solid spheres and microgels may share some common features, it is important to bear in mind that the situation is more complex with microgels which have the ability to interpenetrate, deform and compress in the high-density regimes. Moreover, knowledge about the nature of the microgels’ effective interaction potential in these regimes is still lacking.

### 2.4.1 Cluster configurations

Much of the work done on particle clustering in shrinking emulsion droplets has been performed by Manoharan, Pine, and Yang<sup>88,182–185</sup>, but has also been reported by, for example, Witteman and co-workers<sup>186,187</sup>. In a pioneering study<sup>88</sup>, 844 nm PS spheres confined in 1 to 10  $\mu\text{m}$  toluene droplets were forced to pack together as the toluene was evaporated. Throughout the evaporation process the particles are strongly bound to the oil-water interface. As a consequence, a so-called spherical packing state is encountered, a mechanically stable intermediate where the particles are tightly packed on the surface of the droplet. Further evaporation beyond this point causes the droplet to deform and capillary forces now exert a compressive force that leads to rapid rearrangement of the particles and packing into their final configuration. The resulting clusters, prevented from dissociation due to van der Waals forces between the constituent spheres, are stabilised against aggregation by their surface charge.

Whereas the number of spheres per cluster  $n$  resulting from the evaporation process ranged from 2 to 15 primarily due to the non-uniform size of the initial droplets, it

was found that all clusters of a given  $n$  were identical, regular, polyhedral aggregates, suggesting that they are optimal arrangements in the context of some minimisation principle. The quantity that was minimised turned out to be the second moment of the mass distribution  $M_2 = \sum_{i=1}^n |\mathbf{r}_i - \mathbf{r}_0|^2$ , where  $\mathbf{r}_i$  is the centre coordinate of the  $i$ th sphere and  $\mathbf{r}_0$  is the cluster's centre of mass<sup>188,189</sup>; the configurations of the experimentally obtained clusters (for  $n \leq 11$ ) exactly corresponded to theoretical  $M_2$ -minimised packings calculated by Sloane<sup>190</sup>. The essential element behind  $M_2$  minimisation is the intermediate spherical packing state in which the particles form an ordered arrangement due to long-ranged dipole-dipole repulsion through the oil droplet and Coulomb interactions. This arrangement is identical for all  $n$ -particle droplets and determine all the possible ways in which the droplet can deform and the particles rearrange on further evaporation. An analysis of the degrees of freedom however shows that there is only one possible rearrangement mode. Hence, all  $n$ -clusters have identical configuration.

The same minimal second-moment configurations were obtained when the PS spheres were replaced by PMMA and silica ones (in hexane droplets)<sup>182</sup>, indicating that the forces controlling cluster formation are insensitive to the precise nature of the interactions and surface properties of the spheres. Clustering of water-borne PS and silica spheres in inverted emulsions - water-in-toluene and water-in-hexadecane, respectively - also yielded the same minimal second-moment configurations (with a few exceptions for  $n \geq 7$  where isomeric structures were observed) despite the fact that the particles were observed to reside in the interior of the droplets and not pinned at the interface<sup>183</sup>. Interestingly, the configurations were not affected by the presence of (a large number of much smaller) nanospheres, as revealed with large PS or silica microspheres and small silica or titania nanospheres in hexadecane-in-water droplets<sup>184</sup>. This was also observed for bimodal PS and silica particles in toluene-in-water droplets, and the same authors also prepared binary colloidal clusters through clustering of similar-sized PS and silica microspheres<sup>185</sup>.

#### 2.4.2 Cluster size distributions

The typical method of preparing the initial emulsion involves simply homogenising oil and water, with the particles to be clustered suspended in one of the two phases. Surfactant is used to help stabilise the resulting droplets. This rather uncontrolled emulsification process yields polydisperse droplets and, consequently, a wide distribution of the number of spheres per droplet; a broad spectrum of cluster sizes is therefore obtained following evaporation of the dispersed phase and a fractionation method is required in order to separate clusters of different  $n$ . Because the distribution of particles per oil droplets is statistical, control of the droplet size distribution is crucial in order to obtain a large yield of the desired cluster(s). When the droplets are monodisperse,



the probability that a specific number  $n$  of microgels are captured in a single droplet is governed by Poisson distribution<sup>191,192</sup> only.

Whereas the width of the droplet size distribution is difficult to control in a simple homogenisation process, the (mean)  $n$  can be roughly tuned via the concentration of particles and the (mean) droplet size. However, Zerrouki and co-workers showed that with careful control of the emulsification process - in particular shear rate (in a Couette apparatus) and the viscosity of the continuous phase - the droplet size distribution can be narrowed, thus narrowing also the final cluster size distribution<sup>193</sup>. The use of high-power ultrasonic emulsification has also shown to yield quite uniform droplets and narrow cluster size distributions<sup>186,187</sup>. In the present thesis, however, we turn to so-called droplet microfluidics technology in order to obtain highly monodisperse (microgel-containing) water droplets. Here, as described more in detail in Section. 4.6.3, flows of oil and water in sub-millimetre-sized channels are manipulated in such a way that one of the phases breaks into uniform droplets. This emulsification method has previously been used in the preparation of highly uniform colloidal supraballs via the evaporation route<sup>194–196</sup>.

## 2.5 Small clusters of oppositely charged microgels

In Paper IV (Section 5.6), the electrostatic attraction between oppositely charged ionic microgels is exploited to form small core-satellite-type clusters. Whereas these interactions are well understood and thoroughly investigated for oppositely charged, classical hard colloids - typically modelled as hard spheres with Yukawa-like interactions beyond particle contact<sup>197</sup> - considerably less research has been done on soft particles such as microgels that can interpenetrate, deform and compress. The role of softness was recently addressed by Colla, Blaak and Likos who used molecular dynamics (MD) simulations to study the self-assembly in a fully symmetric, coarse-grained system of oppositely charged ionic microgels<sup>198</sup>. Here, the softness-related short-range elastic repulsion was described by the Hertzian potential<sup>144–147</sup> and varied in strength by varying  $\epsilon$  (Eq. 2.1). Most importantly, as different from the situation with hard particles, the soft Hertzian repulsion allows for microgel interpenetration. Through this interpenetration, oppositely charged microgels neutralise each others charges very efficiently and the minimum of the potential well is (for low  $\epsilon$ ) therefore found well inside the overlap region. This results in the formation of very dense aggregates, thus reducing the system's overall charge inhomogeneity and decreasing the charge ordering commonly seen in charged hard sphere systems. In the remainder of this section, a brief literature review on electrostatically driven assembly of oppositely charged colloids into core-satellite clusters is given, touching on aspects such as cluster size (coordination number; the number  $n$  of satellites  $B$  of size  $R$  adsorbed onto a core  $A$  of size  $r$ ), cluster size distribution and

cluster size configuration.

First, Schade and co-workers studied the adsorption of 1.2  $\mu\text{m}$  amidine-functionalised PS spheres onto 0.49  $\mu\text{m}$  carboxylate-functionalised ones, the two mixed in 100:1 number ratio in order to suppress aggregation and at 10 mM NaCl to set the Debye length to approximately 3 nm<sup>92</sup>. In this system, due to strong van der Waals attractions the satellites irreversibly stick on the cores at contact and cannot rearrange, which precludes the formation of dense or symmetric packings. Nevertheless, for one of the particular size ratios  $R/r$  investigated, 2.45, a yield of 90% irregular, distorted tetrahedra was obtained, which can be compared to the 100% tetrahedra found for  $R/r = 2.41$  when the process was simulated. Due to the irreversible, random binding, these values are well below the value 4.44 for efficient tetrahedral packing. When  $R/r$  was varied in the simulations, only for dimers ( $AB_2$ ) and tetramers ( $AB_4$ ) was 100% yield be obtained. At the critical  $R/r = 2.41$  yielding 100% tetrahedra, the maximum number of satellites that can fit around a core due to packing constraints exactly equals the smallest number of satellites that can be positioned on the core such that another satellite cannot fit.

As observed by Schade, short-range purely attractive interactions (van der Waals) are known to result in irreversible aggregation. This is the reason why Nature instead employs weak interactions in order to successfully achieve high-fidelity self-organised structures. In this respect, (solvent-swollen) microgels are beneficial as they lack van der Waals attractions. This motivated Go and co-workers to form well-defined clusters from oppositely charged, 1.5  $\mu\text{m}$  trifluoroethyl methacrylate (TFMA)-PNIPAM core-shell microgels<sup>199</sup>. In this study, the reversibility of the assembly process was investigated, and it was found that almost all clusters eventually dissociated on addition of NaOH that served to reverse the charge of one of the two particles. The disassembly time was sometimes as long as a few hours, which was explained by the complex coacervates formed between entangled core-satellite polymer networks; disassembly requires the polymer networks to fully disentangle before two particles can apart.

In a study performed by Tagliacruzchi and co-workers, microgels were again employed. Here, positively charged PNIPMAM microgels were used as satellites, but this time carboxylate-coated PS particles were used as cores<sup>200</sup>. The two were assembled at large satellite:core ratios and under salt-free conditions. Here, the authors studied the effect of the  $R/r$  ratio on the coordination number  $n$  in order to deduce if  $n$  is thermodynamically or kinetically controlled. In the case of thermodynamic control the satellites can reorganise on the surface of the core to maximise attractive core-satellite interactions while minimising repulsive satellite-satellite ones. Under conditions of kinetic control such reorganisation is not possible. Hence, under kinetic control the adsorption ceases when the largest free site on the core is smaller than the effective size of a satellite - a process known as random sequential adsorption (RSA). The authors found their experimentally determined coordination numbers (and the irregular geometries of the

clusters) to agree much better with those predicted by RSA than those predicted from a thermodynamically controlled process, thus corroborating Schade's findings.

In contrast, Demirörs and co-workers reported on the preparation of regular clusters from a binary 10:1 mixture of oppositely charged PMMA particles due to an interplay between long-ranged (comparable to the particle size) attractive core-satellites and repulsive satellite-satellite interactions in an intermediate-dielectric constant medium; regular clusters were also obtained in Monte Carlo simulations, with  $R/r = 1$  and using a pair potential composed of a hard-core repulsion plus a Yukawa potential<sup>201</sup>. The authors argued that key to the well-defined preference for particle positions is the intra-cluster satellite-satellite Yukawa repulsion. Furthermore, when the strength of the satellite-satellite repulsion was increased by using more highly charged satellites, lower coordination numbers  $n$  were observed due to a larger effective satellite size. When instead tuning the range of the repulsion via the ionic strength,  $n$  was shown to peak at a certain position with increasing ionic strength due to an interplay between the increasing effective satellite size and the decreasing range of the core-satellite attraction.

Finally, an additional dimension to the electrostatic assembly was added by Mihut and co-workers who used bowl-shaped PS-PNIPMAM core-satellite particles (Section 3.3) as satellites in order to evoke lock-and-key-type interactions<sup>67,94,202,203</sup> with shape-complementary PNIPAM cores of opposite charge<sup>204</sup>. Here, the experimentally observed preference of the cores for the cavity of the satellites was demonstrated by a simple set of calculations considering the minimum electrostatic energy and the van der Waals contribution. Interestingly, and enabled by the lower VPTT of the cores compared to satellites, the coordination number  $n$  could be manipulated with temperature as a core particle below the VPTT can encompass more satellites than one above the VPTT.

*#IAmAScientistBecause there are moments when  
I learn something new in the lab and think, I'm  
the only human that knows this right now.*

- @DrWorms on Twitter

## 3 | Synthesis methods

### Contents

|     |  |    |
|-----|--|----|
| 3.1 | Microgel synthesis . . . . .   | 26 |
| 3.2 | Microgel-microgel coupling . . . . .                                     | 29 |
| 3.3 | Bowl-shaped polystyrene/microgel core-shell particle synthesis . . . . . | 32 |
| 3.4 | PDMS oil droplet synthesis . . . . .                                     | 33 |

In this chapter the most important synthesis methods of the thesis are introduced. Whereas the majority of the chapter focuses on various types of microgel synthesis and post-synthesis functionalisation, an introduction to the preparation of polydimethylsiloxane (PDMS) oil droplets is provided at the end. More comprehensive reviews on microgel synthesis are provided in references<sup>113</sup> and<sup>114</sup>.

### 3.1 Microgel synthesis

#### Reactants and their roles

The PNIPAM and PNIPMAM microgels used in this thesis were prepared by free radical precipitation polymerisation<sup>114</sup> of two main components, NIPAM or NIPMAM as main monomer and BIS as crosslinker (Fig. 3.1A, B and C), as first described in references<sup>110</sup> and<sup>111,112</sup>, respectively. The structural motif that enable NIPAM and NIPMAM to be subject to polymerisation via a radical mechanism is the terminal double bond. BIS, in turn, carries two such motifs, and can thereby act as a crosslinker. The role of the crosslinker is to preserve the particles' structural integrity as they would otherwise dissolve into their constituent water-soluble polymer chains. The 'crosslinking density', the molar amount of BIS added with respect to the main monomer, determines the particle softness and the degree of swelling, with more BIS naturally reducing the softness and the swelling<sup>205</sup>. Moreover, as BIS display faster polymerisation kinetics than the main monomers, a single-batch polymerisation yields particles with an inhomogeneous polymer density profile<sup>121-124,206</sup> (Section 2.1). In order to obtain particles with a homogeneous crosslinker distribution, BIS can be continuously fed to the polymerisation reaction at a rate that serves to keep the monomer-to-crosslinker ratio constant<sup>207</sup>. It is also informative to compare the polymerisation rates of NIPAM and NIPMAM, whose chemical structures only differ by a single methyl group (Fig. 3.1A and B): under the same conditions, full conversion of the monomer is attained after about 20 and 150 minutes for NIPAM and NIPMAM, respectively<sup>111,125</sup>.

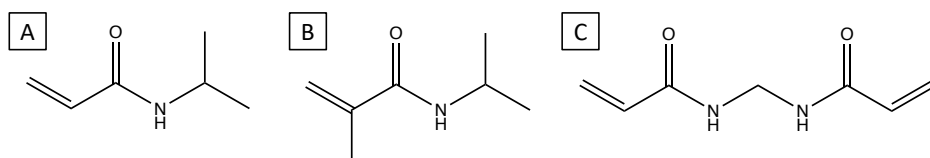


Figure 3.1: Chemical structure of (A-B) the monomers NIPAM and NIPMAM, respectively, and of (C) the crosslinker BIS.

Co-polymerisation of the main monomer and the crosslinker was in this thesis initiated using the free radical initiators potassium persulfate (KPS) or 2,2'-azobis(2-methylpropionamide) dihydrochloride (V50) (Fig. 3.2A and B), which thermally decompose into free radicals at the temperature of the reaction. During the polymerisation reaction, charged initiator residuals become attached to the ends of the polymer chains and serve to confer electrostatic stabilisation. The residuals are negatively and positively charged in the case of KPS (sulfate) and V50 (amidine), respectively. Through the choice of initiator, the charge identity (anionic or cationic) of the resulting microgels can thus be controlled. To control the magnitude of the charge via the amount of initiator is not to recommend however, as this naturally affects the initiation of poly-

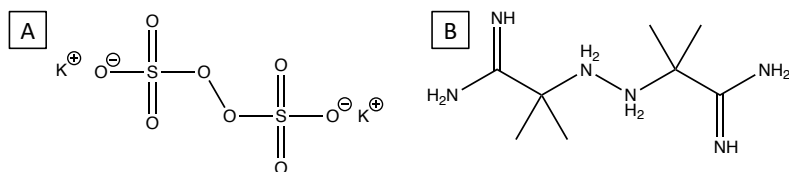


Figure 3.2: Chemical structure of the initiators (A) KPS and (B) V50.

merisation. This is better done using charged co-monomers.

Alongside NIP(M)AM and BIS, co-monomers can be co-polymerised in order to incorporate functional groups. Co-monomers can, for example, confer charge and pH dependence in order to osmotically increase particle swelling as well as adjust the long-ranged electrostatic forces, serve as handles for subsequent attachment of functional molecules, or carry fluorophores. In this thesis, acrylic acid (AAc) and allylamine (AL) (Fig. 3.3A and B) were used as co-monomers for the incorporation of carboxylic acid and amine groups, respectively, and polymerisable rhodamine and fluorescein derivatives were used to label the particles and make them visible under the fluorescence confocal microscope.

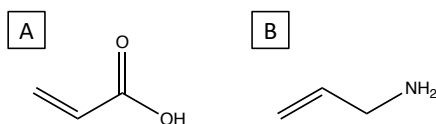


Figure 3.3: Chemical structure of the co-monomers (A) AAc and (B) AL.

Finally, surfactant can be used in the polymerisation to limit the size of the growing particles through a charge stabilisation mechanism<sup>205,208,209</sup>. In the present thesis, sodium dodecyl sulfate (SDS) (Fig. 3.4) was used for this purpose. The particle size is also affected by the choice of polymer, with PNIPMAM particles typically being larger than PNIPAM ones. This is a reflection of the behaviour of the corresponding linear polymers, where PNIPMAM chains take more expanded structures than PNIPAM ones due to a greater intrinsic chain stiffness caused by the extra methyl group<sup>210</sup>.

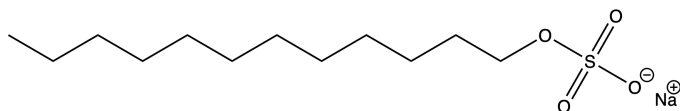


Figure 3.4: Chemical structure of the surfactant SDS.

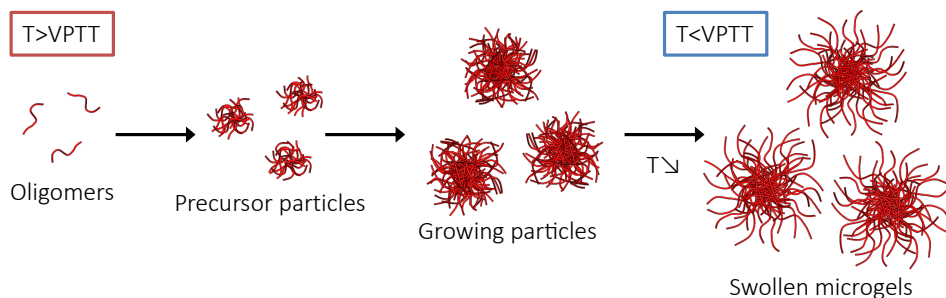


Figure 3.5: Schematic description of microgel formation by precipitation polymerisation.

## Reaction mechanism

Free radical precipitation polymerisation, as any free radical polymerisation, proceeds through initiation, propagation and termination. Initiation of polymerisation takes place on addition of water-soluble thermal initiator to an aqueous solution of monomer and crosslinker (and possibly co-monomers), heated to a temperature above (or close to) the initiator's decomposition temperature. At this elevated temperature, homolytic cleavage of a labile bond within the initiator molecule yield two free radicals per molecule. One such free radical then attack the polymerisable motif in a monomer or crosslinker molecule, on which a new radical is formed that can repeat the process - and so the reaction propagates. Termination occurs when two such radicals combine.

How are then the particles formed? Key to this is the elevated temperature, at which the growing oligomers become insoluble at a critical length, undergo coil-to-globule transition and collapse (precipitate) on each other to form precursor particles (Fig. 3.5). The destiny of such a precursor particle, according to coagulative nucleation theory<sup>125,211</sup>, is to either combine with another precursor particle to form an electrostatically stable unit, a seed, or to grow by addition of monomers and chains from the continuous phase, or by polymerisation of radicals within, until stabilised. As the reaction proceeds and the concentration of monomer and crosslinker decreases in solution, the probability of forming new, stable seeds becomes very low, and growth of already existing seeds becomes the more probable event. The monodispersity of the final product is typically very high (about 5% or so), which stems from the (homogenous) nucleation event being well separated from the growth phase. The fact that the growing particles repel each other electrostatically also serves to preserve the narrow size distribution. The high degree of monodispersity is reflected, most evidently, in the particle's ability crystallise into ordered arrays that Bragg diffract the incident light.

As mentioned above, the elevated temperature has a two-fold role, as it both serves to catalyse the decomposition of the thermal initiator into free radicals as well as en-

sures that precipitation of the growing oligomers takes place. If the thermal initiator is replaced by, for example, a photoinitiator, the polymerisation can be carried out at room temperature. At room temperature, however, the growing polymer chains remain water-soluble, and the resulting product is a macrogel instead of a suspension of discrete particles<sup>212</sup>.

Since the polymerisation proceeds via a radical mechanism, the reaction is sensitive to the presence of oxygen, which has to be excluded as it harvests the radicals. Therefore, before initiation, the monomer solution is deoxygenated by purging with nitrogen gas. Not until the reaction mixture has been well purged and the temperature has been allowed to equilibrate at the desired reaction temperature for some time, the initiator solution is introduced into the vessel under stirring for rapid distribution. Polymerisation starts immediately, as is evident from a rapid increase in turbidity. The reaction is allowed to proceed, under nitrogen atmosphere, for a couple of hours to ensure complete conversion of the starting materials, and is then cooled down to room temperature under stirring. Any coagulum present is removed by filtration through glass wool. Finally, the obtained particle suspension is purified by dialysis or by repeated rounds of centrifugation-decantation-redispersion in order to remove any unreacted monomer or non-bound polymer segments.

## 3.2 Microgel-microgel coupling

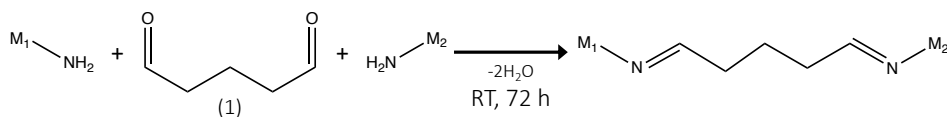
In Paper III (Section 5.5), colloidal molecules are generated through clustering of microgel particles dispersed in evaporating emulsion droplets. To prevent the clusters from dissociating once formed, strategies for creating covalent inter-particle microgel-microgel bonds were investigated in the present thesis and are described below.

### 3.2.1 Amine-dialdehyde coupling

Microgel particles carrying primary amine groups - incorporated during microgel synthesis using amine-carrying co-monomers such as AL<sup>213-216</sup>, *N*-(3-aminopropyl)methacrylamide (APMAM)<sup>217,218</sup> or 2-aminoethylmethacrylate (AEMA)<sup>219</sup> - can be covalently linked using the bifunctional linker glutardialdehyde (GDA). Here, two nucleophilic primary amine groups belonging to two different microgels attack the electrophilic carbonyl carbons of GDA, resulting in a 'bridge' that bonds the two microgels together through two aldimine linkages (Scheme. 3.1). An unwanted side reaction occurs when two amine groups belonging to the same microgel particle attack the same GDA molecule, whereby an intra-particle crosslink forms. In order for the intended inter-particle coupling to take place, the



microgels to be coupled need to be in close proximity before the GDA is introduced. Imine formations are typically carried out at pH 4.5, where the balance between carbonyl oxygen protonation and primary amine deprotonation is optimised.



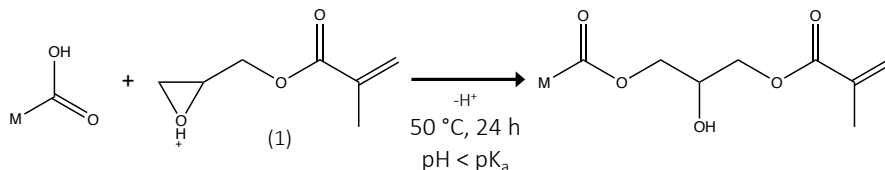
Scheme 3.1: Coupling of two amine-functionalised microgels ( $M_1$  and  $M_2$ ) using the bifunctional crosslinker GDA (1).

### 3.2.2 Post-synthesis polymerisation

Microgels carrying polymerisable groups can be coupled in a post-synthesis polymerisation step. Two methods for attaching polymerisable groups are described in the following.

#### Carboxylic acid-epoxide reaction

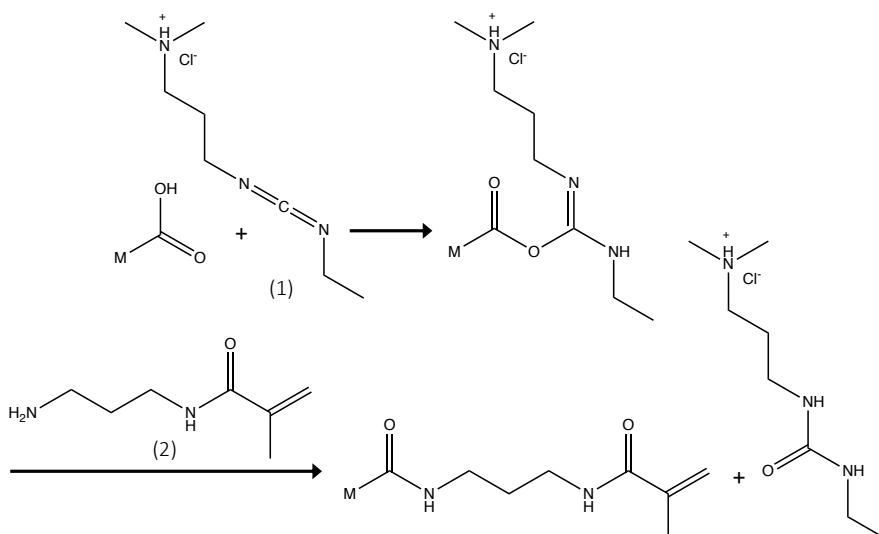
In order to incorporate methacrylate groups that can be linked using (chemical or photo-induced) free radical chemistry, glycidyl methacrylate (GMA) can be attached to carboxylic acid-carrying microgels via an carboxylic acid-epoxide reaction (Scheme. 3.2) as previously reported for linear poly(acrylic acid) (PAAc)<sup>220</sup> and for PMMA/poly(methacrylic acid) (PMAAc) and poly(ethylacrylate) (PEA)/PMAAc particles<sup>221</sup>. Here, the weakly nucleophilic carboxylic acid group attacks the highly electrophilic, highly strained, protonated epoxide group through a ring-opening mechanism. The reaction is performed under conditions where the epoxide is protonated<sup>220</sup>. In case of asymmetrically substituted epoxides, such as the one present in GMA, nucleophilic attack at the more substituted carbon is typically favoured as it better stabilises the intermediate that possesses partial carbocation character. However, the opposite has been reported for GMA attachment to PAAc<sup>220</sup>. Typically, low yields are reported for GMA attachment to carboxylic acid groups<sup>221</sup>, which can be explained by the competition between carboxylic acid and the highly abundant water as a nucleophile.



Scheme 3.2: Acid-catalysed carboxylic acid-epoxide reaction for the attachment of GMA (1) to microgels (M) carrying carboxylic acid groups.

## Carboxylic acid-amine reaction

As an alternative to the acid-epoxide reaction above, polymerisable groups can be incorporated by coupling of the corresponding primary amine-carrying compounds - AL or APMAM for instance - to carboxylic acid-carrying microgels in an 1-ethyl-3-(3-dimethylaminopropyl)carbodiimide (EDC) coupling reaction<sup>222</sup>. EDC is a water soluble, zero-length crosslinking agent that serves to activate the carboxylic acid groups towards nucleophilic attack by the primary amine, resulting in the formation of an amide bond (Scheme. 3.3). It has been used to couple, for instance, biotin<sup>223</sup> and DNA oligonucleotides<sup>224</sup> to PNIPAM. The first step of the process involves nucleophilic attack by the carboxylic acid group on the electron-deficient carbodiimide carbon of EDC, thereby forming an unstable *O*-acylisourea intermediate. In a second step, the EDC residue is displaced in a nucleophilic attack. If the nucleophile is the intended amino group, then the intended amide forms. However, the solvent water may also act as a nucleophile and regenerate the carboxylic acid group. To suppress hydrolysis and thereby increase the efficiency of acid-amine coupling, *N*-hydroxysuccinimide (NHS) is sometimes added to form a more stable NHS ester intermediate<sup>225,226</sup>. The reaction is typically performed in MES buffer at slightly acidic pH.



Scheme 3.3: Attachment of APMAM (2) to microgels (M) carrying carboxylic acid groups using the zero-length crosslinking agent EDC (1).

### 3.3 Bowl-shaped polystyrene/microgel core-shell particle synthesis

In the present thesis, in addition to spherical microgels, the preparation of colloidal molecules from bowl-shaped ones was investigated with the intension of adding an additional dimension to the directional interactions, namely shape complementarity. Here, it was envisioned that bowl-based colloidal molecules, with the cavity of the bowls facing outwards, can be assembled in a lock-and-key-type<sup>67,94,202–204</sup> fashion using spheres that precisely fit the cavities as linkers.

Several methods for the preparation of bowl-shaped (or single-dimple) colloids have been reported in the literature. For instance, radical polymerisation in the aqueous phase was shown to induce buckling in spherical 3-methacryloxypropyl trimethoxysilane (TPM) oil droplets as the droplets acquired a crosslinked shell and, simultaneously, decreased in volume as non-crosslinked TPM oligomers migrated into the water phase<sup>67,203</sup>. In a related approach, dimple formation was induced by first growing crosslinked tetraethoxysilane (TEOS) shells around spherical PDMS oil droplets, and then dissolving the liquid PDMS in a good solvent<sup>64</sup>. In another approach, a single dimple was formed by swelling of spherical linear-PS particles with a mixture of styrene and TPM that were then polymerised<sup>227</sup>. Here, TPM forms a crosslinked shell around the particles whereas polymerisation of styrene in the particle centre causes a volume reduction that, in a manner analogous to that of the previous examples, causes a dimple to form.

In the present thesis, bowl-shaped composite PS/microgel core-shell particles consisting of a PS core and a crosslinked PNIP(M)AM shell were obtained by nano-engineering of the spherical counterparts (Fig. 3.6). In this method, spherical composite PS/microgel core-shell particles are first prepared in a two-step synthesis, an emulsion polymerisation<sup>228</sup> of styrene to yield PS particles followed by a seeded polymerisation of NIP(M)AM during which the PS particles acquire a crosslinked PNIP(M)AM shell<sup>229</sup>. A temperature-controlled swelling mechanism, first demonstrated with polystyrene and poly(methyl methacrylate) (PMMA) particles<sup>65,230</sup>, is then employed in order to transform the spheres into a distinct bowl shape<sup>231,232</sup>. The process proceeds via swelling of the PS cores with styrene, instantaneous freezing in liquid nitrogen (-196 °C), and, finally, slow evaporation (below 0 °C, the melting temperature of water) of the styrene. In the freezing step, solidification of styrene starts from the particle surface, creating a flux from the centre where a void is created. The void grows in the evaporation step, as the styrene flux causes PS chains to migrate towards the particle periphery. As the styrene evaporates, a hole - the cavity - is formed in the shell and its size can be controlled via the evaporation flux<sup>65</sup>. The evaporation process must be carried out below 0 °C in order to preserve the hollow structure, or the particles will

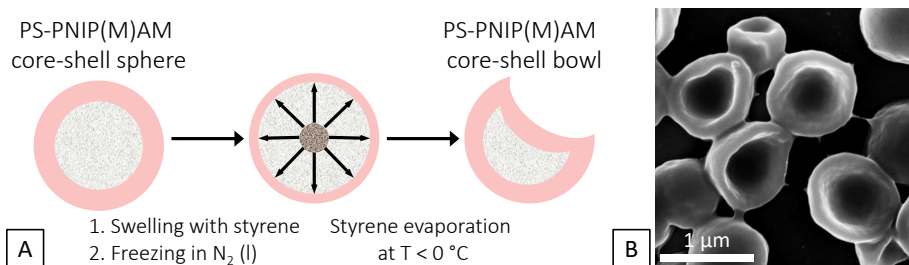


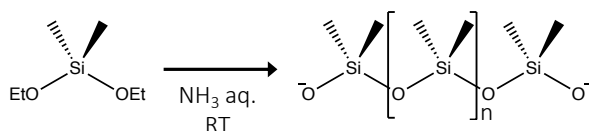
Figure 3.6: (A) Schematic representation of the transformation of spherical composite PS-microgel core-shell particles into bowl-shaped ones. (B) Scanning electron microscopy (SEM) micrograph of bowl-shaped PS-PNIPMAM particles (courtesy of B. Joseph).

else be compressed into spheres by the surrounding liquid water.

### 3.4 PDMS oil droplet synthesis

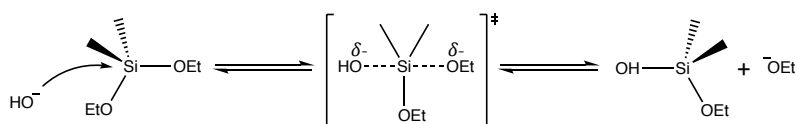
In Paper I and Paper II, the adsorption of microgels to micrometer-sized O/W PDMS emulsion droplets is exploited (Section 5.4). PDMS is the most widely used silicon-based organic polymer. It is typically inert, nontoxic, nonflammable and optically clear. It serves as an important component in silicon grease and in Silly Putty and Kinetic Sand, to which it imparts its characteristic viscoelastic properties. It is also used as an additive in various medicinal drugs, cooking oils and hair and skin care products.

PDMS emulsions can be generated from a mixture of silicon oil and water via traditional comminution routes where energy is inputted to finely disperse the oil phase. The drawback of this method is, however, that it typically results in very wide droplet size distributions. In the present thesis, as a high degree of monodispersity is crucial, an alternative emulsion generation route that offers excellent monodispersity was followed. Here, PDMS was synthesised from the corresponding monomer, dimethyldiethoxysilane (DMDES), via ammonia-catalysed hydrolysis and condensation in water<sup>233</sup> (Scheme. 3.4). The process is analogous to that of the famous Stöber synthesis of colloidal silica particles from TEOS<sup>234</sup> and has also been exploited for the polymerisation of other organosilicon monomers such as 3-(methyldimethoxysilyl)propyl methacrylate (DPM) and TPM<sup>67,203,235,236</sup>.



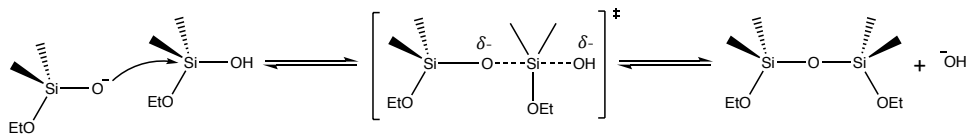
Scheme 3.4: Reaction scheme for the ammonia-catalysed synthesis of (right) PDMS from (left) DMDES.

DMDES consists of a central tetravalent silicon atom of tetrahedral molecular geometry, carrying two methyl groups and two ethoxy groups. In aqueous ammonia solution, the Si-OEt bonds hydrolyses via bimolecular nucleophilic substitution reactions ( $S_N2$ ) at silicon, involving negatively charged, pentavalent transition states<sup>237,238</sup> (Scheme. 3.5). Here, water serves as a nucleophile and replaces an alkoxy group. Ammonia catalyses the reaction by deprotonating the water, thereby rendering it a stronger nucleophile in the shape of a hydroxide ion. Expulsion of the first ethoxy group of DMDES is rate determining; the second hydrolysis step is faster as the electron-withdrawing hydroxyl (-OH) group generated in the first hydrolysis step helps stabilising the transition state of the second step. Several factors influence the hydrolysis rate of organosilanes, such as the concentration of hydroxide ions (the concentration of ammonia, indirectly), and steric and inductive effects.



Scheme 3.5: Base-catalysed hydrolysis of DMDES.

Ammonia catalyses also the subsequent condensation step. The nucleophile is this time an electron-rich, deprotonated silanol group and the reaction proceeds again through nucleophilic attack on the electron-poor silicon centre and via a pentavalent transition state (Scheme. 3.6). The condensation reaction can be either a water or an alcohol condensation depending on whether the leaving group is water or alcohol. In any case, a siloxane bridge (Si-O-Si) is the result, serving to connect two silicon centres originating from two different monomers. The name 'PDMS' is somewhat of a misnomer as the resulting oil phase - as shown by NMR and mass spectrometric analysis - is composed of small, linear and cyclic oligomers, with the cyclic tetramer being the most abundant species<sup>233</sup>.



Scheme 3.6: Base-catalysed condensation of DMDES-derived species.

The formation of monodisperse emulsion oil droplets is believed to proceed via controlled nucleation and growth<sup>233</sup> (Fig. 3.7), as also reported for TPM<sup>235</sup>. The process starts from a two-phase system consisting of initially insoluble DMDES oil in aqueous ammonia solution. The DMDES oil is first finely dispersed by intense shaking or stirring, after which hydrolysis serves to rapidly solubilise it. Condensation reactions then yield PDMS oligomers that, at a critical chain length, separate out of the aqueous

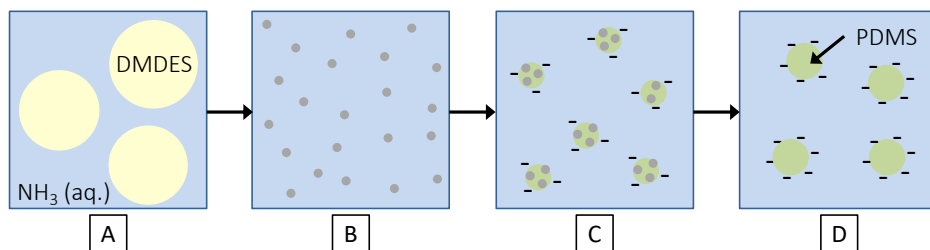


**Figure 3.7:** Schematic representation of DMEDES polymerisation. (A) Polymerisation starts from a two-phase system consisting of DMEDES oil droplets (yellow) dispersed in aqueous ammonia solution (blue). (B) Hydrolysis and condensation of DMEDES produces PDMS oligomers (grey). (C) The oligomers serve as nuclei for PDMS emulsion oil droplets (green), that are eventually stabilised by charge. (D) The emulsion droplets grow by acquiring more PDMS oligomers.

phase to form oil droplet nuclei. The oil droplets grow, without coalescence due to a strongly negative surface charge that develops from dissociation of terminal, acidic silanol groups, by acquiring PDMS oligomers from solution. The turbidity of the solution increases in the process. Liquid droplets are formed since difunctional DMEDES is unable to branch and form crosslinks. The final droplet size ranges from one to five micrometers and can be roughly tuned by adjusting the ammonia concentration and the DMEDES amount, with more ammonia and DMEDES resulting in larger droplets<sup>233</sup>. Due to their surface charge, the corresponding emulsions are long-term kinetically stable, especially so after dialysis that serves to decrease the ionic strength.



*#IAmAScientistBecause a professor said women  
don't do well in chemistry. I proved him wrong.*

- @Chem\_Moneky on Twitter

## 4 | Experimental techniques

### Contents

|     |   |    |
|-----|---|----|
| 4.1 | Light scattering . . . . .                              | 38 |
| 4.2 | Confocal microscopy . . . . .                           | 45 |
| 4.3 | Zetametry . . . . .                                     | 48 |
| 4.4 | Nuclear magnetic resonance (NMR) spectroscopy . . . . . | 51 |
| 4.5 | Sedimentation methods . . . . .                         | 54 |
| 4.6 | Microfluidics . . . . .                                 | 56 |

In this chapter, the experimental techniques used in the thesis are described. Light scattering was used for determination of particle size (radius) and polydispersity, whereas zetametry was used to measure electrophoretic mobility and zeta potential. Direct imaging was done using confocal microscopy. Nuclear magnetic resonance (NMR) spectroscopy was used to evaluate microgel post-synthesis functionalisation. Analytical ultracentrifugation (AUC) was employed for analysis of colloidal molecule size distributions. Colloidal molecule isolation was done using microfluidic deterministic lateral displacement (DLD), whereas droplet-based microfluidic technology was used for emulsion generation. Whereas in-depth introductions to these techniques can be found elsewhere, this chapter aims to provide only rudimentary introductions.



## 4.1 Light scattering

### 4.1.1 Introduction to light scattering

The typical scattering experiment relies on scattering to provide information on the geometry and structure of colloidal particles in dispersion. Whereas both neutrons and x-rays are accessible, (laser) light is by far the most popular type of radiation used to study colloids, as the size of (most) colloids lies near the visible spectrum of light. In a typical light scattering experiment, a coherent (same wavelength, direction of propagation and phase) laser beam illuminates a small volume of the sample. Due to a difference in refractive index  $n$  between the particles and the dispersion medium, the light becomes scattered in all directions, with the intensity  $I$  of the scattered light being dependent on the number of scatterers (particles)  $N$  in the scattering volume  $V$ , and on the scatterers' scattering length density with respect to that of the dispersion medium  $\Delta\rho$ , according to:

$$I(q) = NV^2 \Delta\rho^2 P(q)S(q) \quad (4.1)$$

In Eq. 4.1,  $P(q)$  and  $S(q)$  are the so-called form and structure factors, respectively, and are given by intra- and inter-particle interference effects, respectively. Thus, whereas  $P(q)$  provides information about the scatterers' size and shape,  $S(q)$  provides information about inter-particle interactions. In case of non-interacting particles, as can be assumed for very dilute suspensions,  $S(q)$  is unity (1) and  $I(q) \propto P(q)$ . As in Eq. 4.1,  $I$  is typically expressed as a function of the (magnitude of the) scattering vector  $q$ , which is, if assuming elastic (no energy dissipation in the scattering event) or quasielastic scattering, related to the scattering angle  $\theta$  through:

$$q = |\vec{q}| = \frac{4\pi n_m}{\lambda_0} \sin\left(\frac{\theta}{2}\right) \quad (4.2)$$

where  $\lambda_0$  is the vacuum wavelength of the incoming light and  $n_m$  the refractive index of the medium. In the more physical sense,  $\vec{q}$  represents the difference between the incident wave vector  $\vec{k}_i$  and the scattered wave vector  $\vec{k}_s$ , so  $\vec{q} = \vec{k}_i - \vec{k}_s$  (Fig. 4.1).  $\vec{q}$  has the property:

$$\vec{q}\vec{R} = \phi \quad (4.3)$$

where  $\vec{R}$  the distance vector between any two scattering centres. According to Eq. 4.3 the inner product of  $\vec{q}$  with  $\vec{R}$  yields a phase shift  $\phi$  of two waves scattered from the two centres when arriving at the detector in the far distance. The distribution of all scattering centres in the scattering volume  $V$  thus results in a characteristic interference pattern at the detector. With the (angle-dependent) pattern at hand, one sets out to solve the inverse problem, i.e. deducing the structures that created the specific pattern. This is the basic proposition of a scattering experiment.

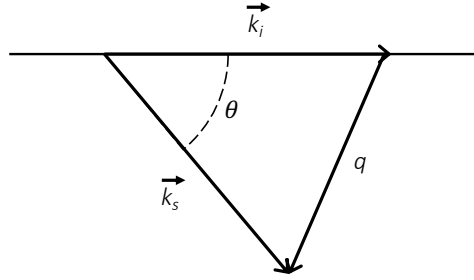


Figure 4.1: Definition of the scattering vector  $\vec{q}$ . The wave vector of the incident beam is denoted  $\vec{k}_i$  and that of the scattered beam  $\vec{k}_s$ .

### 4.1.2 Experimental setup

A typical light scattering system comprises of a number of components. First, a coherent light source, a laser, is used to illuminate the sample. Most of the light passes straight through the sample, but some is scattered by the particles and the intensity of the scattered light is measured by a detector. In order to optimise the performance of the detector, the intensity of the laser is adjusted using an attenuator. The scattered intensity recorded by the detector is processed by a correlator and the information is passed on to a computer.

This experimental setup works well for transparent samples where there are no effects of multiple scattering. Multiple scattering is the phenomenon wherein scattered photons are re-scattered prior to reaching the detector, effectively increasing the ‘randomness’ of the scattered intensity and thereby reducing its correlation in time. As will be apparent downstream (Section 4.1.3), the reduced correlation can in determination of particle hydrodynamic size be interpreted as a faster particle diffusion than the true one. Measurements performed under multiple scattering conditions are therefore biased towards smaller particle sizes.

In order to suppress the effects of multiple scattering, the 3D cross-correlation light scattering technique was developed<sup>239,240</sup>. Here, two scattering experiments are performed simultaneously, on the same scattering volume and at the same scattering vector. By cross-correlating the signals received from the two experiments, the multiple scattering contribution will only give a static contribution to the so-called correlation function (Section 4.1.3), effectively reducing its amplitude, and only the single scattering contribution will affect its relaxation. To avoid cross-talk between the two scattering experiments, the 3D technique was later extended to so-called modulated 3D cross-correlation light scattering<sup>241</sup> where shutters are used in order to very rapidly alternate between the two scattering experiments. This significantly improves the signal-to-noise ratio of the experiment.

### 4.1.3 Static and dynamic light scattering (SLS and DLS)

Light scattering can be subdivided into two broad categories, static and dynamic light scattering (SLS and DLS). In the following two sections the fundamentals of these two techniques are outlined. The discussion is limited to scattering under conditions where Rayleigh-Debye-Gans (RDG) theory is applicable. Its basic assumption is that light is not reflected at the particle boundary nor is it attenuated within the particle. This is typically violated if the particles size is comparable to the wavelength of the laser light or if the particle-solvent refractive index ratio  $m$  is far from 1, i.e. a large refractive index mismatch. The theory for SLS is valid also for X-ray and neutron scattering that differ from SLS only with respect to the much smaller wavelengths (typically 0.1 nm) and the nature of the contrast (electron density and nuclear scattering length density, respectively).

Both techniques, SLS and DLS, were used in this thesis for the purpose of particle size determination, by measuring the time-averaged and fluctuating intensity of the scattered light, respectively. However, when it comes to microgels with an inhomogeneous radial polymer density, SLS typically measure a slightly smaller size compared to DLS. The reason is that SLS probes the more highly scattering particle core whereas DLS builds on hydrodynamics that are affected also by the dangling polymer chains in the periphery of the particles. As the microgel particles used in this thesis were highly monodisperse, as was revealed by CLSM and by sample iridescence, the degree of size polydispersity was seldom quantified. By performing SLS and DLS experiments as a function of temperature, the swelling behaviour of the microgel particles could be studied.

#### Static light scattering (SLS)

Elementary and in-depth introductions to SLS are provided by Colby and Rubinstein<sup>109</sup> and by Zemb and Lindner<sup>242</sup>, respectively.

In SLS, the time-averaged - in order to remove the inherent fluctuations of the signal - intensity  $I$  of the scattered light is measured as a function of the scattering vector  $q$ . As described above, for very dilute suspensions one can assume  $S(q) = 1$  and the dependence of  $I$  on  $q$  is solely expressed through  $P(q)$ . For homogeneous spheres,  $P$  is dependent on both  $q$  and the particle radius  $R$  as:

$$P(qR) = \left[ \frac{3[\sin(qR) - qR \cos(qR)]}{(qR)^3} \right]^2 \quad (4.4)$$

which is graphically displayed in Fig. 4.2. For hard spheres that are large enough to show at least one minimum, Eq. 4.4 can be fitted to the curve in the plot of  $I(q)$  to give

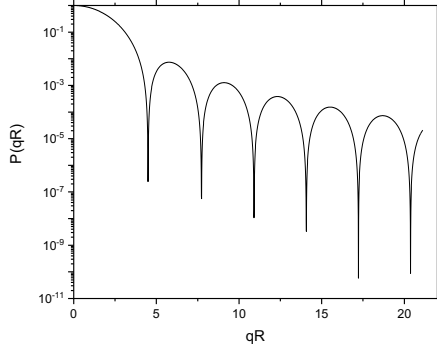


Figure 4.2: The form factor  $P(qR)$  of a hard sphere of radius  $R$ , calculated from Eq. 4.4.

a good estimate for  $R$ . In addition, the depth of the minima provide information about the degree of particle polydispersity. As the  $q$ -position of the minima depends on  $R$ , particle polydispersity serves to ‘smear out’ the minima. In other words, the greater the monodispersity the more pronounced are the minima. To incorporate polydispersity into the model, typically a normal distribution with a standard deviation  $\sigma$  is considered, where this extra parameter can be used to tune the depth of the minima.

For microgel particles,  $P(q)$  has been shown to be well described by Stieger’s fuzzy sphere model<sup>206</sup> where it is assumed that the fuzziness can be accounted for by convoluting the radial box profile for a homogeneous sphere with a Gaussian, and assuming an exponentially decaying polymer density in the loosely crosslinked shell.  $P(q)$  for a fuzzy sphere is given by:

$$P(qR) = \left[ \frac{3[\sin(qR) - qR \cos(qR)]}{(qR)^3} \exp\left(-\frac{(\sigma_s q)^2}{2}\right) \right]^2 \quad (4.5)$$

where  $\sigma_s$  describes the decrease in polymer density outside the box profile that characterises the core. At a distance  $R = R_{box} + 2\sigma_s$  from the centre, the polymer density has decreased by half compared to the core, and at  $R_p = R_{box} + 4\sigma_s$ , the approximate radius measured by scattering, the profile approaches zero. Beyond  $R_p$  a small number of dangling polymer chains contribute only to the hydrodynamics of the particle, and therefore  $R_p$  is expected to be slightly smaller than the hydrodynamic radius  $R_H$  determined by DLS.

Besides size and polydispersity, other sample and particle properties - such as the second virial coefficient  $B_2$ , polymer molecular weight  $M_w$  and radius of gyration  $R_g$  - can be obtained from SLS measurements through construction of so-called Debye and Zimm plots. This will, however, not be further discussed in this thesis.

## Dynamic light scattering (DLS)

Comprehensive introductions to DLS are provided by Zemb and Lindner<sup>242</sup> and by Berne and Pecora<sup>243</sup>.

DLS measures Brownian motion, the movement of particles due to random collisions with the solvent molecules that surround them, defined by a property known as the translational diffusion coefficient  $D$ , and relates this to particle size. In practice, a DLS experiment probes the rate at which the intensity  $I$  of the scattered light, at a given angle, fluctuates with time due to Brownian motion. The fluctuations in  $I$  arise from phase fluctuations of the scattered light waves and a fluctuating interference pattern at the detector. The smaller the particles the more rapid is their motion, and the faster does  $I$  fluctuate. The fluctuations are analysed mathematically using a digital correlator that measures the degree of similarity between two signals over a period of time. The signal at one point in time  $t$  is very similar to the signal at a very short time later  $t + \tau$ , and the two signals are 'strongly correlated'. The degree of correlation reduces with time and at a much later time all correlation is lost. The smaller the particles, the faster the intensity signal changes and the shorter the correlation will persist. In DLS, the timescales are very small, and it takes typically just about one to tens of milliseconds to lose all correlation.

In DLS, the time dependence of the fluctuations in  $I$  is conveniently represented with an intensity autocorrelation function  $g_2(\tau)$ :

$$g_2(\tau) = \frac{\langle I(t) \times I(t + \tau) \rangle}{\langle I(t) \rangle^2} \quad (4.6)$$

The correlations are usually presented graphically as  $g_2(\tau) - 1$  versus  $\tau$  (Fig. 4.3A); perfect correlation ( $\tau \rightarrow 0$ ) is here reported as 1 and no correlation ( $\tau \gg t$ ) is reported as 0. The time at which the correlation starts to significantly decay is an indication of the mean particle size.

The Siegert relation links  $g_2(\tau)$  to the so-called field autocorrelation function  $g_1(\tau)$ :

$$g_2(\tau) = 1 + \beta[g_1(\tau)]^2 \quad (4.7)$$

which can be rewritten as:

$$g_1(\tau) = \frac{1}{\sqrt{\beta}} \sqrt{g_2(\tau) - 1} \quad (4.8)$$

where  $\beta$  is an experimental constant. The autocorrelation functions are naturally functions of  $q$ , and for monodisperse, spherical particles  $g_1(\tau)$  is represented by a single exponential:

$$g_1(\tau) = e^{-q^2 D \tau} \quad (4.9)$$

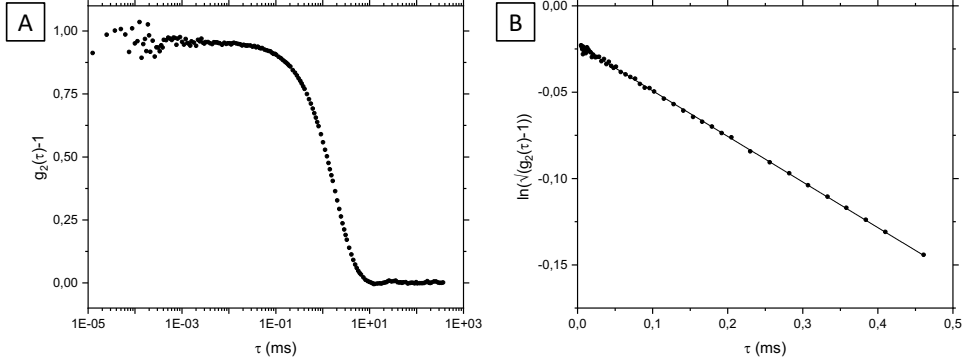


**Figure 4.3:** (A) Autocorrelation function  $g_2(\tau) - 1$  and (B) the corresponding  $\ln(\sqrt{g_2(\tau) - 1})$  versus  $\tau$  plot, from which the decay factor  $\Gamma$  can be obtained from the slope (solid line). The data was obtained with PNIPAM-co-AL microgels of  $R_H$  334 nm suspended in water. Laser wavelength 660 nm, detection angle  $90^\circ$ , temperature  $30^\circ\text{C}$ .

where  $D$  is the measured diffusion coefficient. Combing Eq. 4.8 and Eq. 4.9 gives:

$$\ln\sqrt{g_2(\tau) - 1} = \ln(\sqrt{B}) - \Gamma\tau \quad (4.10)$$

with the decay rate  $\Gamma$ :

$$\Gamma = Dq^2 \quad (4.11)$$

It follows from Eq. 4.10 that from a plot of  $\ln\sqrt{g_2(\tau) - 1}$  versus  $\tau$  (Fig. 4.3B),  $\Gamma$  can be obtained from the slope.  $D$  can then, in turn, be obtained through division by  $q^2$  according to Eq. 4.11. However, the preferred approach in the present thesis was to make a multi-angle measurement, determine  $\Gamma$  for each  $\theta$  and then plot  $\Gamma$  versus  $q^2$  (Eq. 4.11 and Fig. 4.4). In case of monodisperse spheres, a straight line with an intercept 0 and a slope corresponding to  $D$  can be fitted to the data points. A line that is not straight indicates that the sample is polydisperse.

For dilute samples in which the particles can diffuse freely and particle-particle interactions can be assumed negligible, it is straightforward to assume that  $D$  is equal to the self-diffusion coefficient. Knowing  $D$ , the hydrodynamic radius  $R_H$  can be calculated by applying the Stokes-Einstein equation (applicable to spheres):

$$D = \frac{k_B T}{6\pi\eta R_H} \quad (4.12)$$

where  $k_B$  is the Boltzmann constant,  $T$  is the temperature and  $\eta$  the solvent viscosity.

As mentioned above, Eq. 4.9 is valid only for monodisperse particles. To account for polydispersity, a number of methods are available for determining the size distribution from the experimentally obtained  $g_2(\tau) - 1$ . The so-called cumulant expansion

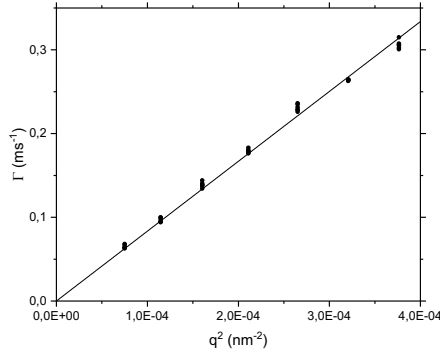


**Figure 4.4:**  $\Gamma$  obtained from a single exponential fit of acquired correlation functions, plotted versus  $q^2$ . The solid line represents a linear fit to the data points. The data was obtained with PNIPAM-co-AL microgels of  $R_H$  334 nm suspended in water. Laser wavelength 660 nm, temperature 30 °C.

method<sup>244</sup> is often used as a first step before more advanced analytical procedures, and involves a series expansion of  $g_1(\tau)$  given by:

$$\ln\sqrt{g_2(\tau) - 1} = \ln(A) - \Gamma\tau \quad (4.13a)$$

$$\ln\sqrt{g_2(\tau) - 1} = \ln(A) - \Gamma\tau + \frac{\mu_2}{2!}\tau^2 \quad (4.13b)$$

$$\ln\sqrt{g_2(\tau) - 1} = \ln(A) - \Gamma\tau + \frac{\mu_2}{2!}\tau^2 - \frac{\mu_3}{3!}\tau^3 \quad (4.13c)$$

Eq. 4.13a (the same as Eq. 4.10), 4.13b, 4.13c are known as the first, second and third order cumulative expansion, respectively. In the case of highly monodisperse samples,  $\ln\sqrt{g_2(\tau) - 1}$  versus  $\tau$  is a perfect straight line (Fig. 4.3B), the cumulant  $\Gamma$  is the same in all three cases and, finally,  $\mu_2$  and  $\mu_3$  are 0. With polydisperse samples, this is no longer the case.

The method of cumulants is suitable for samples that contain a single particle fraction that is not too polydisperse. In that case the second order term in the second cumulant expansion provides the width of the radius distribution according to:

$$width = \frac{\sqrt{\mu_2}}{\Gamma} R_H \quad (4.14)$$

The polydispersity index (PDI), defined as:

$$PDI = \frac{\mu_2}{\Gamma^2} \quad (4.15)$$

is another way of quantifying the distribution. According to this definition, perfectly monodisperse particles has a PDI of 0.

The third cumulative in the third order cumulative expansion, however typically not used, contain information about the symmetry ('skewness') of the distribution, while higher order terms are not very reliable because of noise in the data. As previously mentioned, the cumulant expansion method is suitable for monomodal systems, whereas it cannot be used with multimodal systems. For these more complex distributions an inverse Laplace transformation (ILT), such as Steven Provencher's CONTIN method, can be used, but will not be discussed in more detail here.

## 4.2 Confocal microscopy

Whereas data inferred from (light) scattering techniques are in Fourier space and averaged over large ensembles of system configurations, microscopy yields real-space data and probe local properties. The two techniques thus provide complementary information. The review below focuses on confocal microscopy and will be limited to its application to colloidal systems. As the length scales are in the order of the wavelength of the VIS light source, confocal microscopy is a powerful tool to obtain real-space and real-time information in colloidal systems. The use of confocal microscopy to study colloids is a relatively recent phenomena, and was fuelled by the discovery that monodisperse colloids display a phase behaviour that is much analogous to that seen in atomic systems<sup>8</sup>. Yoshida *et al.* were one of the first to study colloids with a confocal microscope when they in 1991 went deep into a sample of charged PS spheres to observe hexagonal ordering<sup>245</sup>. Extending the capability of the confocal microscope enabled van Blaaderen and Wiltzius to observe the colloidal glass phase in 1995<sup>246</sup>.

### 4.2.1 Principles of operation

Confocal microscopy, as first described by Minsky in 1957<sup>247</sup>, is a development from conventional wide-field optical microscopy whose major drawback is its limited resolution along the  $z$  axis. In confocal microscopy, in-depth discrimination and  $z$  axial resolution is tremendously improved by using one or more pinhole apertures (Fig. 4.5 shows a schematic illustration of an inverted confocal microscope) placed exactly at the conjugate focal plane to the imaged spot (hence the name confocal microscopy). This serves to prevent (most of the) out-of-focus light to reach the detector. The size of the pinhole determines the thickness of the optical slice from which light is collected by the detectors, and smaller pinhole diameters give thinner slices and higher  $z$ -axial resolution - however at a cost of signal intensity. The default pinhole setting is typically 1 Airy unit (AU), which give good balance between of out-of-focus light rejection and signal collection. The Airy unit is described in more detail below.



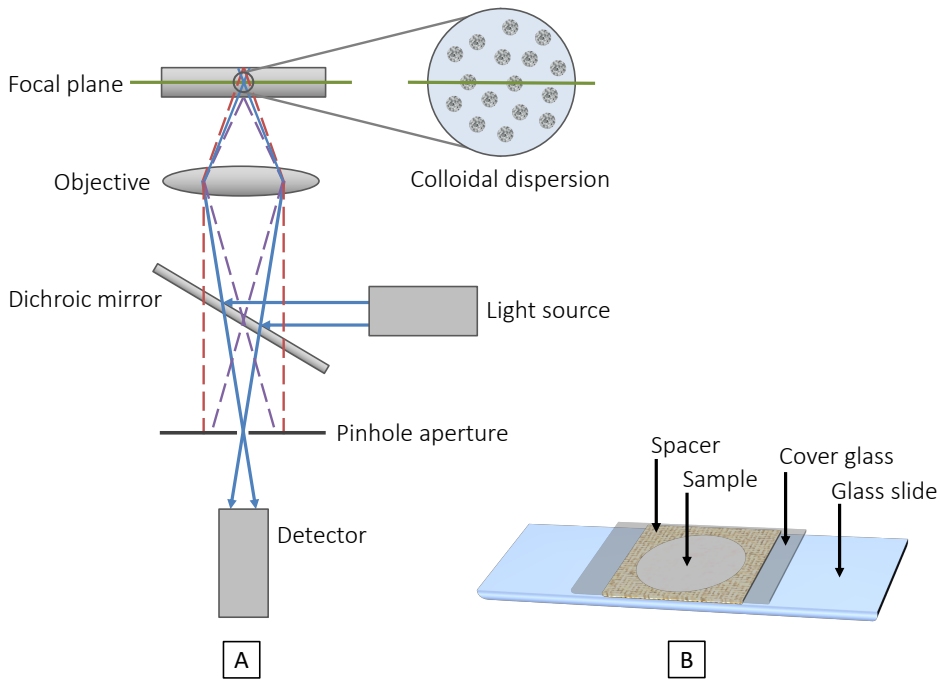


Figure 4.5: (A) Schematic illustration of the setup of an inverted laser scanning confocal microscope. In-focus and out-of-focus light are shown as solid and dotted lines, respectively. (B) Cartoon of a confocal microscopy preparation, with the sample kept between two glass slides separated by an imaging spacer.

The simplest form of a confocal microscope operates in bright-field mode and builds on transmission of light from a continuous light source that is focussed onto the sample using a set of mirrors and lenses. Confocal laser scanning microscopy (CLSM), a variation of confocal microscopy, instead builds on fluorescence and uses a focused, monochromatic laser beam to illuminate the sample in which the objects of interest have been labelled with fluorescent molecules whose excitation wavelength matches the wavelength of the laser. The laser beam is finely focussed to a (diffraction-limited) spot in the focal plane and  $x/y$  images are then constructed by laterally scanning the laser beam over the focal plane using electronically adjustable mirrors, so-called galvanometer mirrors, while measuring variations in fluorescence intensity. In this way, the image is built up pixel-by-pixel and the recorded 2D  $x/y$  image corresponds to an optical cross-section of the sample at that particular  $z$  depth. A dichroic mirror serves to separate the emitted light (fluorescence) from the incident beam, and is projected - through the pinhole - onto a sensitive photomultiplier tube (PMT) or other photon-counting detector. By stacking a series of  $x/y$  images recorded at different  $z$  heights within the sample - which are possible to record as the sample stage can be moved in the  $z$  direction - a 3D reconstruction of the sample can be made in an 'optical tomography' sort of way.

With appropriate acquisition settings (gain, contrast etc.), CLSM image series ( $x/y/z$  or  $x/y/t$ ) can be converted into quantitative data using image processing and analysis protocols that locate and track the particle centres, with Crocker and Grier's Interactive Data Language (IDL) routines<sup>248</sup> being the most well established feature finding algorithms. Hereby, radial distribution functions ( $g(r)$ ) and mean squared displacements (MSD) can be extracted to yield information about structure and dynamics, respectively. Whereas the working distance of the objective, the sample's optical density and variations in refractive index together set the limit for structural data acquisition along the  $z$  axis, which is typically limited to about 200  $\mu\text{m}$ , the rate at which the galvo mirrors can scan the entire  $x/y$  sample plane determines which type (how fast) of dynamic processes that can be studied. Quantitative image analysis will not be discussed any further here, as in the present thesis CLSM was mainly used to estimate - using visual inspection - the size and degree of polydispersity of microgels, oil droplets and colloidal molecules.

#### 4.2.2 Resolution, the Airy disc and the point spread function (PSF)

The so-called numerical aperture (NA) is a measure of an objective's light-gathering ability as only light within a certain maximum angle from the source can be captured. It is related to the maximum half-angle  $\theta$  at which light can still enter the objective:

$$NA = n \sin \theta \quad (4.16)$$

where  $n$  is the refractive index of the objective's working material (air, water or oil). Objectives of higher NA thus capture more light and are valued higher than those of lower NA.

Moreover, the NA determines the resolving power of the objective, the minimum distance between two point sources that allows for the two to still be interpreted as separate objects. As in conventional microscopy, the resolution of a confocal microscope is limited by the diffraction of light. The diffraction pattern arising from a point source illuminating a circular aperture has a strongly peaked intensity in the centre corresponding to the first order diffraction zone, the so-called Airy disc, which decays away from the centre in the  $x$  and  $y$  directions. To obtain a good image of a point source, the size of the pinhole should be set so that only the bright centre of the Airy disc is observed, and not the diffraction pattern around it. To achieve this, the thickness of the confocal slice should match the size of Airy disc. The size of the Airy disc  $r_A$  depends on the laser wavelength  $\lambda$ , on the refractive index of the objective's working material  $n$  and on its NA according to:

$$r_A = \frac{1.22\lambda n}{NA} \quad (4.17)$$

As mentioned above, the size of the pinhole is expressed in Airy units (AU), where 1 AU gives a slice thickness roughly equal to  $r_A$ .

Having defined the size of the Airy disc  $r_A$  generated by a point source, it follows that two such discs cannot be moved any closer than  $r_A$  before they start to overlap, and beyond this point they can no longer be resolved as separated point sources but appear as one. This diffraction-based fundamental resolution limit is known as the diffraction limit  $r_{DL}$  and is given by:

$$r_{DL} = \frac{\lambda}{2NA} \quad (4.18)$$

For a 1.4 NA objective and using a 488 nm light source,  $r_{DL}$  is theoretically about 175 nm, but due to non-ideality in the set-up the practical  $r_{DL}$  is rather in the range of 300-500 nm. Another measure for resolution is given by the Rayleigh criterion, which states that two points can be resolved if the intensity in between their maxima drops by 26%. This drop in intensity correspond to a distance known as the Rayleigh distance, which is about 1.4 times smaller for confocal compared to conventional microscopy. The smaller Rayleigh distance stems from a smaller size of the Airy disc. In addition, confocal microscopy offers greater image contrast, as the difference in intensity between the Airy disc center and the first ring maximum is larger and more intensity is confined in the central peak.

A final remark is that an image recorded by a confocal microscope is not an ideal representation of the object, but distortions occur in the  $x$ ,  $y$  and  $z$  directions. These distortions occur as a response of the imaging system to the point source, and is characterised by the so-called point spread function (PSF). The obtained image is a superposition, a convolution, of the PSF signal and of the real object signal. The PSF is not symmetrical but the distortions are all different. If the optical path is well aligned, the  $x$  and  $y$  distortions are similar, whereas in the  $z$  direction the distortion is typically larger. If the microscope's PSF is known, deconvolution with the PSF can be carried out to obtain the 'real' image. This generally works well in the  $x/y$  plane, but not so well in the  $z$  direction.

### 4.3 Zetametry

Colloids may carry surface charges due to, for example, ionisation of acidic or basic groups or may acquire charges as a result of adsorption of charged species such as ionic surfactants or polyions. These charges result in a repulsive electrical double layer inter-particle force (in the case of like particles), and so the magnitude of the charge is an indication of stability towards (homo)aggregation. The length scale for the range of the

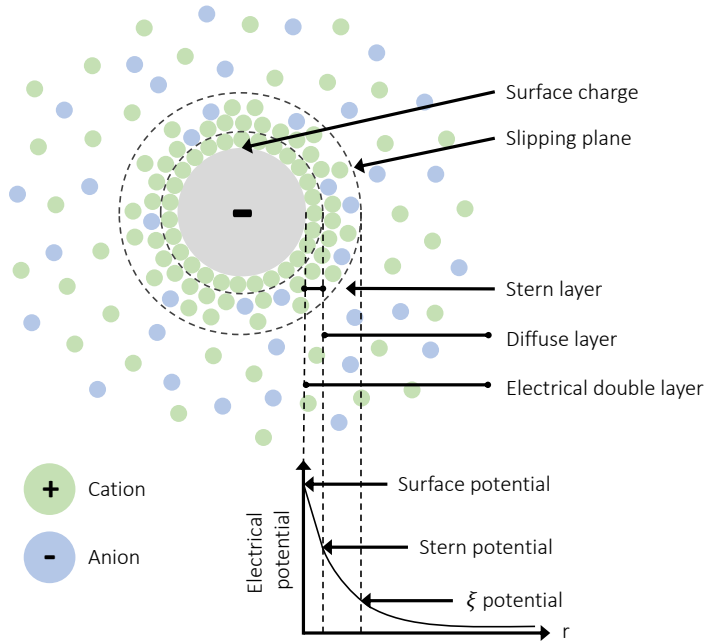


Figure 4.6: Schematic illustration of the counter ion distribution around a charged colloidal particle.

electrostatic repulsion is given by the so-called inverse Debye screening length  $\kappa^{-1}$ :

$$\kappa^{-1} = \sqrt{\frac{\epsilon_0 \epsilon_r k_B T}{\sum (z_i e)^2 c_i}} \quad (4.19)$$

where  $\epsilon_0$  is the vacuum dielectric permittivity,  $\epsilon_r$  the dielectric constant of the medium,  $k_B$  the Boltzmann constant,  $T$  the temperature,  $e$  the elementary charge,  $z_i$  the valency of ion  $i$  and  $c_i$  its concentration. For  $10^{-1}$  M 1:1 monovalent salt,  $\kappa^{-1}$  is about 0.96 nm and increases with decreasing ionic strength to 96 nm at  $10^{-5}$  M (considered deionised).

The presence of a net charge at the particle surface affects the distribution of ions in the surrounding interfacial region, with a build-up of counter ions close to the surface (Fig. 4.6). Strongly bound counter ions close to the surface make up the so-called Stern layer, outside of which less firmly associated ions reside in what is known as the diffuse layer. The two layers together make up the electrical double layer. Within the diffuse layer there is a boundary, referred to as the slipping plane, inside which the particle and its counter ions (and the solvent) form a stable entity. When the particle moves, the ions inside this boundary move with it. The potential at the slipping plane is known as the zeta potential  $\zeta$ , and is typically used as a measure of particle charge.

The zeta potential can be obtained from electrophoresis experiments, in which an electrical field is imposed across a colloidal suspension and the particle velocity  $v$  is meas-

ured. Under the influence of the electrical field, charged particles move in the direction of the electrode of opposite charge. When the field is applied the particles start to accelerate as they experience the electrical force. Almost instantaneously, however, as the electrical force becomes equal to the opposing viscous force, a steady state velocity is reached. In this equilibrium state,  $v$  can be estimated using Stoke's law:

$$\vec{v} = \frac{\vec{F}}{6\pi\eta R} \quad (4.20)$$

where  $\vec{F}$  is the external force experienced by the particle,  $\eta$  the viscosity of the medium and  $R$  the particle radius. For small fields,  $\vec{F}$  can be approximated by the electrical force  $\vec{E}$ . The electrophoretic mobility  $\mu$ , the primary value determined in an electrophoresis experiment, is defined as:

$$\mu = \frac{\vec{v}}{\vec{E}} \quad (4.21)$$

For a particle with charge  $q$  in a field  $\vec{E}$ , the force  $\vec{F}$  is equal to  $q\vec{E}$ . By combining Eq. 4.20 and Eq. 4.21,  $\mu$  can be expressed as:

$$\mu = \frac{q}{6\pi\eta R} \quad (4.22)$$

The equation above has limited use as it is impossible to know to what extent the particle moves independently of the surrounding counter ions. Instead, a sphere of radius  $R'$  and charge  $q'$ , corresponding to the particle and the ions within the slipping plane, is considered. The potential  $\Phi$  at  $R'$  is the aforementioned zeta potential  $\zeta$ . In a system where the Debye-Hückel theory applies,  $\Phi$  decreases exponentially with distance  $r$  from the particle surface:

$$\Phi(r) = \frac{q'}{4\pi\epsilon_0\epsilon_r} \frac{e^{-\kappa r}}{r} \frac{e^{\kappa R'}}{1 + \kappa R'} \quad (4.23)$$

If choosing  $r = R'$  and assuming  $\kappa R' \ll 1$  (small particles),  $\zeta$  is related to  $\mu$  through the Hückel equation:

$$\zeta = \frac{3}{2} \frac{\eta}{\epsilon_r\epsilon_0} \mu \quad (4.24)$$

If instead considering  $\kappa R' \gg 1$  (large particles), the relation between  $\mu$  and  $\zeta$  is given by the Helmholtz-Smoluchowski equation:

$$\zeta = \frac{\eta}{\epsilon_r\epsilon_0} \mu \quad (4.25)$$

Early methods, although still being used, to access electrophoretic mobility and zeta potential included microscopy techniques and manual tracking of particles. In contrast, in the present thesis a combination of electrophoresis and laser Doppler velocimetry

(LDV) was used, known as laser Doppler electrophoresis. In LDV, a (laser) light scattering experiment is performed on a sample subject to electrophoresis. The movement of particles due to the presence of the electrical field will cause the intensity of the detected light to fluctuate with a frequency proportional to the particle velocity. LDV makes use of the fact that the frequency of this fluctuation is equivalent to the Doppler shift between the incident and scattered light, and, using a digital signal processor to extract the characteristic frequencies, the electrophoretic mobility can be obtained from the frequency spectrum.

Whereas zeta potential is the common measure of particle charge, there is an ongoing debate about its meaning in the case of soft colloidal particles such as microgels, as the charges are not located solely at the surface and the particles show ion permeability. This is why the classical models for zeta potential fail for soft spheres, as was shown by Ohshima<sup>249</sup>. For this reason, microgel charge is reported as electrophoretic mobility in the present thesis, and not as zeta potential.

#### 4.4 Nuclear magnetic resonance (NMR) spectroscopy

Nuclear magnetic resonance (NMR) spectroscopy<sup>250–252</sup> makes use of the fact that some nuclei possess a so-called nuclear spin  $I$  that makes them behave like bar magnets; in the presence of an applied magnetic field the nuclear magnets can orient themselves in  $2I + 1$  ways. Nuclei with an odd mass number have spins of  $1/2$ ,  $3/2$ ,  $5/2$ , ..., etc. This short introduction to NMR will be limited to spin  $1/2$  nuclei such as  $^1\text{H}$ ,  $^{13}\text{C}$ ,  $^{15}\text{N}$ ,  $^{19}\text{F}$ ,  $^{29}\text{Si}$  and  $^{31}\text{P}$ .

When a magnetic field is applied, a spin  $1/2$  nucleus can take up either one of only two possible orientations, a low-energy spin aligned ( $\alpha$ ) or a high-energy spin opposed ( $\beta$ ) orientation with respect to the field (Fig. 4.7). The difference in energy  $\Delta E$  between the two is given by:

$$\Delta E = \frac{h\gamma B_0}{2\pi} \quad (4.26)$$

with  $h$  being Planck's constant,  $\gamma$  the gyromagnetic ratio, a measure of the strength of the nuclear magnets and is different for each nucleus, and  $B_0$  the strength of the applied magnetic field.  $\Delta E$  is very small but can be detected by NMR, and it follows from Eq. 4.26 that higher-field instruments are more sensitive than low-field ones.

The number of nuclei  $N$  in the  $\alpha$  and  $\beta$  states is determined by the Boltzmann distribution:

$$\frac{N_\beta}{N_\alpha} = e^{-\frac{\Delta E}{k_B T}} \quad (4.27)$$

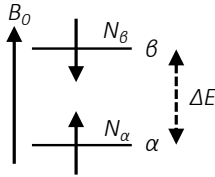


Figure 4.7: Spin  $1/2$  nuclei populate two spin states, a low-energy spin aligned ( $\alpha$ ) and a high-energy spin opposed ( $\beta$ ) one with respect to the applied magnetic field. The  $\alpha$  state is slightly more populated ( $N_\alpha > N_\beta$ ). Nuclei in the  $\alpha$  state can however be promoted to the  $\beta$  one by applying a rf pulse of frequency corresponding to the energy difference  $\Delta E$  between the two states.

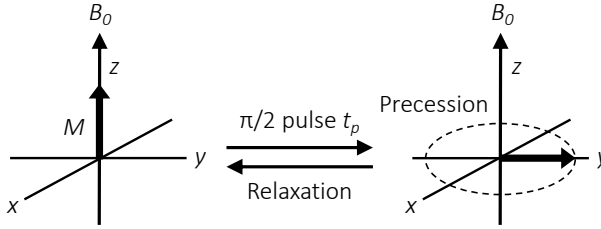


Figure 4.8: In an applied magnetic field, a  $\pi/2$  pulse serves to flip the magnetisation from the  $z$  direction to the  $xy$  plane. Its  $z$  orientation is recovered due to relaxation processes.

where  $k_B T$  is the thermal energy. The  $\alpha$  state is slightly more populated than the  $\beta$  one, but this distribution is changed if applying a radio-frequency (rf) signal matching the frequency at which the nuclei naturally precess in the magnetic field  $B_0$ . Such a rf signal serves to promote spin-flips, more  $\alpha$ -to- $\beta$  than  $\beta$ -to- $\alpha$  ones, and  $N_\beta$  consequently increases. The resonance frequency  $\nu$  is given by:

$$\nu = \frac{\gamma B_0}{2\pi} \quad (4.28)$$

and it follows that  $\nu$  is dependent on both the strength of the applied field and the identity of the nucleus.

In an NMR experiment the rf signal is applied as a single powerful pulse, covering the whole frequency range of the nucleus in question. The pulse generates an oscillating magnetic field  $B_1$  along the  $x$  axis, perpendicular to the applied magnetic field  $B_0$  (along the  $z$  axis). Because of the difference between  $N_\alpha$  and  $N_\beta$ , the sample has a net magnetisation  $M$  that is aligned with  $B_0$  (prior to the pulse). The effect of the pulse is to tip the magnetisation through an angle  $\Theta$  (Fig. 4.8).  $\Theta$  depends on the time of the pulse  $t_p$  according to:

$$\Theta = \gamma B_1 t_p \quad (4.29)$$

Typically,  $t_p$  is chosen so that  $\Theta$  is  $90^\circ$  (known as a  $\pi/2$  pulse), serving to tip the precession of the magnetisation to the  $xy$  plane. Magnetisation oriented along the  $y$  axis is detected by a receiver coil and the frequency of the oscillation ( $+y, 0, -y, 0, +y, \dots$ ,

etc.) is the difference between the NMR resonance frequency and the excitation frequency. The signal decays exponentially with time as relaxation gradually allows nuclei promoted to the  $\beta$  state to return to  $\alpha$ , and so the magnetisation tips back to the  $z$  orientation. The decaying signal is known as a free induction decay (FID). By Fourier transformation (FT) of the FID from the time domain to the frequency domain, the decaying signal is converted to a frequency signal. This yields a FT spectrum, with absorption against frequency, which is the useful output of an NMR experiment. As it is inconvenient to characterise the positions of the signals (peaks) in the FT spectrum by assigning them their absolute frequency, they are typically referenced with respect to a standard compound, almost always tetramethylsilane (TMS), and normalised by the operating frequency:

$$\delta = \frac{v_s (\text{Hz}) - v_{\text{TMS}} (\text{Hz})}{\text{operating frequency (MHz)}} \quad (4.30)$$

where  $\delta$  is known as the chemical shift.  $\delta$  is unit-less and is expressed in parts per million (p.p.m.) to make the scale more manageable. By definition, the standard has a  $\delta$  value of 0. By convention, FT spectra are plotted with  $\delta$  increasing from right to left.

So, what then can one learn from a NMR experiment and from a FT spectrum? NMR has undoubtedly been used the most by organic chemists, for determination of the structure of organic compounds. This is possible due to the fact that nuclei that are in different electronic environments come into resonance at different frequencies. This electronic non-equivalency has its locus in a phenomenon known as shielding. Shielding is caused by circulating electrons in the neighbourhood of each nucleus, generating small induced magnetic fields that oppose the applied field. The result is that the magnetic field at the nucleus is weaker than the applied field - the nucleus is shielded. Nuclei in different positions in a molecule are shielded to different extents due to differences in electron population, and thus come into resonance at different frequencies and so have their own characteristic chemical shifts in the FT spectrum. An example of a FT spectrum is shown in Fig. 4.9 where the signal from more shielded protons appear upfield, towards the right of the spectrum, and more deshielded protons appear downfield, towards the left. Besides characteristic frequencies, structure determination is aided by the fact that the adsorption of a signal in a ( $^1\text{H}$ ) FT spectrum is (generally) proportional to the number of nuclei coming into resonance at the frequency of that signal. This means that the area under the peaks is proportional to the number of protons being detected.



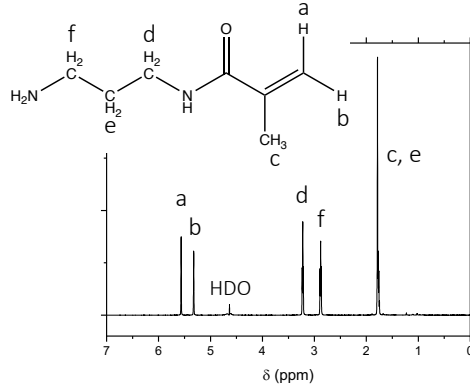


Figure 4.9: 600 MHz 1D  $^1\text{H}$  FT NMR spectrum of APMAA, recorded in  $\text{D}_2\text{O}$  at 25  $^\circ\text{C}$ .

## 4.5 Sedimentation methods

Sedimentation methods rely on observations of the settling of colloidal particles under the influence of gravity<sup>5</sup>. Here, the gravitational force  $G$  acting on a particle is resisted by a frictional force  $F$  due to the viscosity of the medium. The two forces are given by:

$$G = (\rho_p - \rho_m) \frac{4}{3} \pi R^3 g \quad (4.31)$$

and

$$F = 6\pi\eta Rv \quad (4.32)$$

respectively, with  $\rho_p$  the density of the particle,  $\rho_m$  the density of the medium,  $\eta$  the viscosity of the medium and  $g$  the gravitational acceleration. As shown by Stokes, when the two forces are balanced, the particle fall at a constant velocity, termed the sedimentation velocity  $v$ . For a non-deformable, smooth, spherical particle sedimenting under Stokes conditions,  $v$  is proportional to the square of the particle radius  $R$  according to:

$$v = \frac{2(\rho_p - \rho_m)gR^2}{9\eta} \quad (4.33)$$

For colloids, Earth's gravitational force is typically not strong enough to induce sedimentation in reasonable time, but a drastic improvement in rate can be achieved with (ultra)centrifugation.

It follows from Eq. 4.33 that  $R$  can be obtained by measuring  $v$ . In practice, however, one measures the time  $t$  required for the particles to fall a known distance  $h$ . Besides being used for analytical purposes (i.e. to assess  $R$  distributions) (Section 4.5.1), sedimentation methods can also be used for preparative purposes where the goal is to separate and harvest one or several particle populations within a sample.

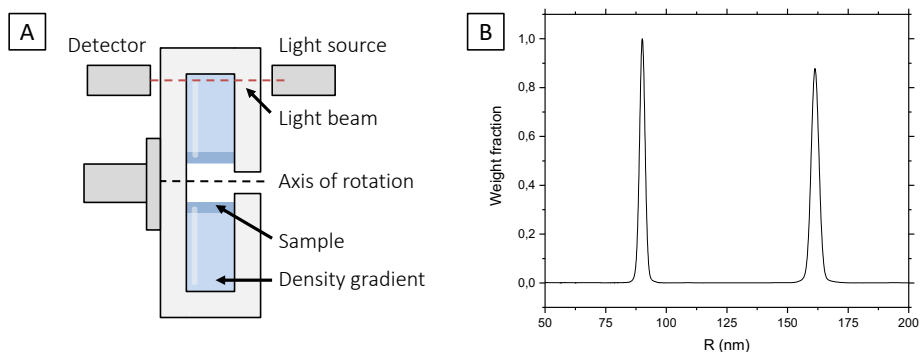


Figure 4.10: (A) Schematic cross sectional view of an analytical centrifuge disc. (B) Analytical centrifugal sedimentation trace recorded for a binary mixture of PS/PNIPAM composite particles (2-8 wt% sucrose, 24000 rpm).

### 4.5.1 Analytical ultracentrifugation (AUC)

Analytical ultracentrifugation (AUC)<sup>253–255</sup> is a sedimentation method used to assess particle sizes and particle size distributions. The  $v \propto R^2$  relationship (Eq. 4.33) ensures that particles differing in size only by a few percent still sediment at significantly different velocities to be accurately resolved as distinct populations.

Analytical centrifugation run with the same principles as (preparative) density gradient centrifugation. In the analytical centrifuge used in the present thesis, particles are injected at the centre of an optically clear, rotating disc containing a density gradient made from layered sucrose solutions of increasing density towards the rim of the disc (Fig. 4.10A). The purpose of the gradient is to counteract the effect of a higher apparent density in the sample due to the presence of particles and to thereby suppress streaming. During sedimentation, a sample containing a mixture of particles of narrow sizes separates into distinct, narrow bands as the different-sized particles possess different sedimentation velocities. At the rim of the disc, an absorbance detector is located that detects the particles as they pass. When particles pass the detector, the intensity of the detector light beam is attenuated due to scattering and absorption by the particles. This reduces the voltage produced by the detector and a software converts this voltage signal to an absorption value. Based on the absorption value, and accounting for elapsed time and the efficiency of light scattering by the particles, a particle size distribution - weight versus size - is generated (Fig. 4.10B). The degree of accuracy in the particle size determination depends on assigning accurate values to a number of key parameters, most importantly particle refractive index, absorption (a constant that describes the rate at which light intensity falls with distance as it passes through the particle) and non-sphericity, which govern the particles' light scattering efficiency, or, the so-called effective light scattering cross section  $Q_{net}$ . Based on  $Q_{net}$  and using Mie theory, the raw data (absorption versus time) is converted into a particle size distribution (weight

versus size).

The conditions under which well-resolved peaks are observed in analytical centrifuge can be translated into a preparative rate-zonal centrifugation, as has been shown elsewhere<sup>88,183,186,222</sup>. Here, a narrow sample zone is applied on top of a density gradient within a centrifugation tube. During centrifugation, which should be shorter than the time required for complete sedimentation, particles of the same size fall the same distance in the tube, resulting in the formation of distinct bands or zones that can be harvested.

## 4.6 Microfluidics

Microfluidics<sup>256–259</sup> deals with the behaviour, precise control and manipulation of fluids constrained to networks of channels of, at least in one dimension, sub-millimetre size. It is a relatively young research area, often regarded as being born with the groundbreaking publication by Manz *et al.* from 1990, where a high-pressure liquid chromatography column was integrated onto a small silicon chip<sup>260</sup>. Today, microfluidics find applications in various areas outside of analytical chemistry, such as small-molecule<sup>261,262</sup> and colloidal synthesis<sup>263</sup>, biology<sup>264,265</sup>, drug discovery<sup>266,267</sup> and point-of-care (PoC) sensing and diagnostics<sup>268,269</sup>. Benefits of microfluidics include cheap and easy device fabrication, and, due to the small length scales, portability, low liquid volume consumption and short processing time.

### 4.6.1 Fluidics at the microscale

Fluids behave very differently on the micrometer scale compared to the length scales that we are used to from our every day life. As microfluidics devices are miniaturised, the surface area-to-volume ratio is high and surface forces dominate. One effect of these surface forces is the occurrence of laminar flow, characterised by being ordered and predictable, in contrast to turbulent flow that is chaotic and unpredictable. Turbulent flow occurs, for instance, when water is poured into a glass. The two regimes (laminar and turbulent) are associated with different so-called Reynolds number  $Re$ <sup>270</sup>, which reflects the relative importance of inertial and viscous forces.  $Re$  is, for cylindrical channels, given by:

$$Re = \frac{\rho v_0 L_0}{\eta} \quad (4.34)$$

with  $\rho$  and  $\eta$  the fluid density and viscosity, respectively,  $v_0$  the characteristic velocity and  $L_0$  the characteristic length scale.  $L_0$  is often equated with the hydraulic diameter

$D_H$ :

$$D_H = 4 \frac{A}{P_w} \quad (4.35)$$

where  $A$  is the cross-sectional area of the flow and  $P_w$  is the wetted perimeter of the cross-section. Laminar flow is typically present, in cylindrical channels, for  $Re \lesssim 2300$ , and the viscous forces are dominating. However, with the small length scales present in microfluidics devices, typically  $Re < 1$ .

The word ‘laminar’ stems from Latin, and translates to ‘thin sheet of material’. This is a good description of laminar flow, where the fluid can be regarded as consisting of non-mixing parallel flows, laminae. However, even under conditions of laminar flow, due to (random) diffusion the different laminae eventually mix to give a uniform, radial concentration profile. Typically, considering the relatively short processing times associated with microfluidics, diffusion only starts to become significant for particles below  $1 \mu\text{m}$ . In most cases, diffusion is an unwanted phenomena, as it reduces the ability to predict a particle’s position in the device at a certain time. For microfluidic particle-sorting (Section 4.6.4), diffusion acts to decrease sorting efficiency. Diffusion can however be reduced by increasing viscosity or decreasing the temperature (Eq. 4.12), or by speeding up the flow rate (within reasonable limits). The relative importance of of advective and diffusive transport is given by the dimensionless Péclet number  $Pe$ :

$$Pe = \frac{Lv}{D} \quad (4.36)$$

where  $D$  is the diffusion coefficient, and  $L$  and  $v$  the characteristic length and velocity of the system, respectively.

An important feature of laminar flow is its parabolic velocity profile. The parabolic profile develops due to the viscous drag exerted by the channel walls, close to which the flow can be regarded as (essentially) static. This is known as the non-slip boundary condition. Instead, the maximum velocity is found in the centre of the channel.

## 4.6.2 Microfluidic device fabrication

The microfluidic devices used in the present thesis were fabricated using the soft lithography technique<sup>271–273</sup>, widely popular due to its rapid turn-around time and low cost. In soft lithography, an elastomeric stamp with patterned relief structures on its surface is used to transfer these structures onto another substrate. The stamp, first of all, is manufactured by ultraviolet (UV) lithography (Fig. 4.11A) and starts with the coating of a silicon wafer with SU-8, an epoxy-based negative photoresist that solidifies through crosslinking when exposed to UV light. In order to solidify only selected parts of the

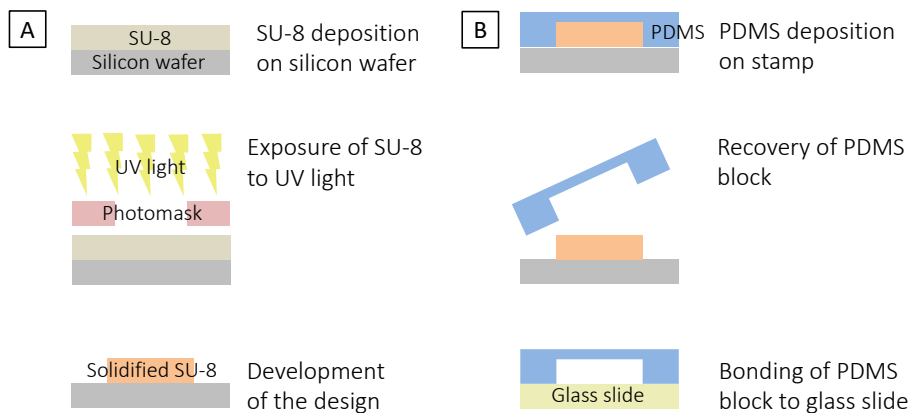


Figure 4.11: Sketch of microfluidic device fabrication. (A) A silicon wafer-supported stamp with patterned SU-8 relief structures is prepared by UV lithography. (B) By soft lithography, the pattern is replicated in PDMS. Bonding of the PDMS block onto a glass substrate yields the desired microfluidics device.

SU-8, a photomask is used that shields parts of the SU-8 from the UV light. The non-UV-exposed, non-crosslinked SU-8 can then be removed through dissolution - a step known as development - and a stamp, or replica moulding master, with the desired design is obtained.

By negative stamping (Fig. 4.11B), the SU-8 structures on the stamp are replicated in PDMS, a widely used silicon-based polymer offering good thermal stability, optical transparency, gas permeability and various surface modification options. First, the stamp is treated with a fluorinated silane in order to ensure easy lift-off of PDMS downstream in the process. A degassed mixture of pre-polymer (Sylgard 184) and curing agent is then poured over the SU-8 stamp, and cured at elevated temperature. After recovery of the PDMS block following curing, holes for inlets and outlets are punched. Finally, the channels are sealed by transferring the block to a glass cover slip. The PDMS and the glass, both extensively cleaned beforehand, are strongly bond together by oxygen plasma treatment, which is the last step of the device fabrication. The device is now ready to be used, but is typically first subjected to some kind of surface treatment that depends on the application. In the present thesis, droplet microfluidics devices (Section 4.6.3) were rendered hydrophobic through treatment with fluorinated silanes, whereas the deterministic lateral displacement (DLD) devices (Section 4.6.4) were functionalised with a polyethylene glycol (PEG) silane to minimise particle sticking. Including the time spent on microfluidics device design, typically two days, going from idea to a ready-to-use device takes about five days.

### 4.6.3 Droplet microfluidics

Droplet microfluidics<sup>274-278</sup> concerns the manipulation of two-phase flows in microfluidic channels in order to, with high speed (100 Hz-100 kHz) and precise control over size and content, form femto-to-picoliter-sized emulsion droplets, ‘mini-labs’, to which molecules, particles or cells are confined. While conventional methods for emulsion formation - typically involving shearing of two immiscible liquids - generally results in wide droplet size distributions, droplet microfluidics allows for production of droplets of high monodispersity. Usually, the coefficient of variation ( $CV$ ), the standard deviation of the diameter over the arithmetic mean, is below 5%. Droplet microfluidics has for this reason found applications in areas where emulsion monodispersity is important, such as small-molecule and particle synthesis, drug delivery and biosensing<sup>276,279,280</sup>. For instance, in the present thesis and inspired by earlier work<sup>88,195</sup>, we turned to droplet microfluidics to be able to compartmentalise small numbers of microgel building blocks inside monodisperse water droplets (Section 5.5). Here, droplet monodispersity serves to reduce the distribution of the number of microgels per water droplet, in a subsequent step destined to form colloidal molecules through evaporation of the water. Still inevitably following a statistical Poisson distribution<sup>192</sup>, the monodispersity of the colloidal molecules is considerably improved compared to the conventional comminution method<sup>88,195</sup>.

As in other areas of fluid dynamics, droplet microfluidics can be characterised by a set of dimensionless parameters, useful for the understanding of the relative importance of different effects and forces<sup>281</sup>. The so-called capillary number  $Ca$ , for instance, compares viscous stresses to interfacial tension and can be written as:

$$Ca = \frac{\eta v}{\gamma} \quad (4.37)$$

with  $\eta$  the viscosity,  $\gamma$  the interfacial tension and  $v$  the characteristic velocity. If droplets are formed under conditions of low  $Ca$ , the interfacial tension exceeds the viscous stresses, with the result that spherical droplets are formed in order to minimise the surface-to-volume ratio. In case viscous forces dominate, droplets are deformed.

Together with the  $Ca$ , two additional dimensionless parameters, namely the viscosity ratio  $\sigma$  and the flow rate ratio  $\phi$ , govern the mode of droplet formation (discussed in more detail below). These two parameters are given by

$$\sigma = \frac{\eta_d}{\eta_c} \quad (4.38)$$

and

$$\phi = \frac{\Phi_d}{\Phi_c} \quad (4.39)$$

respectively, where the subscripts  $d$  and  $c$  refers to dispersed and continuous phase, respectively.

Whether a water-in-oil (W/O) or an oil-in-water (O/W) emulsion forms in a microfluidics device depends, foremost, on the relative channel wetting ability of the two liquid phases. If the device walls are hydrophobic a W/O emulsion is formed, and if hydrophilic a O/W one. Measures typically have to be undertaken in order to suppress adhesion of the dispersed phase to the channel walls, which can be accomplished through various coatings. Once formed, the stability of the droplets can be enhanced using surfactants that due to their amphiphilic nature adsorbs to the liquid-liquid interface and serves to decrease the interfacial tension, thereby reducing the droplets' tendency to coalesce.

In droplet generation, besides the high monodispersity that was touched upon above, high droplet generation frequency together with ability to tune the frequency as well as the droplet size, is desired. Whereas a multitude of different droplet generation techniques exist, they will not all be reviewed in the present thesis. However, an important distinction is made between active and passive droplet generation<sup>282</sup>. Whereas the former relies on external actuation - via, for instance, magnetic, electric or centrifugal fields, or by manipulation of viscosities, flow velocities, interfacial tension or channel wettability - to form droplets by inducing interfacial instabilities, the latter relies solely on hydrodynamic forces. Despite the high versatility of active devices, (flow focussing) passive droplet generation was the method of choice for the present thesis due to its simpler operation, more stable performance, higher droplet generation frequency and greater droplet monodispersity.

In passive droplet generation, the generation frequency is controlled through the dispersed-to-continuous phase flow velocity, which also, together with the channel width, determine droplet size. Whereas a plethora of different device configurations for droplet generation exist<sup>283-287</sup>, a so-called flow focussing device<sup>288-291</sup> was used in the present thesis. Here, droplets are formed as the two phases are forced through a narrow constriction where continuous phase is introduced from two side channels and the dispersed phase through a central one (Fig. 4.12). This results in a symmetric shearing of the dispersed phase liquid thread, enabling stable generation of small, monodisperse droplets at high frequencies.

In flow focussing droplet generation, several so-called droplet generation modes are possible, and which one that is in play depends on factors such as device geometry, interfacial tension, fluid viscosities and channel wetting. In the present thesis, droplets were generated in squeezing mode. Here, the liquid thread of the dispersed phase liquid blocks the constriction for the continuous phase. This leads to a pressure build-up upstream, which results in the droplet being squeezed and deformed until the point where

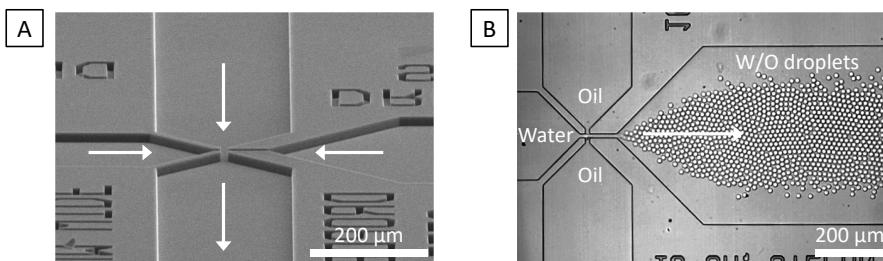


Figure 4.12: (A) Scanning electron microscopy (SEM) micrograph of the 10  $\mu\text{m}$  nozzle size constriction in the flow focussing device used in the present paper. (B) With the flow focussing geometry, monodisperse ( $CV$  1.9%) W/O droplets form in squeezing mode. The aqueous phase is water and the oil phase is HFE-7500 supplemented with 2 wt% Pico-Surf1 surfactant.

it is finally pinched off. Squeezing mode is also known as the geometry-controlled mode, as the droplet size is to a large extent determined by the geometry of the device.

#### 4.6.4 Deterministic lateral displacement (DLD)

Deterministic lateral displacement (DLD) is one of many microfluidics-based particle-sorting techniques<sup>292–295</sup>, and is used for sorting of particles on the basis of their size. When first introduced, it displayed an unprecedented resolution of  $\sim 10$  nm for PS particles<sup>296</sup>. It can be applied either for analytical purposes where quantitative or qualitative information about the sample is given as a result of the separation, or for preparative purposes where the goal is to purify and collect one or more particle populations in the sample. This thesis is concerned with the latter, which was used for the isolation of colloidal molecules by removal of single microgel particles.

In microfluidic particle-sorting techniques, as in droplet microfluidics, a distinction is made between passive and active methods. Whereas active methods require external force fields - for instance ultrasonic standing waves<sup>297</sup>, and electric<sup>298,299</sup> and magnetic fields<sup>300</sup> - to accomplish sorting, passive methods, such as DLD, rely solely on channel geometry and hydrodynamic forces. An additional distinction is made between bulk sorting and continuous sorting. In bulk sorting, in a chromatography-like manner different particle populations get separated along the axis of travel and arrive at the outlet reservoir at different points in time. As bulk sorting limits sample injection to a single point in time, continuous sorting is more attractive. Here, the sample is continuously injected at a certain lateral point in the device and as the particles are transported with the flow they are subjected to secondary force at an angle, typically perpendicular, to the flow direction that causes them to deflect - to be laterally displaced - from the direction of flow. As different particles respond differently to the force, they can be collected from different outlets. The outlets can be laterally positioned so to capture a certain



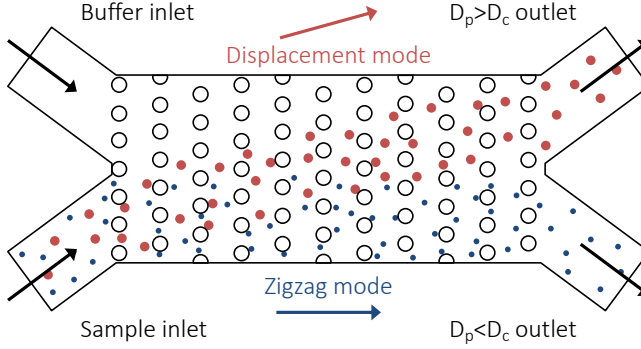


**Figure 4.13:** Sketch of a DLD device in which small ( $D_p < D_c$ , blue) and large particles ( $D_p > D_c$ , red) are separated due to interactions with an array of perpendicular posts (black) and be collected from different outlet reservoirs. The small particles travel (overall) in the direction of the fluid flow (zigzag mode) and exit the device at the same lateral position as where they entered. The large particles, on the other hand, are laterally displaced and travel at an angle with respect to the fluid flow (displacement mode).

particle population. This is enabled by the deterministic nature of the separation, i.e. it does not involve any random processes but relies on laminar flow and the consequent order and predictability of the behaviour of the fluid.

The deflection from the direction of flow in DLD sorting is due to hydrodynamic and steric interactions between the particles and a symmetrical array of vertically standing, typically cylindrical, obstacles referred to as posts (Fig. 4.13). The interactions with the post array cause particles larger than a certain cut-off size, known as the critical diameter  $D_c$ , to travel at an angle with respect to the fluid flow. This mode of travelling is called displacement mode. On the other hand, particles smaller in size than  $D_c$  travel in the overall direction of the flow, in so-called zigzag mode.

A DLD device's  $D_c$  is determined by several parameters of the post array (Fig. 4.14). These parameters include the centre-to-centre distance between two neighbouring posts  $\lambda$ , the post diameter  $D_{post}$ , the so-called row-shift  $\Delta\lambda$ , which is the distance by which every row in the array is shifted laterally with respect to the previous one, and period of the array  $N$  given by:

$$N = \frac{\lambda}{\Delta\lambda} \quad (4.40)$$

In the place of  $D_{post}$ , the distance, or gap, between two neighbouring posts  $G$ , defined as:

$$G = \lambda - D_{post} \quad (4.41)$$

is typically stated.

In the DLD device, the flow can be divided into multiple laminae of the same volumetric flow rate (Fig. 4.15). The width of a single lamina is typically chosen so that it transports  $\Phi = \Phi_{gap}/N$ , with  $\Phi_{gap}$  the total volumetric flow rate through a gap between

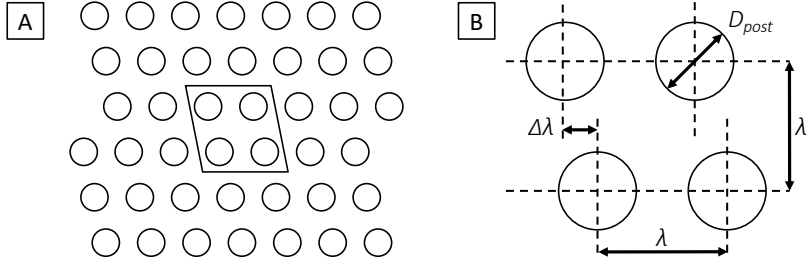


Figure 4.14: (A) A rhombic unit cell highlighted in an array of posts in a DLD device. (A) The critical diameter  $D_c$  is determined by, most importantly, the post diameter  $D_{post}$ , the post-post centre-to-centre distance  $\lambda$ , the row shift  $\Delta\lambda$  and the gap given by  $G = \lambda - D_{post}$ .

two neighbouring posts. Due to the parabolic flow profile, the central laminae between two posts are narrower than the ones closer to the posts. For each row in the device, the lamina is diverted, and not until after  $N$  rows the lamina is back at its original relative position. In this environment, the decision point for the size-based particle separation occurs is the gap. At this position, a particle smaller than  $D_c$  (that is  $D_p < D_c$ ) resides within its original lamina whereas for  $D_p > D_c$  the particle is pushed into the neighbouring one. Here,  $D_p < D_c$  holds true if  $D_p < 2\beta_1$ , where  $\beta_1$  is the width of the lamina in which the particle resides at the gap. If  $D_p > 2\beta_1$ , lateral displacement occurs. This decision is repeated at each gap (each row), resulting in lateral displacement of particles larger in size than  $D_c$ . It follows that  $D_c = 2\beta_1$ . The following empirically deduced formula<sup>301</sup> has been extensively used in order to estimate DLD device  $D_c$ s:

$$D_c = 1.4GN^{-0.48} \quad (4.42)$$

Analytical solutions to the critical diameter, including corrections for the influence of post shape and device geometry on the flow profile, exist but do not agree as well with experimental separation results as the empirical formula does. This is believed to be related to flow perturbation in the gap, induced by the presence of particles. As some factors that effect  $D_c$ , such as post shape and device depth, are left out in Eq. 4.42 computational fluid dynamic (CFD) simulations can be used as an additional tool.

Whereas DLD devices with a single  $D_c$  are able to distinguish only between particles smaller than or larger than this  $D_c$  (bimodal separation), devices with multiple critical diameters in series, referred to as sections, are able to separate more complex mixtures. The presence of multiple sections allows for sorting into additional bins, with  $n$  sections enabling sorting into up to  $n + 1$  bins. Multiple sections can be achieved in different ways. According to Eq. 4.42,  $D_c$  can be altered by varying either the gap  $G$  or the period  $N$  along the device. As a smaller  $G$  can potentially lead to clogging, it is more common to alter  $N$ . As the deflection angle decreases with decreasing  $D_c$  (and  $N$ ), sections of low  $D_c$  should typically occupy a major part of the device.

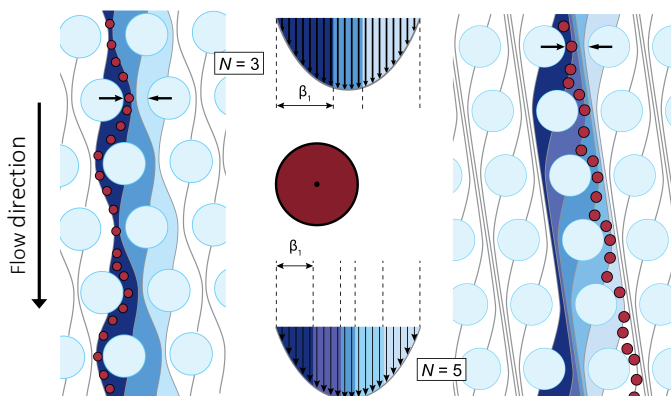


Figure 4.15: (Left) A colloidal particle (maroon) of size  $D_p < 2\beta_1$  resides within the same lamina as it travels through the DLD device. (Right) If instead  $D_p > 2\beta_1$ , the colloid is, at each row, pushed into the neighbouring lamina and so travels in displacement mode. Figure courtesy of S. H. Holm.

In the above description of the basis of separation in DLD, the particles trajectories are often thought of in terms of pure zigzag or pure displacement mode, which is the ideal case. This is a simplified model, as several factors can affect the particle trajectories as the particles travel the device. The two perhaps most important factors are particle softness and shape, which is highly relevant for the separation of soft and anisotropic microgel-based colloidal molecules. Whereas softness allows for deformation under shear forces that leads to a smaller effective particle size, anisotropy is problematic since the particle orientation at the decision point in each row will determine whether zigzag or displacement mode is in play up until the next decision point. An additional problem occurs if the particles have affinity for, and stick to, the walls and posts of the device. This, first of all, results in a larger effective post size, and, secondly, in clogging of the device. Finally, in order to suppress the effects of particle-particle interactions, and in order to achieve high throughput, the sample cannot be too concentrated.

Particle properties, such as shape, are not alone responsible for inducing mixed separation modes (zigzag and displacement simultaneously) and thereby decrease the separation efficiency in DLD. Mixed modes can also stem from properties of the device, often related to fabrication limitations that may introduce defects. These defects can be introduced, for instance, during photolithography, in case of non-uniform illumination. The overexposure of some areas and underexposure of others can cause the post size and the critical diameter to vary. Related problems also occur if the posts are not completely vertical.

*#IAmAScientistBecause I like having a job that lets me act and feel superior to people who are much better paid in more stable careers.*

- @NIH\_Bear on Twitter

## 5 | Summary of main results

### Contents

|     |  |    |
|-----|--|----|
| 5.1 | Short recapitulation: The knowledge gap and the solution . . . . .                 | 66 |
| 5.2 | Microgels - ideal building blocks . . . . .  | 67 |
| 5.3 | Some general remarks on the preparation of colloidal molecules . . . . .           | 67 |
| 5.4 | Interfacial tension-driven anchoring to small emulsion oil droplets . . . . .      | 68 |
| 5.5 | Evaporation-induced assembly from W/O emulsions . . . . .                          | 79 |
| 5.6 | Electrostatic attraction-driven assembly of oppositely charged microgels . . . . . | 84 |

In this chapter, the main results of the papers are summarised, with emphasis on design and development of methods for obtaining temperature-responsive colloidal molecules from soft microgel spheres. In addition, a few ongoing research projects are briefly described.

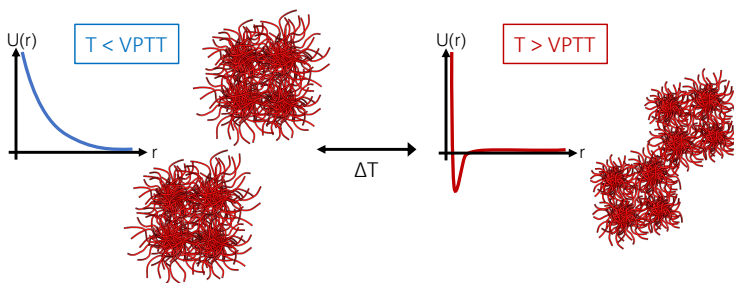


Figure 5.1: The use of temperature-responsive microgels as building blocks allows for tuning of the volume fraction and interactions of the corresponding colloidal molecules with temperature.

## 5.1 Short recapitulation: The knowledge gap and the solution

When colloidal molecules first appeared on the scientific scene - now more than a decade ago - a huge interest was sparked in the scientific community as scientists immediately began to imagine previously inaccessible colloidal structures as feasible targets for self-assembly, thus allowing access to advanced, for instance optically active, materials. However, as is evident from the astonishing lack of scientific publications in the area - with one notable exception involving DNA-mediated assembly<sup>104</sup> - the success in experimentally realising such assemblies has been severely hampered due to the non-spherical shape of the colloidal molecules, which facilitates trapping in glassy or amorphous states where positional and orientational defects cannot easily heal. This puts greater demands on our ability to control and tune the inter-particle interactions during assembly, which is difficult with the charged hard sphere colloidal molecules seen so far. With this thesis, we aim to relieve this issue by developing methods for preparing microgel-based colloidal molecules that allow for convenient tuning of the interactions - as well as of the volume fraction - using temperature as an external stimulus (Fig. 5.1).

To the best of our knowledge, there are only two published reports on the synthesis of colloidal molecules from microgels, both from the same research group at Nankai University and published in 2016 and 2018, respectively<sup>222,302</sup>. In both cases, colloidal molecules were elegantly obtained from a binary crystal, where one type of microgel was surrounded exclusively by the second type and click chemistry<sup>303</sup> was implemented to bind the two together. The drawback of this method is, however, its complexity, as binary crystals are notoriously difficult to make. Moreover, the number of microgels per cluster, which is determined by the arrangements of the microgels in the crystal, cannot be easily tuned without completely altering the crystal structure.

## 5.2 Microgels - ideal building blocks

Besides their temperature-responsiveness, microgels serve as ideal building blocks for several reasons. First, their colloidal size allows for them to be studied using a number of experimental techniques such as light, X-ray and neutron scattering, and confocal and electron microscopy. Second, microgels are nearly density-matched with water, which means that sedimentation effects are small. Third, microgels are easy and cheap to prepare in large quantities and with high monodispersity, and their chemical composition and properties can be conveniently adjusted through incorporation of different co-monomers during synthesis.

## 5.3 Some general remarks on the preparation of colloidal molecules

This thesis features three fundamentally different methods for assembling spherical, temperature-responsive microgels into well-defined colloidal molecule-like clusters with a small number of interaction sites. Common for all three of them are however a few criteria that we tried to fulfil during method design and development and which are summarised in the following bullet list. **The method should...**

- **...be simple.** The method should be as simple as possible, making it readily accessible to a wide range of scientists. It should be completed in just a few simple steps, and should involve only commercially available chemicals and easily accessible equipment.
- **...be reproducible.** The method should be robust, reliable and reproducible.
- **...be up-scalable.** The method should be of bulk character and/or be easily up-scalable to yield a large amount of colloidal molecules.
- **...yield discrete colloidal molecules.** The method should yield discrete, stable colloidal molecules and any aggregation should be suppressed.
- **...yield colloidal molecules of narrow size distribution.** The method should yield monodisperse colloidal molecules with respect to the number of microgels per colloidal molecule. Monodispersity is a necessity for any subsequent self-assembly to successfully result in a periodic structure.

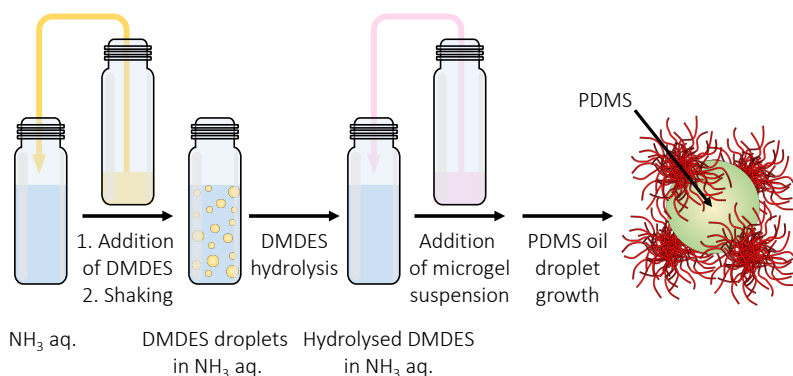


Figure 5.2: Schematic overview of the in situ microgel-Pickering emulsion method for colloidal molecule preparation.

- **...yield regular colloidal molecules.** The method should result in all colloidal molecules consisting of a certain number of microgels having the same, regular shape. Monodispersity with respect to shape (and size) is essential for the success of any subsequent self-assembly.
- **...offer control over size/valency.** The method should offer tunability and control with respect to the number of microgels per cluster. Considering each microgel an interaction site, this directly translates into valency which governs the number of neighbours in a self-assembling structure.

## 5.4 Interfacial tension-driven anchoring to small emulsion oil droplets

In Paper I and Paper II, we introduce a new route to microgel-based colloidal molecules where the well-documented interfacial activity of microgels<sup>161–167</sup> is exploited. Here, we use monodisperse PDMS oil mini-emulsion droplets - prepared via ammonia-catalysed hydrolysis and condensation of DMEDES monomer<sup>233</sup> - as anchors to which the microgels adsorb to lower the interfacial tension and the total free energy of the system.

The key findings presented in Paper I and Paper II are summarised in the following two sections. The results presented in Paper I provide a proof of concept for the potential of a so-called in situ microgel-Pickering emulsion method for the preparation of colloidal molecule-like microgel-decorated oil droplets (Fig. 5.2). In Paper II, the method is refined in order to yield the target colloidal molecules, with well-defined microgel interaction sites, and is also extended to the preparation of patchy colloidal molecules.

**Table 5.1:** Summary of the microgel systems used in Paper 1. All of them had a BIS crosslinker content of 5 mol%.

| Microgel          | Polymer | Dye         | $R_H$ (20/50 °C)<br>[nm] | $\mu$ (20/50 °C)<br>[ $\cdot 10^{-8} \text{ m}^2 \text{ V}^{-1} \text{ s}^{-1}$ ] |
|-------------------|---------|-------------|--------------------------|---|
| MG <sub>1</sub>   | PNIPAM  | Rhodamine   | 298 / 186                | +0.53 / +1.95   |
| MG <sub>1,2</sub> | PNIPAM  | Rhodamine   | 319 / 211                | +0.58 / +2.99   |
| MG <sub>2</sub>   | PNIPAM  | Fluorescein | 448 / 277                | +0.82 / +3.25   |
| MG <sub>3</sub>   | PNIPAM  | Rhodamine   | 244 / 154                | -1.56 / -3.79   |
| MG <sub>4</sub>   | PNIPAM  | Fluorescein | 494 / 317                | +0.72 / +1.93   |

#### 5.4.1 Main results of Paper 1

In Paper 1, five different temperature-responsive microgels were used as building blocks, all of them crosslinked using 5 mol% BIS but different with respect to polymer identity, fluorescent label, size and charge (Table. 5.1). All of the microgels were weakly charged as no co-monomers were incorporated; their charges originated from initiator residuals alone (KPS for the anionic microgel and V50 for the cationic ones). Their temperature-responsive behaviour was reflected in a decrease in  $R_H$  measured by DLS as well as in an increase of the magnitude of  $\mu$  measured by zetametry. The reduction of volume fraction accompanying the reduction of  $R_H$  was visualised by CLSM, through melting of a MG<sub>1</sub> crystal (7.5 wt%) into a fluid as the temperature was raised to 30 °C. Under conditions of strong electrostatic screening (100 mM KCl), a further increase in temperature across the VPTT resulted in the formation of a volume-spanning gel network as a result of attractive van der Waals interactions.

Crucial for a subsequent assembly of the microgels into colloidal molecules, the interfacial activity of the MG<sub>1,2</sub> microgels was investigated by CLSM using large, silicon oil emulsion droplets to provide an oil-water interface. The microgels were observed to densely pack into a well-ordered hexagonal array at the oil-water interface, with a center-to-center distance smaller than that expected from their hydrodynamic diameter  $D_H$  in bulk (506 versus 638 nm), thus reflecting their soft repulsive potential and ability to interpenetrate<sup>126,127</sup>.

In order to assemble the temperature-responsive, interface active microgels into colloidal molecules, small emulsion oil droplets were used as anchors. Here, two requirements needed to be fulfilled. First, in order to limit the number of microgels - the number of interaction sites - per oil droplet, the oil droplets needed to be comparable in size to the microgels. Second, high oil droplet monodispersity was essential in order to yield a monodisperse colloidal molecule product, thus immediately disqualifying conventional high-energy input comminution methods known to result in wide droplet size distributions. Both requirements could be fulfilled by following an



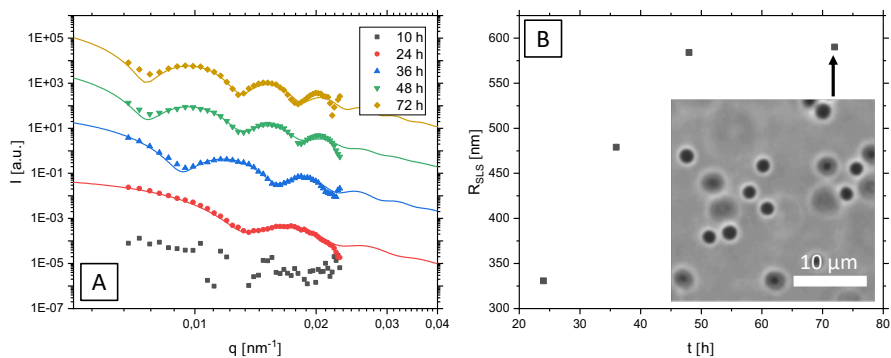


Figure 5.3: (A) Evolution of  $I(q)$  with time, measured by SLS for growing PDMS oil mini-emulsion droplets. Lines represent fits using a polydisperse sphere model. (B) Evolution of  $R_{SLS}$  of PDMS oil mini-emulsion droplets with time.  $R_{SLS}$  was obtained from the fits in (A). The inset micrograph shows 72-hour-old PDMS oil mini-emulsion droplets.

emulsion synthesis route involving ammonia-catalysed hydrolysis and condensation of DMDES monomer to yield monodisperse, micron-sized PDMS oil mini-emulsion droplets in aqueous solution<sup>233</sup>. Moreover, we could benefit from the fact that PDMS has a refractive index (1.40) close to that of water, resulting in, first of all, low-turbidity emulsions suitable for CLSM studies, and, second, reduced attractive van der Waals attractions. In addition, the density of PDMS ( $0.97 \text{ g/cm}^3$ ) is slightly lower than that of water, whereas that of microgels is slightly higher, thus enabling studies of the resulting density-matched microgel-decorated oil droplets without sedimentation or creaming effects.

Before any attempts to prepare colloidal molecules, the PDMS oil mini-emulsion droplets were characterised. First, the growth of oil droplets prepared from 0.01 v/v DMDES in pH 10.8 ammonia solution was studied by SLS (Fig. 5.3A). Here, small aliquots of the emulsion were taken out at certain time points, were diluted by a factor ten to slow down the growth, and were then measured. At 10 hours, no measurable angular dependence of the intensity of the scattered light was observed as the intensity was simply too low. At 24 hours and longer, however, the presence of a series of well-defined minima pointed to the presence of rather monodisperse oil droplets. The SLS data were fitted using a polydisperse sphere model, where the positions and depth of the minima were fitted to yield the oil droplet radius  $R_{SLS}$  and polydispersity, respectively. The evolution of the radius with time is initially steep but eventually levels off as the monomer supply is consumed (Fig. 5.3B). The polydispersity was in all cases below 10%. The obtained emulsions proved to be stable for weeks - longer if dialysed - due to the presence of deprotonated silanols residing at the oil-water interface conferring electrostatic stabilisation. The negative surface charge was reflected in  $\mu$ , measured by zetametry to  $-3.67 \cdot 10^{-8} \text{ m}^2 \text{V}^{-1} \text{s}^{-1}$ .

As a first step towards colloidal molecules, obtained mini-emulsions were added

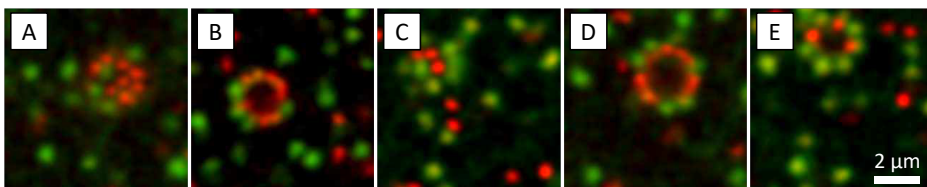
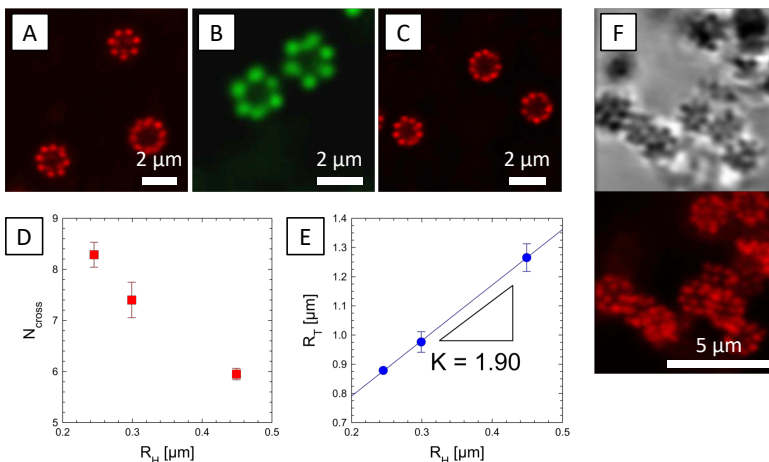


Figure 5.4: CLSM micrographs (20 °C) of PDMS oil mini-emulsion droplets decorated with MG1 and MG4 microgels, obtained by slow addition of emulsion to the 1:1 binary microgel mixture.

to MG1 and MG4 microgel suspensions, respectively, which yielded monodisperse, colloidosome-like microgel-decorated oil droplets. The observed number of microgels in the cross-section  $N_{cross}$  - on average 9.5 and 6.4 for the smaller MG1 and the larger MG4, respectively - was used to calculate the total number of microgels per oil droplet  $N_T$  - 31-32 for MG1 and 13-14 for MG4 - using the well-known relationship for the maximum packing of spheres on a sphere<sup>304</sup>. In an attempt to reduce the number of effective interaction sites, the emulsion was then instead added to a 1:1 MG1-MG4 mixture. Here, the high-VPTT MG4 PNIPMAM microgels were considered as spacers effectively separating the low-VPTT MG1 PNIPAM microgel interaction sites. Interestingly, the two microgels were not randomly distributed at the interface but appeared to coexist in the form of domains (Fig. 5.4). Moreover, there appeared to be a strong preference for MG1 over MG4 adsorption, but the locus of this preferential adsorption was not further investigated.

To reach even smaller oil droplet sizes and an even smaller number of microgels per droplet, a so-called in situ microgel-Pickering emulsion approach was developed (Fig. 5.2). Here, a microgel suspension was added to a just-hydrolysed DMEDES solution, and so the oil droplets grew in the presence of (an excess of) microgels. This approach successfully yielded microgel-decorated oil droplets with the MG1, MG2 and MG3 microgels (Fig. 5.5A-C); with MG4, however, aggregation was observed and was attributed to the large size of the microgels resulting in a less homogeneously covered and less well protected interface. CLSM studies of the MG1, MG2 and MG3-decorated oil droplets revealed, not surprisingly, that both  $N_{cross}$  and  $N_T$  increased with decreasing microgel size (given by  $R_H$ ) (Fig. 5.5D). Moreover, the overall size of the microgel-decorated oil droplets  $R_T$  was found to linearly increase with increasing size of the microgels, with a slope  $K=1.90$  (Fig. 5.5E). Extrapolation to  $R_H=0$  yielded a droplet radius ( $R_d=410$  nm) smaller than that observed for droplets grown in the absence of microgels, indicating that the growth is somehow limited by the presence of the microgels. From  $K$  and using a simple model treating the microgels as non-deformable spheres wetting a liquid droplet, the effective contact angle  $\theta_{eff}$  was estimated to 33.8, 32.5 and 37.3° for MG1, MG2 and MG3, respectively. The relatively low  $\theta_{eff}$  reflects the microgels' strong preference for the water phase over the oil phase.



**Figure 5.5:** CLSM micrographs (20 °C) showing (A) MG1, (B) MG2 and (C) MG3-decorated PDMS oil mini-emulsion droplets obtained with the in situ approach. (D-E) Influence of microgel size ( $R_H$ ) on (D) the number of microgels in the oil droplet cross-section  $N_{cross}$ , and (E) the overall size of the assemblies  $R_T$ . (F) Bright-field (top) and fluorescence (bottom) CLSM micrographs showing the network structure formed by MG1-decorated oil droplets in 100 mM KCl and at 35 °C.

Using the MG<sub>I</sub>-decorated oil droplets, the ability of the microgels to serve as temperature-responsive interaction sites was demonstrated using CLSM. Here, an increase in temperature across the VPTT under conditions of strong electrostatic screening (100 mM KCl) resulted in reversible association of the microgel-decorated oil droplets (of the excess microgels) (Fig. 5.5F). This confirmed that the temperature response of the individual microgels was conferred to the assemblies via the microgel interaction sites.

Since the number of microgels per oil droplet after three days of in situ oil droplet growth was still too large for the assemblies to be classified as colloidal molecules, the evolution of  $N_T$  with time was studied by CLSM in order to assess whether smaller, colloidal molecule-like assemblies were present in the early stages of oil droplet growth. Here, MG<sub>I</sub> assemblies of  $N_T=2$  to  $N_T=5$  - likely held together by capillary forces<sup>305</sup> - were indeed observed after 30 minutes of oil droplet growth, and grew to  $N_T=18-19$  after one day (Fig. 5.6). Observation of these small, colloidal molecule-like assemblies, together with a putative possibility to halt further oil droplet growth via an efficient quench, provided a first but promising proof of concept for the potential of the in situ approach for colloidal molecule preparation.

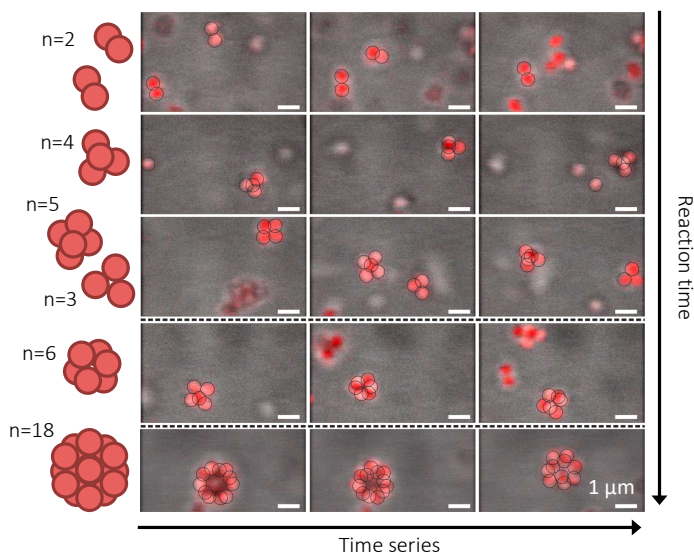
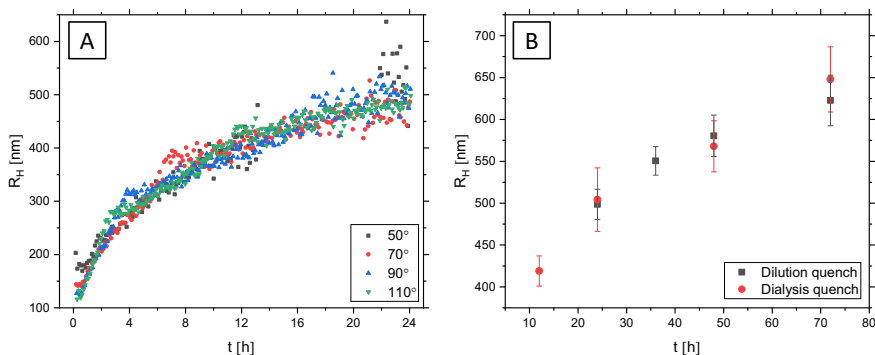


Figure 5.6: Overlay of bright-field and fluorescence CLSM micrographs (20 °C) showing the evolution of  $N_T$  for MG1-decorated PDMS oil mini-emulsion droplets with time.

#### 5.4.2 Main results of Paper II

Paper II serves as a follow-up paper, where the microgel-Pickering emulsion approach introduced in Paper I is refined. Briefly, it involves a more detailed study of the growth of PDMS oil mini-emulsion droplets and microgel-decorated oil droplets with time. This allows us to localise the time point corresponding to the target colloidal molecule size/valency, and, following suppression of further growth, the target colloidal molecules can be isolated. Finally, using a mixture of PNIPAM and PNIPMAM microgels, we extend the microgel-Pickering emulsion approach to the preparation of so-called patchy colloidal molecules. By definition, a patchy particle exhibits one or more well-defined interaction sites - patches - (ideally) at prescribed locations on the surface, through which it can experience strongly anisotropic, highly directional interactions with neighbouring particles<sup>27,306–311</sup>.

In Paper II, 478 nm ( $R_H$  at 20 °C), rhodamine-labelled PNIPAM-co-AAc microgels were used as building blocks. The microgels were crosslinked using 5.0 mol% BIS and their AAc content was 7.5 mol%. Their temperature-responsive behaviour was characterised using DLS where a decrease of  $R_H$  to 212 nm was observed on increasing the temperature to 54 °C. The deswelling was, first of all, accompanied by an increase in  $\mu$ , from  $-1.90 \cdot 10^{-8}$  at 20 °C to  $-3.39 \cdot 10^{-8} \text{ m}^2\text{V}^{-1}\text{s}^{-1}$  at 50 °C, measured by zetametry. Second, the concomitant reduction of the volume fraction was observed to induce melting of a crystal (3.7 wt%) into a fluid by increasing the temperature to 40 °C.



**Figure 5.7:** (A) PDMS oil droplet growth probed via the evolution of  $R_H$  with time  $t$  up to 24 h, measured by 3D DLS at four different angles.  $t=0$  corresponds to the time of addition of DMEDES to the ammonia solution;  $t=10$  min corresponds to the start of the measurements. The oil droplets were prepared from 0.01 v/v DMEDES in 0.1 v/v ammonia solution. (B) Evolution of  $R_H$  of oil droplets with growth time  $t$ . Data represented by filled grey squares were obtained following a ten-fold dilution of (an aliquot of) the emulsion whereas data represented by red circles were obtained following a 72 hours dialysis quench.

Under suppression of the electrostatic repulsion (5 mM HCl), the same temperature ramp instead served to trigger a repulsive-to-attractive transition that caused the microgels to associate into a volume-spanning network. Finally, the interface activity of the microgels was confirmed by their adsorption to large silicon oil droplets. The microgels' strong preference for water over oil was reflected in their position in the interface, studied by CLSM; the microgels were observed to reside on the water-side with only a small anchoring in the oil. CLSM furthermore revealed the microgels' organisation into a 2D hexagonal crystal at the interface, mediated by inter-particle repulsion in the plane of the interface.

Just as in Paper I, in Paper II the PDMS oil mini-emulsions were prepared by hydrolysis and condensation of DMEDES in aqueous ammonia solution<sup>233</sup>. Here, a DMEDES amount of 0.01 v/v and an ammonia amount of 0.1 v/v were used, yielding highly monodisperse oil droplets stabilised by negative surface charges ( $\zeta=-110.6$  mV). As the characterisation of PDMS oil droplet growth provided in Paper I did not comprise the first 24 hours, in Paper II the evolution of the oil droplet size in this region was studied in situ by 3D DLS (Fig. 5.7A). Here, the oil droplet radius ( $R_H$ ) was observed to initially increase steeply, after which the growth rate began to slowly level off. After 24 hours of growth, the radius approached 500 nm. This is in good agreement with the radius given by SLS, 473 nm, which was obtained by fitting of the form factor  $P(q)$  with a Mie scattering profile of polydisperse, homogeneous spheres. The fitting yielded a polydispersity of 5.0%, which corroborated the high droplet monodispersity observed by CLSM.

Next, the feasibility of a dialysis growth quench in order to suppress further oil droplet growth, via monomer and ammonia depletion, was investigated. This was motivated by

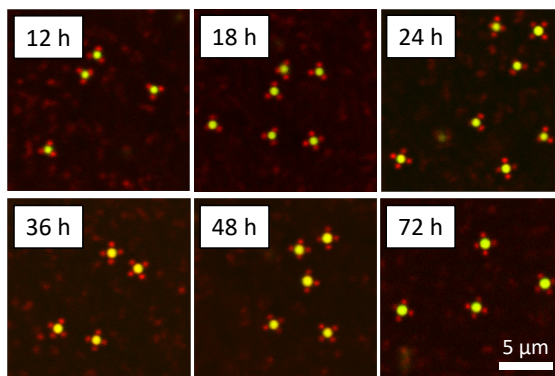


**Figure 5.8:** CLSM micrographs (20 °C) showing the evolution of the size/valency of the microgel-decorated oil droplets with time. The oil droplets were prepared from 0.01 v/v PM546-dyed DMEDES in 0.1 v/v ammonia solution containing 0.5 wt% microgels. The assemblies are adsorbed to the cover slip.

the (possible) need to halt further oil droplet growth in the in situ microgel-Pickering emulsion process once the target colloidal molecule-like microgel-decorated oil droplets were formed. Here, small aliquots of the growing emulsion were extracted and put for dialysis at certain time points, 12, 24, 48 and 72 hours. Following 72 hours of dialysis, the size of the oil droplets was measured by DLS, and was compared to the size measured following a simple dilution quench (Fig. 5.7B). The results confirmed that dialysis can be employed to effectively suppress further oil droplet growth.

The in situ microgel-Pickering emulsion approach developed in Paper I, was used also in Paper II. However, to obtain colloidal molecules with a small number - around four - of well-defined defined interaction sites, larger and more highly charged (stronger repulsive) microgels were employed in Paper II. Based on the evolution of the valency - the number of microgels per oil droplet - with time for neutral ( $\mu=+0.53 \cdot 10^{-8} \text{ m}^2\text{V}^{-1}\text{s}^{-1}$  at 20 °C), smaller ( $R_H= 299 \text{ nm}$  at 20 °C) microgels, we hypothesised that the target colloidal molecules would not be present until after the initial, steep growth phase. The evolution of the valency was studied by CLSM, at 12, 18, 24, 36, 48 and 72 hours (Fig. 5.8). Already at 12 hours, monodisperse, valency-four colloidal molecules of tetrahedral geometry were observed. The valency increased with growth time to about six to seven at 72 hours. The adsorbed microgels were well separated at the interface, arranged regularly due to the inter-particle repulsion that serves to maximise the inter-particle distances.

As the target colloidal molecules with four microgel interaction sites per droplet were found at 12 hours of oil droplet growth,  $t=12$  hours was naturally chosen as the point of the dialysis quench. After dialysis quenching, the colloidal molecules - still tetrahedral, valency-four ones, as determined by CLSM - were isolated by removal of excess microgels using DLD technology. This served to remove the vast majority of excess micro-

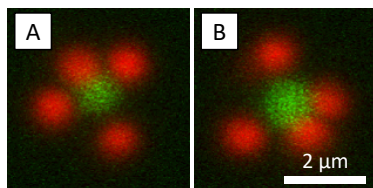


Figure 5.9: CLSM  $xyz$  maximum intensity projections (20 °C), constructed from 15  $xy$  frames collected over a  $z$ -distance of 2.94  $\mu\text{m}$ , showing isolated tetrahedral microgel-decorated oil droplets adsorbed to the glass cover slip.

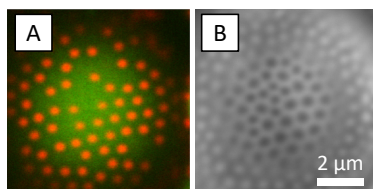
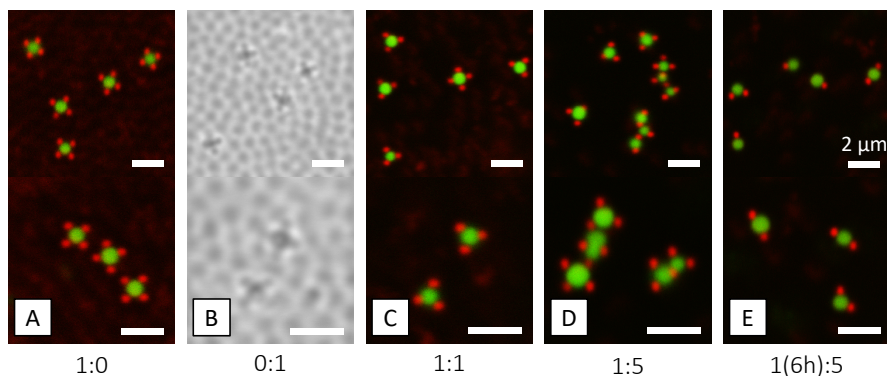


Figure 5.10: (A) Fluorescence and (B) bright-field CLSM micrographs (20 °C) of PM546-dyed silicon oil emulsion droplets simultaneously decorated with PNIPAM-co-AAc (rhodamine-labelled) and PNIPMAM-co-AAc microgels (unlabelled).

gels. However, due to issues with microgel sticking to the walls and posts of the device which decreases the performance of the device, a small amount of microgels ended up as contaminants in the colloidal molecule reservoir. CLSM micrographs of the isolated tetrahedral clusters are shown in Fig. 5.9. These results altogether demonstrate how the in situ microgel-Pickering emulsion approach, in combination with dialysis quenching and DLD sorting, can be successfully employed to generate monodisperse colloidal molecules of a specific, target valency.

The remaining part of Paper II features a sub-study in which the microgel-Pickering emulsion approach was extended to the preparation of patchy colloidal molecules. Such colloidal molecules are highly attractive as they can be used to study the influence of attractive patches with directional interactions on, for example, self-assembly and diffusion. In this part of the study, two different microgels were used, one rhodamine-labelled, 401 nm ( $R_H$  at 20 °C) PNIPAM-co-AAc microgel and one unlabelled, 355 nm PNIPMAM-co-AAc one. Both were moderately crosslinked (4.8 and 4.9 mol% BIS, respectively) and had an AAc content of 4.8 mol%. In this sub-study, the low-VPTT PNIPAM microgels were employed to play the role of the effective patches whereas the high-VPTT PNIPMAM ones served as passive spacer particles.

Before attempting any preparation of colloidal molecules, the simultaneous adsorption of the two microgels to the interface of an emulsion comprising large silicon oil droplets was studied. Both microgels were observed to adsorb to the interface, arranging in a (distorted) hexagonal array (Fig. 5.10). However, and as also reported in Paper I, preferential adsorption of one type of microgel, the PNIPAM one, was observed but



**Figure 5.11:** CLSM micrographs (20 °C) showing examples of PDMS oil droplets prepared in the presence of PNIPAM-co-AAc (rhodamine-labelled) and PNIPMAM-co-AAc (unlabelled) microgels of the following number ratios (PNIPAM:PNIPMAM): (A) 1:0, (B) 0:1, (C) 1:1, (D) 1:5 with PNIPAM added at  $t=0$  and (E) 1:5 with PNIPAM added at  $t=6$  hours. The oil droplets were prepared from 0.01 v/v PM546-dyed DMDES and 0.05 v/v ammonia solution and grown for 48 hours.

its locus was not investigated in more detail. Instead, the in situ microgel-Pickering emulsion approach was now employed in order to prepare patchy colloidal molecules. Whereas the two microgels were observed to independently adsorb to the oil-water interface to form microgel-decorated oil droplets (Fig. 5.11A-B), the PNIPAM microgels were selectively recruited to the interface when a binary 1:1 microgel mixture was used (Fig. 5.11C). Attempts to tweak the adsorption in favour of PNIPMAM by using a 1:5 PNIPAM:PNIPMAM mixture merely caused aggregation by a bridging mechanism as the PNIPAM microgels were still preferentially adsorbed but no longer present in excess (Fig. 5.11D). As a work-around, the PNIPAM microgels were in the next experiment added at a later stage, after six hours, when the the interface was already covered by PNIPMAM microgels. With this approach, patchy colloidal molecules carrying, typically, one or two PNIPAM interaction sites were successfully obtained (Fig. 5.11E). Whereas this small set of experiments only constitute a first proof of concept for this approach, the results clearly demonstrate the potential of the microgel-Pickering emulsion approach for the preparation of patchy colloidal molecules.

#### 5.4.3 Ongoing investigations: attempts to solidify the oil droplets

As difunctional DMDES is unable to branch and form crosslinks, the microgel-decorated oil droplets featured in Paper I and Paper II consist of a liquid central oil droplet. In order to preserve the structures longterm, we are currently investigating the possibility to exchange (part of) the DMDES for DPM or TMP that carry methacrylate groups that can be utilised for solidification through free radical-induced polymerisation<sup>67,203,235,236</sup>. So far, we have successfully prepared monodisperse emulsions



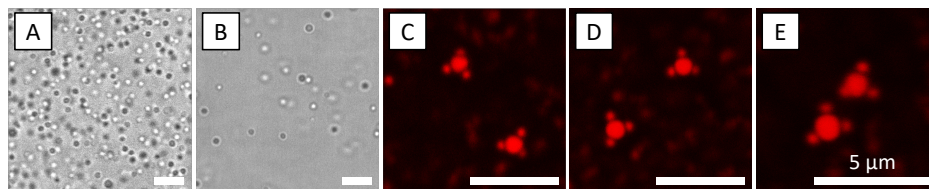


Figure 5.12: (A) Emulsion prepared from 0.016 v/v TPM and 0.3 v/v  $\text{NH}_3$  according to a literature procedure<sup>67</sup> and grown for 12 hours. (B) Same as in A but at ten-fold dilution. (C-E) Examples of microgel-decorated TPM oil droplets (undyed) with (possibly) microgels engulfed inside, prepared by mixing the diluted emulsion with PNIPAM-co-AAc microgels. Scale bars are 10  $\mu\text{m}$  in A-B, 5  $\mu\text{m}$  in C-D and 2  $\mu\text{m}$  in E.

from TPM (Fig. 5.12A-B), which on mixing with microgels yield colloidal molecule-like assemblies (Fig. 5.12C-E) alongside, unfortunately, a large number of aggregates. Interestingly, based on the localisation of the red fluoresce, it appears that, besides the microgels adsorbed to the interface, microgels are also engulfed by the TPM droplets and reside in their interior.

Whereas the initial results look promising, future experiments will have to reveal whether or not the use of TPM is the right way to go to solidify the oil droplets. An alternative could be to use the trifunctional monomer monomethyltriethoxysilane (MMTES); a 50:50 v/v mixture of DMDES and MMTES has previously been used to prepare crosslinked, inorganic microgel particles<sup>312</sup>.

#### 5.4.4 Ongoing investigations: attempts to evoke lock-and-key interactions

An ongoing study focuses on replacing the spherical microgels with bowl-shaped, PS-PNIP(M)AM core-shell ones that will allow for the implementation of lock-and-key principles in a second assembly step where spherical particles that precisely fit the cavity of the bowls serve as linkers. A prerequisite for such lock-and-key type bonding, which can be driven by electrostatic<sup>231</sup> or depletion interactions<sup>67</sup>, is naturally that the preferred orientation of the bowls is one where the cavity faces outwards, towards the water phase. Initial results from CLSM however indicate that the cavities of adsorbed bowls are randomly oriented (Fig. 5.13) and that the bowls are (more or less) rotationally locked in place once adsorbed. It is unlikely that the orientation of the cavities can be manipulated in this system. Moreover, it appears that the bowls have a lower affinity for the oil droplets than the pure microgels have: the oil droplets are typically not fully covered by bowls.

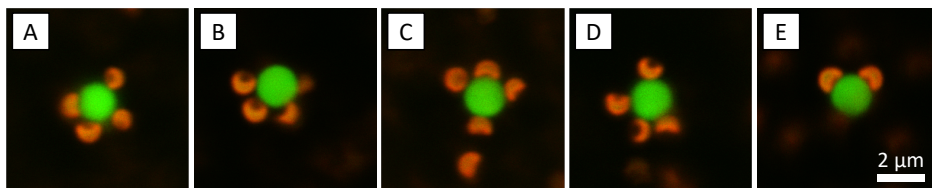


Figure 5.13: CLSM micrographs (20 °C) showing examples of pyrromethene 546-dyed PDMS oil droplets decorated by bowl-shaped PNIPMAM-PS core-shell particles, prepared through addition of bowls to a PDMS O/W emulsion prepared from 0.025 v/v DMDES and 0.1 v/v NH<sub>3</sub> and grown for 24 hours.

## 5.5 Evaporation-induced assembly from W/O emulsions

In Paper III, we present a method for the preparation microgel-based colloidal molecules that builds on evaporation of water from microgel-containing W/O emulsion droplets (Fig. 5.14), in turn generated using droplet microfluidics to yield droplets of exquisite monodispersity. In this paper, a mixture of PNIPAM and PNIPMAM microgels is used in order to form bicomponent colloidal molecules that possess patchy interactions at temperatures in between the two VPTTs. The main results of Paper III are summarised in the following section.

### 5.5.1 Main results of Paper III

In Paper III, two microgel systems were employed, one rhodamine-labelled, 332 nm ( $R_H$  at 20 °C in water) PNIPAM microgel and one fluorescein-labelled, 202 nm PNIPMAM one. The two were moderately crosslinked with 5 mol% BIS. Through co-polymerisation with AAc (22 mol%), carboxylic acid groups were incorporated and subsequently used as handles for attachment of methacrylate-carrying GMA, thereby enabling the preparation of stable colloidal molecules through microgel-microgel cross-linking. As revealed by NMR, the degree of GMA functionalisation was low, albeit still sufficient to induce crosslinking as was demonstrated through the preparation of stable macrogels. Both microgels responded to changes in temperature: a decrease of  $R_H$  and an increase of  $\mu$  with increasing temperature was measured by DLS and zeta-metry, respectively. Using CLSM, when the temperature was raised to above the VPTT under conditions where the electrostatic repulsion was suppressed (1 mM HCl and 100 mM KCl), both microgels were observed to undergo a reversible repulsive-to-attractive transition leading to the formation of a volume-spanning network structure. When a binary mixture was used, due to the difference in VPTT between the two, the resulting network had a core-shell character with the low-VPTT PNIPAM microgels in the core and the high-VPTT PNIPMAM ones in the shell. The difference in VPTT is crucial for the objective of Paper III, to prepare bicomponent colloidal molecules where

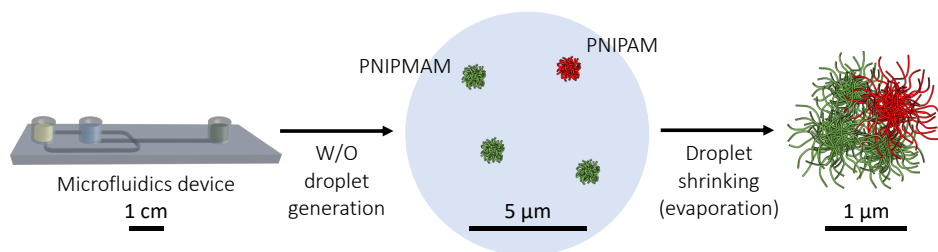


Figure 5.14: Evaporation of water from monodisperse, microfluidics-generated, microgel-containing water-in-oil emulsion droplets yields colloidal molecule-like microgel assemblies.

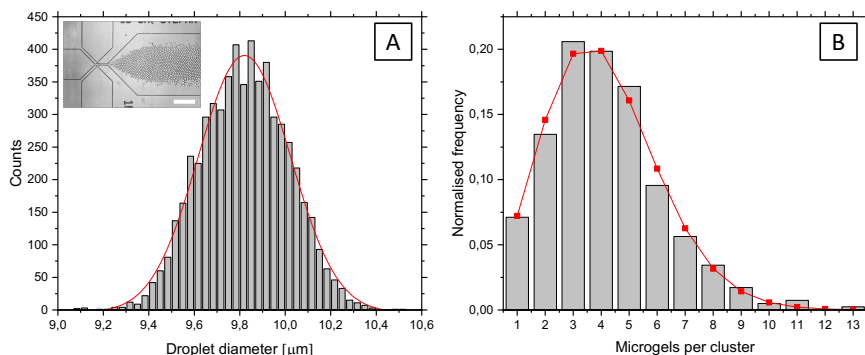


Figure 5.15: (A) Water droplet size distribution together with a Gaussian fit (red line;  $n=10\,653$ ,  $R^2=0.99$ ). Inset shows droplet generation at the constriction. The scale bar is  $200\ \mu\text{m}$ . (B) Histogram showing the experimentally determined distribution of microgels per cluster (in oil) together with a ZTP fit (red line).

patchy interactions can be induced.

To prepare colloidal molecules, we used a droplet microfluidic device to generate microgel-containing W/O emulsion droplets and induced assembly of the encapsulated microgels by allowing the water to evaporate, thereby packing the microgels into dense, colloidal-molecule like clusters. To allow for evaporation, a fluorinated hydrocarbon oil with a (relatively) high water solubility was used as continuous phase. The use of microfluidic technology allowed us to generate highly monodisperse water droplets of radius  $9.83 \pm 0.19\ \mu\text{m}$  (Fig. 5.15A), typically at a rate of  $10000\ \text{s}^{-1}$ . The use of monodisperse water droplets considerably sharpens the cluster size distribution compared to conventional comminution methods that are known to yield (highly) polydisperse droplets and therefore widen the cluster size distribution; if the droplets are monodisperse, the distribution of the number of microgels per droplet obeys a simple Poisson distribution. The use of a suspension containing  $0.00103\ \text{wt}\%$  PNIPAM and  $0.00158\ \text{wt}\%$  PNIPMAM (corresponding to a 1:3 number ratio) yielded - based on counting of the number of microgels in the resulting dense clusters in oil and subsequent fitting the acquired histogram with a zero truncated Poisson (ZTP) distribution that takes into

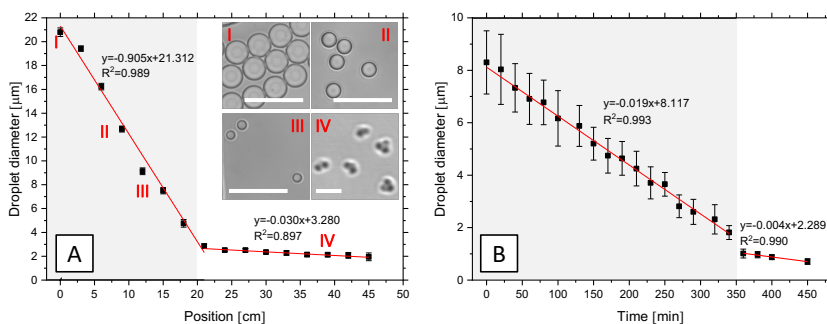


Figure 5.16: (A) Shrinking of water droplets generated with the long device was monitored on-chip.  $x = 0$  denotes the point where the main channel is split into the six meandering channels. Error bars are typically smaller than the symbol size. Scale bars are 50  $\mu\text{m}$  in micrographs I-III and 2  $\mu\text{m}$  in IV. (B) Shrinking of droplets generated with the short device was instead performed and monitored off-chip.  $t = 0$  denotes the time point at which the emulsion was transferred from the device outlet to a vial for water evaporation under stirring. Red lines represent linear fits.

consideration that droplets containing zero microgels were not accounted for - a mean of 4.12 microgels per droplet (Fig. 5.15B). This demonstrates that our method can be used to generate a library of colloidal molecules with a narrow size distribution in a single step. Since the distribution of cluster sizes inevitably follows a Poisson distribution, the yield of a certain cluster size is always limited. However, by prolonging the droplet generation time, or through the use of many parallel devices, the yield of a specific cluster size can still be high. For cases where it is desirable to obtain a single cluster size, strategies such as on-chip pre-focusing of the microgels or post-generation sorting of the colloidal molecules can be employed.

Two different microfluidics devices were used for droplet generation, one shorter device offering high generation frequency and one longer device with six meandering channels offering long droplet residence times and the ability to monitor the droplet shrinking process on-chip; the shrinking of droplets generated with the short device was instead performed and monitored off-chip. In both cases, droplet shrinking was characterised by two distinct phases, an initially steep, linear reduction of the droplet diameter followed by shrinking at a considerably lower rate enabled by the rearrangement of the microgels inside the droplets (Fig. 5.16). The final cluster size was determined by the balance between droplet Laplace pressure and the microgels' finite ability to interpenetrate, deform and compress<sup>126,127</sup>.

Following complete water evaporation, the clusters were crosslinked using 2-hydroxy-2-methylpropiophenone (HMPP), a photoinitiator that has previously been shown to effectively induce crosslinking of other GMA-functionalised microgels.<sup>313</sup> After crosslinking, the clusters were transferred from oil to water through a series of extensive washing steps. CLSM studies of the obtained clusters revealed that certain configurations - linear dimers, (distorted) trigonal trimers and (distorted) tetrahedral or square

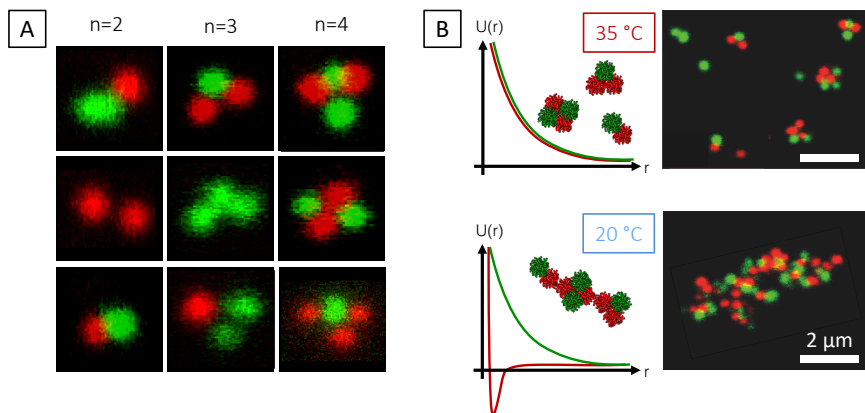


Figure 5.17: (A) CLSM micrographs (20 °C) showing examples of crosslinked, colloidal molecule-like clusters after transfer from oil into water. (B) Association of the clusters can be induced through an increase in temperature from 20 to 35 °C, in 1 mM HCl and 100 mM KCl to suppress the electrostatic stabilisation, mediated by the repulsive-to-attractive transition of the PNIPAM patches.

planar tetramers, for example - seemed to be favoured (Fig. 5.17A), likely due to packing efficiency reasons during droplet shrinking. When the temperature of the sample was raised to between the two VPTTs, under suppression of electrostatic repulsion (by 1 mM HCl and 100 mM KCl), reversible association of the clusters was observed as a response to the repulsive-to-attractive transition of the PNIPAM interaction sites (Fig. 5.17B), thereby reflecting the patchy nature of the clusters.

### 5.5.2 Ongoing investigations: a new microgel-microgel coupling approach

As the GMA-to-carboxylic acid attachment reaction featured in Paper III proceeds with very low (yet still sufficient) efficiency, we are currently looking into alternative methods for the attachment of polymerisable groups capable of inducing microgel-microgel crosslinking. Here, we have recently adapted an EDC coupling scheme to attach methacrylamide-carrying APMAM to the carboxylic acid groups of PNIP(M)AM-*co*-AAc microgels. Successful attachment was confirmed by  $^1\text{H}$  NMR, through appearance of characteristic peaks corresponding to the two vinyl protons of APMAM (Fig. 5.18). Whereas the efficiency of APMAM attachment has not yet been quantified, the relatively strong signals in the NMR spectrum indicates a considerable enhancement compared to that of the GMA attachment.

It is also worth mentioning that we have investigated crosslinking using AL-functionalised microgels in combination with the crosslinker GDA. However, likely due to internal crosslinking being favoured, stable colloidal molecules were never obtained following oil-to-water transfer. Still, stable macrogels could be prepared with

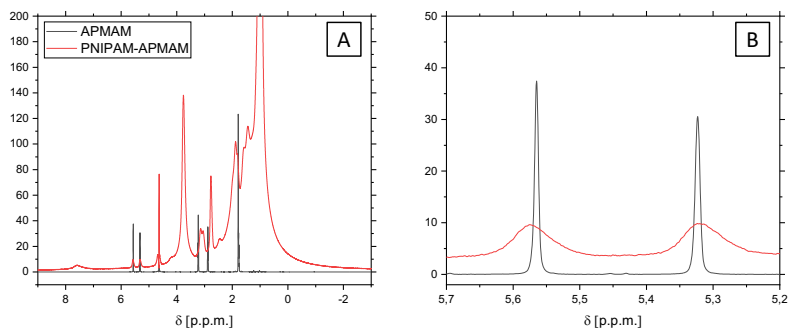


Figure 5.18: (A) 600 MHz 1D  $^1\text{H}$  FT NMR spectrum of APMAM (black line) and APMAM-functionalised PNIPAM microgels (red line), recorded in  $\text{D}_2\text{O}$  at 25  $^\circ\text{C}$ . (B) The appearance of vinyl peaks in the 5.7-5.2 p.p.m. region is indicative of APMAM attachment to the microgels.

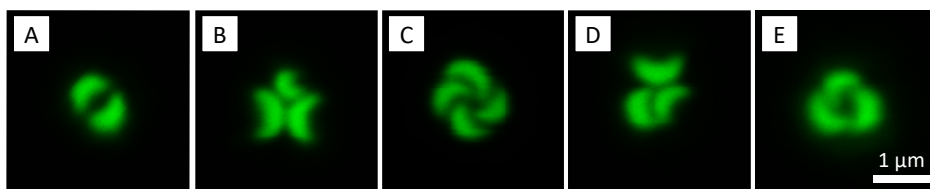
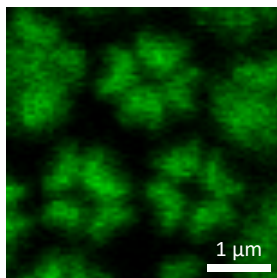


Figure 5.19: CLSM micrographs (20  $^\circ\text{C}$ ) showing examples of clusters of bowl-shaped PNIPAM-PS core-shell particles in hydrofluoroether (HFE) oil, prepared by evaporation of water from microfluidics-generated, bowl-containing water-in-oil emulsion droplets. The PS cores are labelled with pyromethene 546. The bowl-shaped particles were synthesised by J. J. Crassous and J-M. Meijer and were assembled by F. Peng.

this approach.

### 5.5.3 Ongoing investigations: attempts to evoke lock-and-key interactions

As bowl-shaped PS-microgel core-shell particles adsorbed onto oil droplets unfortunately seem to displayed a random orientation (Section 5.4.4), currently under investigation are instead clusters of bowls formed with the water droplet evaporation method. As previously mentioned, small clusters of bowls where the cavities face outwards are the target, in order to be able to evoke lock-and-key interactions in a subsequent assembly step. It is hypothesised that shrinking of the water droplets poses a certain organisation on the bowls as their available space becomes restricted<sup>68</sup>, but initial results however indicate that their orientation is again random, with perhaps a slight preference for stacking one bowl in the other (Fig. 5.19). We are currently looking into possibilities of manipulating the orientation of the bowls by adding like-charged (same charge as the bowls), shape-complementary (to the cavity) spherical microgels to the shrinking water droplets. Here, due to electrostatic repulsion, an orientation where the contact area between bowl and sphere is large - i.e sphere in cavity - should be disfavoured. As anticipated, cavity-outwards orientations (Fig. 5.20) appear more frequently, but this



**Figure 5.20:** CLSM micrograph (20 °C) showing examples of ‘cavity out-clusters’ in HFE oil, prepared from bowl-shaped PNIPMAM-PS core-shell particles in the presence of shape-complementary, like-charged spherical microgels. The PS cores are labelled with pyromethene 546 whereas the spherical microgels are non-fluorescent (not shown). The bowl-shaped particles were synthesised by J. J. Crassous and J-M. Meijer and were assembled by F. Peng.

needs to be better quantified in order to draw any conclusions.

## 5.6 Electrostatic attraction-driven assembly of oppositely charged microgels

In Paper IV, we introduce a new approach to assemble microgels into colloidal molecules, where the electrostatic attraction between oppositely charged microgels is utilised to drive the assembly. As schematically depicted in Fig. 5.21, we start from high ionic strength conditions where the electrostatic interactions are screened, and induce assembly through dialysis; the assembly results in the formation of colloidal molecule-like clusters with a core-satellite morphology. The most important results of Paper IV are reviewed in the following section.

### 5.6.1 Main results of Paper IV

In Paper IV, four microgel systems - referred to as B<sub>474</sub>, A<sub>115</sub>, A<sub>220</sub> and A<sub>394</sub> (Table 5.2) - were employed as building blocks for AB<sub>n</sub> core-satellite-type colloidal molecules: one anionic one and three cationic ones of different sizes, destined to serve as satellites (*B*) and cores (*A*), respectively. Positive and negative charges, a prerequisite for an electrostatically driven assembly, were incorporated thorough co-polymerisation with AAc and AL, respectively. The microgels were all moderately crosslinked (3.1-4.8 mol% BIS). Two of the microgels, B<sub>474</sub> and A<sub>394</sub>, were fluorescently labelled, with rhodamine and fluorescein, respectively. The four microgel systems were selected from a large microgel library, primarily based on their size. All of the microgels responded to an increase in temperature, as was evident from a decrease of  $R_H$  with increasing

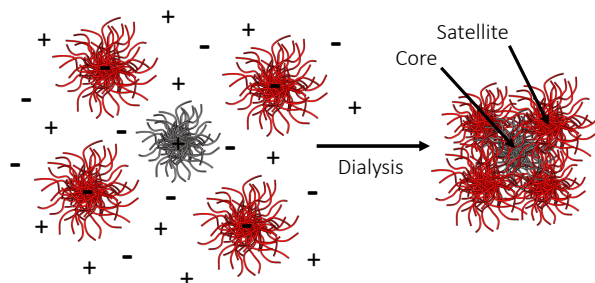


Figure 5.21: Induced by a reduction of ionic strength through dialysis, electrostatic attraction drives the ‘parking’ of charged microgels onto oppositely charged ones, thus yielding core-satellite-type colloidal molecules.

Table 5.2: Summary of the microgel systems used in Paper iv.

| Microgel | Polymer                | BIS [mol%] | $R_H$ (20/55 °C) [nm] | $\mu$ (20 °C) [ $\cdot 10^{-8} \text{ m}^2 \text{ V}^{-1} \text{ s}^{-1}$ ] | B474:Axxx (20 °C) [nm/nm] |
|----------|------------------------|------------|-----------------------|---|---------------------------|
| B474     | PNIPAM- <i>co</i> -AAc | 4.8        | 474 / 233             | -2.46   | -                         |
| A115     | PNIPAM- <i>co</i> -AL  | 4.6        | 115 / 70              | +2.80   | 4.12                      |
| A220     | PNIPAM- <i>co</i> -AL  | 4.4        | 220 / 113             | +3.14   | 2.15                      |
| A394     | PNIPAM- <i>co</i> -AL  | 3.1        | 394 / 197             | +2.47   | 1.20                      |

temperature. The temperature response of the B474 microgels was also characterised by CLSM, where an increase in temperature across the VPTT, under salt-free conditions, served to melt a crystal (3.7 wt%) into a fluid state as the volume fraction was reduced. Under conditions where the electrostatic repulsion was suppressed (5 mM HCl), crossing the VPTT instead served to induce a repulsive-to-attractive transition as evident from the microgels’ association into a volume-spanning network structure.

To assemble the satellites and cores, two methods were initially investigated. In the first method, the (A220) cores were added slowly to an excess of satellites (48:1) under deionised conditions, meaning that long-range electrostatic interactions are in play already from the start. In the second method, the two microgels were instead mixed at high ionic strength and not until the cores were well distributed among the satellites their assembly was initiated by dialysis. Whereas aggregates, large and small, formed by alternating cores and satellites, were common with the first method, the second method resulted almost exclusively in the small, target clusters. The second method consequently became the method of choice for subsequent experiments.

Three different-sized microgels were used as cores in order to evaluate the influence of the  $B:A$  size ratio on the size - or valency  $n$  - of the resulting  $AB_n$ -type colloidal molecules. Not surprisingly,  $n$  was observed to decrease with an increasing  $B:A$  size ratio, from  $n=6$  (A394) to  $n=2$  (A115) via  $n=4$  (A220), as evaluated by CLSM (Fig. 5.22). Together with the  $AB_2$  clusters, a small number of  $AB_3$  ones was observed. If geomet-



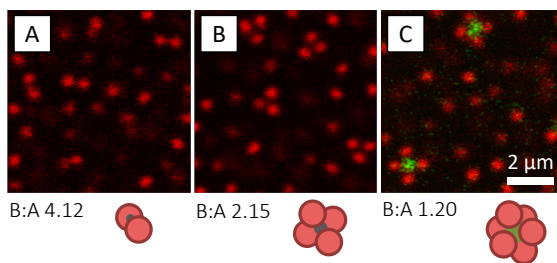


Figure 5.22: CLSM micrographs (20 °C) showing  $AB_n$ -type clusters, in an excess of B474 satellites, at three different  $B:A$  size ratios: (A) 4.12, (B) 2.15, and (C) 1.20.

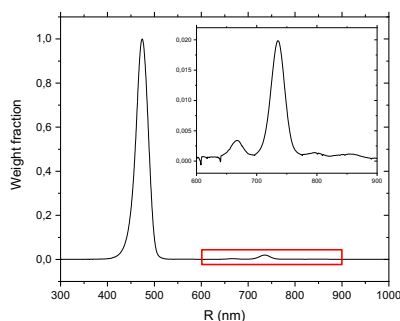


Figure 5.23: Cluster size distribution measured by AUC for the suspension harvested following assembly of B474 satellites and A220 cores. The inset shows a magnification of the 600-900 nm region (red box).

rically allowed, a finite probability for such  $AB_3$  clusters remains if the strength of the satellite-satellite repulsion is not too large at the point where the ongoing reduction of the ionic strength and the increasing core-satellite attraction permanently fixes a given cluster configuration. Similarly, a small number of  $AB_3$  clusters coexisted with the  $AB_4$  ones, which we attribute to ‘parking spaces’ on the cores being unoccupied also at long times. The same goes for the small number of  $AB_5$  clusters observed alongside the  $AB_6$  ones. The clusters size distribution obtained with the A220-B474 core-satellite combination was determined by AUC, yielding, besides a peak corresponding to the excess satellites, two distinct peaks corresponding to the  $AB_3$  and  $AB_4$  clusters, respectively (Fig. 5.23). By peak integration, it was determined that the  $AB_4$  clusters constituted 90% of the total cluster population by weight, which can probably be boosted further by careful optimisation.

Quite remarkably, for all A-B combinations investigated, regular clusters were obtained: linear dimers, tetrahedral tetramers and octahedral hexamers, respectively. We attribute the symmetric distribution of the adsorbed satellites to the electrostatic satellite-satellite repulsion that serves to maximise their distances. This maximisation is enabled by the slow decrease of ionic strength during the dialysis process that only slowly serves to increase the strength of the core-satellite (and satellite-satellite) interactions. This

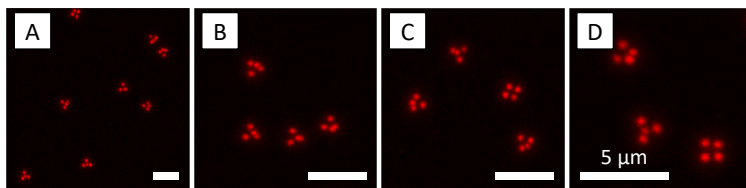


Figure 5.24: CLSM  $xyz$  maximum intensity projections (20 °C), constructed from 40  $xy$  frames collected over a  $z$ -distance of 3.27  $\mu\text{m}$ , showing isolated  $AB_4$ -type clusters of tetrahedral geometry adsorbed to the glass cover slip.

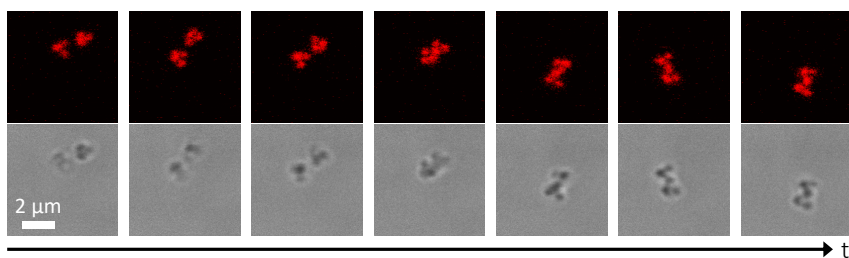


Figure 5.25: CLSM micrographs showing the association of two  $AB_4$ -type clusters, induced by an increase of temperature from 30 to 35 °C in 5 mM HCl. The top and bottom panels show fluorescence and bright-field micrographs, respectively.

allows the particles to initially rearrange and find their optimum positions, which are slowly ‘frozen’ as the core-satellite attraction grows stronger. We also found the clusters to be remarkably stable as they did not dissociate under conditions of high salinity (100 mM KCl) or acidity (5 mM HCl). We attribute the lack of dissociation to, first of all, extensive interpenetration and entanglement of the fuzzy shells of the core and satellite microgels. Second, resembling the situation of linear polyion adsorption to an oppositely charged surface, it is highly unlikely that all core-satellite ion pairs dissociates at the same time and the entire satellite can desorb before re-pairing occurs.

The tetrahedral  $AB_4$  clusters obtained from A220 and B474 were efficiently isolated from excess satellites using microfluidic DLD sorting technology; CLSM micrographs of isolated clusters are shown in Fig. 5.24. Removal of the excess satellites allowed us to, by CLSM, clearly visualise the attractive-to-repulsive transition of the clusters when the temperature was increased across the VPPT under conditions of suppressed electrostatic repulsion (5 mM HCl) (Fig. 5.25).

### 5.6.2 Ongoing investigations: attempts to make patchy particles

The electrostatic attraction-driven assembly method is currently employed with the intention of preparing tricomponent colloidal molecules where the core particles carry a mixture of PNIPAM and PNIPMAM satellites. A large number of different satellite

combinations have been investigated, always with the outcome that one type of microgel is exclusively adsorbed. Changing the number ratio in favour for the non-adsorbing type of microgel merely induces aggregation as the preferentially adsorbing one is no longer in large excess with respect to the cores. As it is extremely difficult to synthesise two microgels that are electrostatically equivalent and have the same affinity for the cores, this route to patchy colloidal molecules will (likely) not be further pursued.

*#IAmAScientistBecause of Carl Sagan and Ken Sakamura whose TV shows I watched when I was a kid. Also 'cause I'd be terrible in any other job.*

- @HirokiSayama on Twitter

## 6 | Conclusions and outlook

In conclusion, in an effort to address the problems with trapping of particle positions and orientations associated with the self-assembly of anisotropic, hard sphere-like colloidal molecules, in this thesis three conceptually simple, robust and up-scalable methods for the preparation of colloidal molecules from PNIPAM and PNIPMAM microgel spheres were developed, where the colloidal molecules inherit the unique properties of their constituents, including the soft and deformable nature and the temperature-responsiveness with respect to size, volume fraction and interactions. We believe that the transfer of these particle properties - the temperature-tunable volume fraction (size) and interactions in particular - from the single particle level to the colloidal molecule level constitute an important step towards successful assembly of colloidal molecules into novel crystal structures with emergent (temperature-switchable) properties. The photonic diamond structure, which has earned an almost Holy Grail-like status in the material science area and ranks the highest on the list of most wanted crystal structures, should be accessible from tetrahedral colloidal molecules. However, for the structure to possess a full photonic band gap, the pure microgels - due to their low refractive index - should be replaced by core-shell ones containing an inorganic core. Beside their role as powerful, anisotropic building blocks, the colloidal molecules prepared in the present thesis are expected to find use as model systems, for instance as 'big molecules' for the study of various phase transition phenomena in real space. They may also serve as simple models for complex anisotropic colloids such as bio-colloids.

With the generation of colloidal molecules presented in the present thesis, a set of new scientific questions has naturally appeared. Most interesting is perhaps to explore the phase diagram of the colloidal molecules, this by varying the number density (concentration), with temperature and/or ionic strength as additional parameters to tune the volume fraction and the nature and range of the inter-particles interactions in situ. We envision to extract information on structure and dynamics via radial distribution functions ( $g(r)$ s) and mean squared displacements (MSDs), respectively, obtained from image analysis and particle tracking know-how in our group. How do the colloidal molecules organise? How do they interact? Can we make them crystallise? In addition, we

would like to continue to explore the possibility of creating patchy colloidal molecules from PNIPAM-PNIPMAM mixtures and the use of bowl-shaped core-shell microgels to evoke lock-and-key-type bindings.

# References

- [1] International Union of Pure and Applied Chemistry. <https://goldbook.iupac.org/html/C/C01172.html>. Accessed: 2018-10-06.
- [2] Evans, D. F. & Wennerström, H. *The colloidal domain: where physics, chemistry, biology, and technology meet* (Wiley-VCH New York, 1999).
- [3] Hunter, R. J. *Foundations of colloid science* (Oxford University Press, 2001).
- [4] Everett, D. H. *et al. Basic principles of colloid science* (Royal Society of Chemistry, 2007).
- [5] Hamley, I. W. *Introduction to Soft Matter: synthetic and biological self-assembling materials* (John Wiley & Sons, 2013).
- [6] Poon, W. Colloids as big atoms. *Science* **304**, 830–831 (2004).
- [7] De Kruif, C., Rouw, P., Jansen, J. & Vrij, A. Hard sphere properties and crystalline packing of lyophilic silica colloids. *Le Journal de Physique Colloques* **46**, (C3)295–308 (1985).
- [8] Pusey, P. & Van Megen, W. Phase behaviour of concentrated suspensions of nearly hard colloidal spheres. *Nature* **320**, 340–342 (1986).
- [9] Pusey, P. N. & van Megen, W. Observation of a glass transition in suspensions of spherical colloidal particles. *Physical Review Letters* **59**, 2083 (1987).
- [10] Pusey, P., Van Megen, W., Bartlett, P., Ackerson, B., Rarity, J. & Underwood, S. Structure of crystals of hard colloidal spheres. *Physical Review Letters* **63**, 2753 (1989).
- [11] Pusey, P., Van Megen, W., Underwood, S., Bartlett, P. & Ottewill, R. Colloidal fluids, crystals and glasses. *Journal of Physics: Condensed Matter* **2**, SA373 (1990).
- [12] Van Megen, W. & Pusey, P. Dynamic light-scattering study of the glass transition in a colloidal suspension. *Physical Review A* **43**, 5429 (1991).
- [13] Pusey, P., Poon, W. C., Ilett, S. & Bartlett, P. Phase behaviour and structure of colloidal suspensions. *Journal of Physics: Condensed Matter* **6**, A29 (1994).
- [14] Kegel, W. K. & van Blaaderen, A. Direct observation of dynamical heterogeneities in colloidal hard-sphere suspensions. *Science* **287**, 290–293 (2000).
- [15] Gasser, U., Weeks, E. R., Schofield, A., Pusey, P. & Weitz, D. Real-space imaging of nucleation and growth in colloidal crystallization. *Science* **292**, 258–262 (2001).
- [16] Anderson, V. J. & Lekkerkerker, H. N. Insights into phase transition kinetics from

- colloid science. *Nature* **416**, 811 (2002).
- [17] Pham, K. N., Puertas, A. M., Bergenholtz, J., Egelhaaf, S. U., Moussaid, A., Pusey, P. N., Schofield, A. B., Cates, M. E., Fuchs, M. & Poon, W. C. Multiple glassy states in a simple model system. *Science* **296**, 104–106 (2002).
- [18] Yethiraj, A. & van Blaaderen, A. A colloidal model system with an interaction tunable from hard sphere to soft and dipolar. *Nature* **421**, 513 (2003).
- [19] de Villeneuve, V. W., Dullens, R. P., Aarts, D. G., Groeneveld, E., Scherff, J. H., Kegel, W. K. & Lekkerkerker, H. N. Colloidal hard-sphere crystal growth frustrated by large spherical impurities. *Science* **309**, 1231–1233 (2005).
- [20] Schall, P., Cohen, I., Weitz, D. A. & Spaepen, F. Visualizing dislocation nucleation by indenting colloidal crystals. *Nature* **440**, 319 (2006).
- [21] Lu, P. J. & Weitz, D. A. Colloidal particles: crystals, glasses, and gels. *Annual Review of Condensed Matter Physics* **4**, 217–233 (2013).
- [22] Li, B., Zhou, D. & Han, Y. Assembly and phase transitions of colloidal crystals. *Nature Reviews Materials* **1**, 15011 (2016).
- [23] Whitesides, G. M. & Grzybowski, B. Self-assembly at all scales. *Science* **295**, 2418–2421 (2002).
- [24] Xia, Y., Gates, B., Yin, Y. & Lu, Y. Monodispersed colloidal spheres: old materials with new applications. *Advanced Materials* **12**, 693–713 (2000).
- [25] Li, F., Josephson, D. P. & Stein, A. Colloidal assembly: the road from particles to colloidal molecules and crystals. *Angewandte Chemie International Edition* **50**, 360–388 (2011).
- [26] Glotzer, S. C. & Solomon, M. J. Anisotropy of building blocks and their assembly into complex structures. *Nature Materials* **6**, 557 (2007).
- [27] Zhang, J., Luijten, E. & Granick, S. Toward design rules of directional Janus colloidal assembly. *Annual Review of Physical Chemistry* **66**, 581–600 (2015).
- [28] Israelachvili, J. N. *Intermolecular and surface forces* (Academic Press, 2011).
- [29] Sanders, J. Diffraction of light by opals. *Acta Crystallographica Section A: Crystal Physics, Diffraction, Theoretical and General Crystallography* **24**, 427–434 (1968).
- [30] Marlow, F., Sharifi, P., Brinkmann, R. & Mendive, C. Opals: status and prospects. *Angewandte Chemie International Edition* **48**, 6212–6233 (2009).
- [31] Parker, A. R. 515 million years of structural colour. *Journal of Optics A: Pure and Applied Optics* **2**, R15 (2000).
- [32] Yoshioka, S. & Kinoshita, S. Effect of macroscopic structure in iridescent color of the peacock feathers. *Forma* **17**, 169–181 (2002).
- [33] Parker, A. R., Welch, V. L., Driver, D. & Martini, N. Structural colour: opal analogue discovered in a weevil. *Nature* **426**, 786 (2003).
- [34] Zi, J., Yu, X., Li, Y., Hu, X., Xu, C., Wang, X., Liu, X. & Fu, R. Coloration strategies in peacock feathers. *Proceedings of the National Academy of Sciences of the United States of America* **100**, 12576–12578 (2003).
- [35] Galusha, J. W., Richey, L. R., Gardner, J. S., Cha, J. N. & Bartl, M. H. Discovery of a

- diamond-based photonic crystal structure in beetle scales. *Physical Review E* **77**, 050904 (2008).
- [36] Wickham, S., Poladian, L., Large, M. & Vukusic, P. Control of iridescence in natural photonic structures: the case of butterfly scales. In *Optical Biomimetics*, 147–176e (Elsevier, 2012).
- [37] Yablonovitch, E. Inhibited spontaneous emission in solid-state physics and electronics. *Physical Review Letters* **58**, 2059 (1987).
- [38] John, S. Strong localization of photons in certain disordered dielectric superlattices. *Physical Review Letters* **58**, 2486 (1987).
- [39] Ho, K., Chan, C. T. & Soukoulis, C. M. Existence of a photonic gap in periodic dielectric structures. *Physical Review Letters* **65**, 3152 (1990).
- [40] Colvin, V. L. From opals to optics: colloidal photonic crystals. *MRS Bulletin* **26**, 637–641 (2001).
- [41] Maldovan, M. & Thomas, E. L. Diamond-structured photonic crystals. *Nature Materials* **3**, 593 (2004).
- [42] Hynninen, A.-P., Thijssen, J. H., Vermolen, E. C., Dijkstra, M. & Van Blaaderen, A. Self-assembly route for photonic crystals with a bandgap in the visible region. *Nature Materials* **6**, 202 (2007).
- [43] Cong, H., Yu, B., Tang, J., Li, Z. & Liu, X. Current status and future developments in preparation and application of colloidal crystals. *Chemical Society Reviews* **42**, 7774–7800 (2013).
- [44] van Blaaderen, A. Materials science: colloids get complex. *Nature* **439**, 545 (2006).
- [45] Solomon, M. J. Directions for targeted self-assembly of anisotropic colloids from statistical thermodynamics. *Current Opinion in Colloid & Interface Science* **16**, 158–167 (2011).
- [46] Sacanna, S. & Pine, D. J. Shape-anisotropic colloids: building blocks for complex assemblies. *Current Opinion in Colloid & Interface Science* **16**, 96–105 (2011).
- [47] Cademartiri, L., Bishop, K. J., Snyder, P. W. & Ozin, G. A. Using shape for self-assembly. *Philosophical Transactions of the Royal Society A* **370**, 2824–2847 (2012).
- [48] Sacanna, S., Pine, D. J. & Yi, G.-R. Engineering shape: the novel geometries of colloidal self-assembly. *Soft Matter* **9**, 8096–8106 (2013).
- [49] van Anders, G., Ahmed, N. K., Smith, R., Engel, M. & Glotzer, S. C. Entropically patchy particles: engineering valence through shape entropy. *ACS Nano* **8**, 931–940 (2013).
- [50] Petukhov, A. V., Tuinier, R. & Vroege, G. J. Entropic patchiness: effects of colloid shape and depletion. *Current Opinion in Colloid & Interface Science* **30**, 54–61 (2017).
- [51] Torquato, S. & Jiao, Y. Dense packings of the platonic and archimedean solids. *Nature* **460**, 876 (2009).
- [52] Damasceno, P. F., Engel, M. & Glotzer, S. C. Predictive self-assembly of polyhedra into complex structures. *Science* **337**, 453–457 (2012).
- [53] Avendaño, C. & Escobedo, F. A. Packing, entropic patchiness, and self-assembly of non-convex colloidal particles: a simulation perspective. *Current Opinion in Colloid & Interface Science* **30**, 62–69 (2017).



- [54] Chen, Z., Ye, S., Evans, S. D., Ge, Y., Zhu, Z., Tu, Y. & Yang, X. Confined assembly of hollow carbon spheres in carbonaceous nanotube: a spheres-in-tube carbon nanostructure with hierarchical porosity for high-performance supercapacitor. *Small* **14**, 1704015 (2018).
- [55] Maeda, H. & Maeda, Y. Liquid crystal formation in suspensions of hard rodlike colloidal particles: direct observation of particle arrangement and self-ordering behavior. *Physical Review Letters* **90**, 018303 (2003).
- [56] Mohraz, A. & Solomon, M. J. Direct visualization of colloidal rod assembly by confocal microscopy. *Langmuir* **21**, 5298–5306 (2005).
- [57] Solomon, M. J. & Spicer, P. T. Microstructural regimes of colloidal rod suspensions, gels, and glasses. *Soft Matter* **6**, 1391–1400 (2010).
- [58] Mukhija, D. & Solomon, M. J. Nematic order in suspensions of colloidal rods by application of a centrifugal field. *Soft Matter* **7**, 540–545 (2011).
- [59] Kuijk, A., van Blaaderen, A. & Imhof, A. Synthesis of monodisperse, rodlike silica colloids with tunable aspect ratio. *Journal of the American Chemical Society* **133**, 2346–2349 (2011).
- [60] Kuijk, A., Byelov, D. V., Petukhov, A. V., van Blaaderen, A. & Imhof, A. Phase behavior of colloidal silica rods. *Faraday discussions* **159**, 181–199 (2012).
- [61] Ozaki, M., Kratochvil, S. & Matijević, E. Formation of monodispersed spindle-type hematite particles. *Journal of Colloid and Interface Science* **102**, 146–151 (1984).
- [62] Ozaki, M. & Matijević, E. Preparation and magnetic properties of monodispersed spindle-type  $\gamma$ -Fe<sub>2</sub>O<sub>3</sub> particles. *Journal of Colloid and Interface Science* **107**, 199–203 (1985).
- [63] Ishikawa, T. & Matijević, E. Formation of monodispersed pure and coated spindle-type iron particles. *Langmuir* **4**, 26–31 (1988).
- [64] Zoldesi, C. I. & Imhof, A. Synthesis of monodisperse colloidal spheres, capsules, and microballoons by emulsion templating. *Advanced Materials* **17**, 924–928 (2005).
- [65] Im, S. H., Jeong, U. & Xia, Y. Polymer hollow particles with controllable holes in their surfaces. *Nature Materials* **4**, 671 (2005).
- [66] Riley, E. K. & Liddell, C. M. Confinement-controlled self assembly of colloids with simultaneous isotropic and anisotropic cross-section. *Langmuir* **26**, 11648–11656 (2010).
- [67] Sacanna, S., Irvine, W., Chaikin, P. M. & Pine, D. J. Lock and key colloids. *Nature* **464**, 575 (2010).
- [68] Marechal, M., Kortschot, R. J., Demirörs, A. F., Imhof, A. & Dijkstra, M. Phase behavior and structure of a new colloidal model system of bowl-shaped particles. *Nano Letters* **10**, 1907–1911 (2010).
- [69] Jing, W., Du, S. & Zhang, Z. Synthesis of polystyrene particles with precisely controlled degree of concaveness. *Polymers* **10**, 458 (2018).
- [70] Rossi, L., Sacanna, S., Irvine, W. T., Chaikin, P. M., Pine, D. J. & Philipse, A. P. Cubic crystals from cubic colloids. *Soft Matter* **7**, 4139–4142 (2011).
- [71] Meijer, J.-M., Hagemans, F., Rossi, L., Byelov, D. V., Castillo, S. I., Snigirev, A., Snigireva, I., Philipse, A. P. & Petukhov, A. V. Self-assembly of colloidal cubes via

- vertical deposition. *Langmuir* **28**, 7631–7638 (2012).
- [72] Johnson, P. M., van Kats, C. M. & van Blaaderen, A. Synthesis of colloidal silica dumbbells. *Langmuir* **21**, 11510–11517 (2005).
- [73] Marechal, M. & Dijkstra, M. Colloidal hard dumbbells under gravity: structure and crystallization. *Soft Matter* **7**, 1397–1408 (2011).
- [74] Forster, J. D., Park, J.-G., Mittal, M., Noh, H., Schreck, C. F., O'Hern, C. S., Cao, H., Furst, E. M. & Dufresne, E. R. Assembly of optical-scale dumbbells into dense photonic crystals. *ACS Nano* **5**, 6695–6700 (2011).
- [75] Sugimoto, T., Khan, M. M., Muramatsu, A. & Itoh, H. Formation mechanism of monodisperse peanut-type  $\alpha$ -Fe<sub>2</sub>O<sub>3</sub> particles from condensed ferric hydroxide gel. *Colloids and Surfaces A: Physicochemical and Engineering Aspects* **79**, 233–247 (1993).
- [76] Lee, S. H., Gerbode, S. J., John, B. S., Wolfgang, A. K., Escobedo, F. A., Cohen, I. & Liddell, C. M. Synthesis and assembly of nonspherical hollow silica colloids under confinement. *Journal of Materials Chemistry* **18**, 4912–4916 (2008).
- [77] Sheu, H., El-Aasser, M. & Vanderhoff, J. Phase separation in polystyrene latex interpenetrating polymer networks. *Journal of Polymer Science Part A: Polymer Chemistry* **28**, 629–651 (1990).
- [78] Chaturvedi, N., Juluri, B. K., Hao, Q., Huang, T. J. & Velegol, D. Simple fabrication of snowman-like colloids. *Journal of Colloid and Interface Science* **371**, 28–33 (2012).
- [79] van Blaaderen, A. Chemistry: colloidal molecules and beyond. *Science* **301**, 470–471 (2003).
- [80] Duguet, E., Désert, A., Perro, A. & Ravaine, S. Design and elaboration of colloidal molecules: an overview. *Chemical Society Reviews* **40**, 941–960 (2011).
- [81] Zhang, Z., Keys, A. S., Chen, T. & Glotzer, S. C. Self-assembly of patchy particles into diamond structures through molecular mimicry. *Langmuir* **21**, 11547–11551 (2005).
- [82] Noya, E. G., Vega, C., Doye, J. P. & Louis, A. A. The stability of a crystal with diamond structure for patchy particles with tetrahedral symmetry. *The Journal of Chemical Physics* **132**, 234511 (2010).
- [83] Romano, F., Sanz, E. & Sciortino, F. Crystallization of tetrahedral patchy particles in silico. *The Journal of Chemical Physics* **134**, 174502 (2011).
- [84] Morphew, D., Shaw, J., Avins, C. & Chakrabarti, D. Programming hierarchical self-assembly of patchy particles into colloidal crystals via colloidal molecules. *ACS Nano* **12**, 2355–2364 (2018).
- [85] Wang, Y., Wang, Y., Breed, D. R., Manoharan, V. N., Feng, L., Hollingsworth, A. D., Weck, M. & Pine, D. J. Colloids with valence and specific directional bonding. *Nature* **491**, 51–55 (2012).
- [86] Sacanna, S., Rossi, L. & Pine, D. J. Magnetic click colloidal assembly. *Journal of the American Chemical Society* **134**, 6112–6115 (2012).
- [87] Hong, L., Cacciuto, A., Luijten, E. & Granick, S. Clusters of amphiphilic colloidal spheres. *Langmuir* **24**, 621–625 (2008).
- [88] Manoharan, V. N., Elsesser, M. T. & Pine, D. J. Dense packing and symmetry in small clusters of microspheres. *Science* **301**, 483–487 (2003).

- [89] Yin, Y. & Xia, Y. Self-assembly of monodispersed spherical colloids into complex aggregates with well-defined sizes, shapes, and structures. *Advanced Materials* **13**, 267–271 (2001).
- [90] Kraft, D. J., Vlug, W. S., van Kats, C. M., van Blaaderen, A., Imhof, A. & Kegel, W. K. Self-assembly of colloids with liquid protrusions. *Journal of the American Chemical Society* **131**, 1182–1186 (2008).
- [91] Kraft, D. J., Groenewold, J. & Kegel, W. K. Colloidal molecules with well-controlled bond angles. *Soft Matter* **5**, 3823–3826 (2009).
- [92] Schade, N. B., Holmes-Cerfon, M. C., Chen, E. R., Aronzon, D., Collins, J. W., Fan, J. A., Capasso, F. & Manoharan, V. N. Tetrahedral colloidal clusters from random parking of bidisperse spheres. *Physical Review Letters* **110**, 148303 (2013).
- [93] Meng, G., Arkus, N., Brenner, M. P. & Manoharan, V. N. The free-energy landscape of clusters of attractive hard spheres. *Science* **327**, 560–563 (2010).
- [94] Wang, Y., Wang, Y., Zheng, X., Yi, G.-R., Sacanna, S., Pine, D. J. & Weck, M. Three-dimensional lock and key colloids. *Journal of the American Chemical Society* **136**, 6866–6869 (2014).
- [95] Kraft, D. J., Ni, R., Smallenburg, F., Hermes, M., Yoon, K., Weitz, D. A., van Blaaderen, A., Groenewold, J., Dijkstra, M. & Kegel, W. K. Surface roughness directed self-assembly of patchy particles into colloidal micelles. *Proceedings of the National Academy of Sciences of the United States of America* **109**, 10787–10792 (2012).
- [96] Wolters, J. R., Avisati, G., Hagemans, F., Vissers, T., Kraft, D. J., Dijkstra, M. & Kegel, W. K. Self-assembly of ‘Mickey Mouse’ shaped colloids into tube-like structures: experiments and simulations. *Soft Matter* **11**, 1067–1077 (2015).
- [97] Kegel, W. K., Breed, D., Elsesser, M. & Pine, D. J. Formation of anisotropic polymer colloids by disparate relaxation times. *Langmuir* **22**, 7135–7136 (2006).
- [98] Kim, J.-W., Larsen, R. J. & Weitz, D. A. Synthesis of nonspherical colloidal particles with anisotropic properties. *Journal of the American Chemical Society* **128**, 14374–14377 (2006).
- [99] Kim, J.-W., Larsen, R. J. & Weitz, D. A. Uniform nonspherical colloidal particles with tunable shapes. *Advanced Materials* **19**, 2005–2009 (2007).
- [100] Park, J.-G., Forster, J. D. & Dufresne, E. R. Synthesis of colloidal particles with the symmetry of water molecules. *Langmuir* **25**, 8903–8906 (2009).
- [101] Reculosa, S., Poncet-Legrand, C., Ravaine, S., Mingotaud, C., Duguet, E. & Bourgeat-Lami, E. Syntheses of raspberry-like silica/polystyrene materials. *Chemistry of Materials* **14**, 2354–2359 (2002).
- [102] Reculosa, S., Mingotaud, C., Bourgeat-Lami, E., Duguet, E. & Ravaine, S. Synthesis of daisy-shaped and multipod-like silica/polystyrene nanocomposites. *Nano Letters* **4**, 1677–1682 (2004).
- [103] Perro, A., Duguet, E., Lambert, O., Taveau, J.-C., Bourgeat-Lami, E. & Ravaine, S. A chemical synthetic route towards ‘colloidal molecules’. *Angewandte Chemie* **121**, 367–371 (2009).
- [104] Ducrot, É., He, M., Yi, G.-R. & Pine, D. J. Colloidal alloys with preassembled clusters

- and spheres. *Nature Materials* **16**, 652 (2017).
- [105] Baker, W., Mason, W. & Heiss, J. Mechanical properties of discrete polymer molecules. *Journal of Polymer Science* **8**, 129–155 (1952).
- [106] Saunders, B. R. & Vincent, B. Microgel particles as model colloids: theory, properties and applications. *Advances in Colloid and Interface Science* **80**, 1–25 (1999).
- [107] Heskins, M. & Guillet, J. E. Solution properties of poly(*N*-isopropylacrylamide). *Journal of Macromolecular Science: Part A - Chemistry* **2**, 1441–1455 (1968).
- [108] Schild, H. G. Poly(*N*-isopropylacrylamide): experiment, theory and application. *Progress in Polymer Science* **17**, 163–249 (1992).
- [109] Rubinstein, M. & Colby, R. H. *Polymer physics*, vol. 23 (Oxford University Press New York, 2003).
- [110] Pelton, R. & Chibante, P. Preparation of aqueous latices with *N*-isopropylacrylamide. *Colloids and Surfaces* **20**, 247–256 (1986).
- [111] Duracher, D., Eläissari, A. & Pichot, C. Preparation of poly(*N*-isopropylmethacrylamide) latexes - kinetic studies and characterization. *Journal of Polymer Science Part A: Polymer Chemistry* **37**, 1823–1837 (1999).
- [112] Duracher, D., Eläissari, A. & Pichot, C. Characterization of cross-linked poly(*N*-isopropylmethacrylamide) microgel latexes. *Colloid and Polymer Science* **277**, 905–913 (1999).
- [113] Pelton, R. Temperature-sensitive aqueous microgels. *Advances in Colloid and Interface Science* **85**, 1–33 (2000).
- [114] Pich, A. & Richtering, W. Microgels by precipitation polymerization: synthesis, characterization, and functionalization. In *Chemical Design of Responsive Microgels*, 1–37 (Springer, 2010).
- [115] Brijjita, J. & Schurtenberger, P. Responsive hydrogel colloids: structure, interactions, phase behaviour, and equilibrium and non-equilibrium transitions of microgel dispersions. *Current Opinion in Colloid & Interface Science* (2019).
- [116] Shibayama, M. & Tanaka, T. Volume phase transition and related phenomena of polymer gels. In *Responsive gels: volume transitions I*, 1–62 (Springer, 1993).
- [117] Wiese, S., Spiess, A. C. & Richtering, W. Microgel-stabilized smart emulsions for biocatalysis. *Angewandte Chemie* **125**, 604–607 (2013).
- [118] Kiser, P. F., Wilson, G. & Needham, D. Lipid-coated microgels for the triggered release of doxorubicin. *Journal of Controlled Release* **68**, 9–22 (2000).
- [119] Pérez, J. H., López, M. S.-P., López-Cabarcos, E. & López-Ruiz, B. Amperometric tyrosinase biosensor based on polyacrylamide microgels. *Biosensors and Bioelectronics* **22**, 429–439 (2006).
- [120] Serpe, M. J., Kim, J. & Lyon, L. A. Colloidal hydrogel microlenses. *Advanced Materials* **16**, 184–187 (2004).
- [121] Varga, I., Gilányi, T., Meszaros, R., Filipcsei, G. & Zrinyi, M. Effect of cross-link density on the internal structure of poly(*N*-isopropylacrylamide) microgels. *The Journal of Physical Chemistry B* **105**, 9071–9076 (2001).
- [122] Saunders, B. R. On the structure of poly(*N*-isopropylacrylamide) microgel particles.

*Langmuir* **20**, 3925–3932 (2004).

- [123] Reufer, M., Diaz-Leyva, P., Lynch, I. & Scheffold, F. Temperature-sensitive poly(*N*-isopropyl-acrylamide) microgel particles: A light scattering study. *The European Physical Journal E* **28**, 165–171 (2009).
- [124] Boon, N. & Schurtenberger, P. Swelling of micro-hydrogels with a crosslinker gradient. *Physical Chemistry Chemical Physics* **19**, 23740–23746 (2017).
- [125] Wu, X., Pelton, R., Hamielec, A., Woods, D. & McPhee, W. The kinetics of poly(*N*-isopropylacrylamide) microgel latex formation. *Colloid and Polymer Science* **272**, 467–477 (1994).
- [126] Conley, G. M., Aebischer, P., Nöjd, S., Schurtenberger, P. & Scheffold, F. Jamming and overpacking fuzzy microgels: deformation, interpenetration, and compression. *Science Advances* **3**, e1700969 (2017).
- [127] Mohanty, P. S., Nöjd, S., van Gruijthuisen, K., Crassous, J. J., Obiols-Rabasa, M., Schweins, R., Stradner, A. & Schurtenberger, P. Interpenetration of polymeric microgels at ultrahigh densities. *Scientific Reports* **7**, 1487 (2017).
- [128] Pelton, R., Pelton, H., Morphesis, A. & Rowell, R. Particle sizes and electrophoretic mobilities of poly(*N*-isopropylacrylamide) latex. *Langmuir* **5**, 816–818 (1989).
- [129] Daly, E. & Saunders, B. R. Temperature-dependent electrophoretic mobility and hydrodynamic radius measurements of poly(*N*-isopropylacrylamide) microgel particles: structural insights. *Physical Chemistry Chemical Physics* **2**, 3187–3193 (2000).
- [130] Wu, J., Zhou, B. & Hu, Z. Phase behavior of thermally responsive microgel colloids. *Physical Review Letters* **90**, 048304 (2003).
- [131] Gottwald, D., Likos, C., Kahl, G. & Löwen, H. Phase behavior of ionic microgels. *Physical Review Letters* **92**, 068301 (2004).
- [132] Senff, H. & Richtering, W. Temperature sensitive microgel suspensions: colloidal phase behavior and rheology of soft spheres. *The Journal of Chemical Physics* **111**, 1705–1711 (1999).
- [133] Hellweg, T., Dewhurst, C., Brückner, E., Kratz, K. & Eimer, W. Colloidal crystals made of poly(*N*-isopropylacrylamide) microgel particles. *Colloid and Polymer Science* **278**, 972–978 (2000).
- [134] Debord, J. D. & Lyon, L. A. Thermoresponsive photonic crystals. *The Journal of Physical Chemistry B* **104**, 6327–6331 (2000).
- [135] Lyon, L. A., Debord, J. D., Debord, S. B., Jones, C. D., McGrath, J. G. & Serpe, M. J. Microgel colloidal crystals. *The Journal of Physical Chemistry B* **108**, 19099–19108 (2004).
- [136] St. John, A. N., Breedveld, V. & Lyon, L. A. Phase behavior in highly concentrated assemblies of microgels with soft repulsive interaction potentials. *The Journal of Physical Chemistry B* **111**, 7796–7801 (2007).
- [137] Meng, Z., Cho, J. K., Debord, S., Breedveld, V. & Lyon, L. A. Crystallization behavior of soft, attractive microgels. *The Journal of Physical Chemistry B* **111**, 6992–6997 (2007).
- [138] Cho, J. K., Meng, Z., Lyon, L. A. & Breedveld, V. Tunable attractive and repulsive interactions between pH-responsive microgels. *Soft Matter* **5**, 3599–3602 (2009).
- [139] Lyon, L. A. & Fernandez-Nieves, A. The polymer/colloid duality of microgel suspen-

- sions. *Annual Review of Physical Chemistry* **63**, 25–43 (2012).
- [140] Romeo, G., Fernandez-Nieves, A., Wyss, H. M., Acierno, D. & Weitz, D. A. Temperature-controlled transitions between glass, liquid, and gel states in dense p-NIPA suspensions. *Advanced Materials* **22**, 3441–3445 (2010).
- [141] Yunker, P. J., Chen, K., Gratale, M. D., Lohr, M. A., Still, T. & Yodh, A. Physics in ordered and disordered colloidal matter composed of poly(*N*-isopropylacrylamide) microgel particles. *Reports on Progress in Physics* **77**, 056601 (2014).
- [142] Heyes, D. & Brańka, A. Interactions between microgel particles. *Soft Matter* **5**, 2681–2685 (2009).
- [143] Fritz, G., Schädler, V., Willenbacher, N. & Wagner, N. J. Electrosteric stabilization of colloidal dispersions. *Langmuir* **18**, 6381–6390 (2002).
- [144] Riest, J., Mohanty, P., Schurtenberger, P. & Likos, C. N. Coarse-graining of ionic microgels: theory and experiment. *Zeitschrift für Physikalische Chemie* **226**, 711–735 (2012).
- [145] Paloli, D., Mohanty, P. S., Crassous, J. J., Zaccarelli, E. & Schurtenberger, P. Fluid-solid transitions in soft-repulsive colloids. *Soft Matter* **9**, 3000–3004 (2013).
- [146] Mohanty, P. S., Paloli, D., Crassous, J. J., Zaccarelli, E. & Schurtenberger, P. Effective interactions between soft-repulsive colloids: experiments, theory, and simulations. *The Journal of Chemical Physics* **140**, 094901 (2014).
- [147] Colla, T. & Likos, C. N. Effective interactions in polydisperse systems of penetrable macroions. *Molecular Physics* **113**, 2496–2510 (2015).
- [148] Bergman, M. J., Gnan, N., Obiols-Rabasa, M., Meijer, J.-M., Rovigatti, L., Zaccarelli, E. & Schurtenberger, P. A new look at effective interactions between microgel particles. *Nature Communications* **9**, 5039 (2018).
- [149] Verwey, E. J. W. & Overbeek, J. T. G. *Theory of the stability of lyophobic colloids* (Elsevier, 1948).
- [150] Rasmusson, M., Routh, A. & Vincent, B. Flocculation of microgel particles with sodium chloride and sodium polystyrene sulfonate as a function of temperature. *Langmuir* **20**, 3536–3542 (2004).
- [151] Wu, J., Huang, G. & Hu, Z. Interparticle potential and the phase behavior of temperature-sensitive microgel dispersions. *Macromolecules* **36**, 440–448 (2003).
- [152] Zhou, J., Wang, G., Zou, L., Tang, L., Marquez, M. & Hu, Z. Viscoelastic behavior and in vivo release of microgel dispersions with inverse thermo-reversible gelation. *Bio-macromolecules* **9**, 142 (2008).
- [153] Zaccone, A., Crassous, J. J., Béri, B. & Ballauff, M. Quantifying the reversible association of thermosensitive nanoparticles. *Physical Review Letters* **107**, 168303 (2011).
- [154] Holmqvist, P., Mohanty, P., Nägele, G., Schurtenberger, P. & Heinen, M. Structure and dynamics of loosely cross-linked ionic microgel dispersions in the fluid regime. *Physical Review Letters* **109**, 048302 (2012).
- [155] Nöjd, S., Mohanty, P. S., Bagheri, P., Yethiraj, A. & Schurtenberger, P. Electric field driven self-assembly of ionic microgels. *Soft Matter* **9**, 9199–9207 (2013).
- [156] Zaccone, A., Crassous, J. J. & Ballauff, M. Colloidal gelation with variable attraction energy. *The Journal of Chemical Physics* **138**, 104908 (2013).

- [157] Dybal, J., Trchová, M. & Schmidt, P. The role of water in structural changes of poly(*N*-isopropylacrylamide) and poly(*N*-isopropylmethacrylamide) studied by FTIR, Raman spectroscopy and quantum chemical calculations. *Vibrational Spectroscopy* **51**, 44–51 (2009).
- [158] Appel, J., de Lange, N., van der Kooij, H. M., van de Laar, T., ten Hove, J. B., Kodger, T. E. & Sprakel, J. Temperature controlled sequential gelation in composite microgel suspensions. *Particle & Particle Systems Characterization* **32**, 764–770 (2015).
- [159] Minami, S., Watanabe, T., Suzuki, D. & Urayama, K. Viscoelasticity of dense suspensions of thermosensitive microgel mixtures undergoing colloidal gelation. *Soft Matter* **14**, 1596–1607 (2018).
- [160] Immink, J. N., Maris, J. E., Crassous, J. J., Stenhammar, J. & Schurtenberger, P. Reversible formation of thermoresponsive binary particle gels with tunable structural and mechanical properties. *ACS Nano* (2019).
- [161] Ngai, T., Behrens, S. H. & Auweter, H. Novel emulsions stabilized by pH and temperature sensitive microgels. *Chemical Communications* 331–333 (2005).
- [162] Ngai, T., Auweter, H. & Behrens, S. H. Environmental responsiveness of microgel particles and particle-stabilized emulsions. *Macromolecules* **39**, 8171–8177 (2006).
- [163] Tsuji, S. & Kawaguchi, H. Thermosensitive Pickering emulsion stabilized by poly(*N*-isopropylacrylamide)-carrying particles. *Langmuir* **24**, 3300–3305 (2008).
- [164] Brugger, B., Rosen, B. A. & Richtering, W. Microgels as stimuli-responsive stabilizers for emulsions. *Langmuir* **24**, 12202–12208 (2008).
- [165] Monteux, C., Marliere, C., Paris, P., Pantoustier, N., Sanson, N. & Perrin, P. Poly(*N*-isopropylacrylamide) microgels at the oil–water interface: interfacial properties as a function of temperature. *Langmuir* **26**, 13839–13846 (2010).
- [166] Destribats, M., Lapeyre, V., Wolfs, M., Sellier, E., Leal-Calderon, F., Ravaine, V. & Schmitt, V. Soft microgels as Pickering emulsion stabilisers: role of particle deformability. *Soft Matter* **7**, 7689–7698 (2011).
- [167] Richtering, W. Responsive emulsions stabilized by stimuli-sensitive microgels: emulsions with special non-Pickering properties. *Langmuir* **28**, 17218–17229 (2012).
- [168] Zhang, J. & Pelton, R. Poly(*N*-isopropylacrylamide) at the air/water interface. *Langmuir* **12**, 2611–2612 (1996).
- [169] Zhang, J. & Pelton, R. The dynamic behavior of poly(*N*-isopropylacrylamide) at the air/water interface. *Colloids and Surfaces A: Physicochemical and Engineering Aspects* **156**, 111–122 (1999).
- [170] Deshmukh, O. S., van den Ende, D., Stuart, M. C., Mugele, F. & Duits, M. H. Hard and soft colloids at fluid interfaces: adsorption, interactions, assembly & rheology. *Advances in Colloid and Interface Science* **222**, 215–227 (2015).
- [171] Style, R. W., Isa, L. & Dufresne, E. R. Adsorption of soft particles at fluid interfaces. *Soft Matter* **11**, 7412–7419 (2015).
- [172] Mehrabian, H., Harting, J. & Snoeijer, J. H. Soft particles at a fluid interface. *Soft Matter* **12**, 1062–1073 (2016).
- [173] Brugger, B., Rütten, S., Phan, K.-H., Möller, M. & Richtering, W. The colloidal supra-

- structure of smart microgels at oil–water interfaces. *Angewandte Chemie* **121**, 4038–4041 (2009).
- [174] Destribats, M., Lapeyre, V., Sellier, E., Leal-Calderon, F., Schmitt, V. & Ravaine, V. Water-in-oil emulsions stabilized by water-dispersible poly(*N*-isopropylacrylamide) microgels: understanding anti-Finkle behavior. *Langmuir* **27**, 14096–14107 (2011).
- [175] Geisel, K., Isa, L. & Richtering, W. Unraveling the 3D localization and deformation of responsive microgels at oil/water interfaces: a step forward in understanding soft emulsion stabilizers. *Langmuir* **28**, 15770–15776 (2012).
- [176] Komura, S., Hirose, Y. & Nonomura, Y. Adsorption of colloidal particles to curved interfaces. *The Journal of Chemical Physics* **124**, 2411041–2411044 (2006).
- [177] Ershov, D., Sprakel, J., Appel, J., Stuart, M. A. C. & van der Gucht, J. Capillarity-induced ordering of spherical colloids on an interface with anisotropic curvature. *Proceedings of the National Academy of Sciences of the United States of America* **110**, 9220–9224 (2013).
- [178] Pieranski, P. Two-dimensional interfacial colloidal crystals. *Physical Review Letters* **45**, 569 (1980).
- [179] Hurd, A. J. The electrostatic interaction between interfacial colloidal particles. *Journal of Physics A: Mathematical and General* **18**, L1055 (1985).
- [180] Lucassen, J. Capillary forces between solid particles in fluid interfaces. *Colloids and Surfaces* **65**, 131–137 (1992).
- [181] Vella, D. & Mahadevan, L. The ‘cheerios effect’. *American Journal of Physics* **73**, 817–825 (2005).
- [182] Yi, G.-R., Manoharan, V. N., Michel, E., Elsesser, M. T., Yang, S.-M. & Pine, D. J. Colloidal clusters of silica or polymer microspheres. *Advanced Materials* **16**, 1204–1208 (2004).
- [183] Cho, Y.-S., Yi, G.-R., Kim, S.-H., Pine, D. J. & Yang, S.-M. Colloidal clusters of microspheres from water-in-oil emulsions. *Chemistry of Materials* **17**, 5006–5013 (2005).
- [184] Cho, Y.-S., Yi, G.-R., Lim, J.-M., Kim, S.-H., Manoharan, V. N., Pine, D. J. & Yang, S.-M. Self-organization of bidisperse colloids in water droplets. *Journal of the American Chemical Society* **127**, 15968–15975 (2005).
- [185] Cho, Y.-S., Yi, G.-R., Kim, S.-H., Elsesser, M. T., Breed, D. R. & Yang, S.-M. Homogeneous and heterogeneous binary colloidal clusters formed by evaporation-induced self-assembly inside droplets. *Journal of Colloid and Interface Science* **318**, 124–133 (2008).
- [186] Wagner, C. S., Lu, Y. & Wittemann, A. Preparation of submicrometer-sized clusters from polymer spheres using ultrasonication. *Langmuir* **24**, 12126–12128 (2008).
- [187] Wagner, C. S., Fischer, B., May, M. & Witteman, A. Templated assembly of polymer particles into mesoscopic clusters with well-defined configurations. *Colloid and Polymer Science* **288**, 487–498 (2010).
- [188] Lauga, E. & Brenner, M. P. Evaporation-driven assembly of colloidal particles. *Physical Review Letters* **93**, 238301 (2004).
- [189] Manoharan, V. N. Colloidal spheres confined by liquid droplets: Geometry, physics, and physical chemistry. *Solid State Communications* **139**, 557–561 (2006).



- [190] Sloane, N. J., Hardin, R. H., Duff, T. & Conway, J. H. Minimal-energy clusters of hard spheres. *Discrete & Computational Geometry* **14**, 237–259 (1995).
- [191] Hinds, W. C. *Aerosol technology: properties, behavior, and measurement of airborne particles* (John Wiley & Sons, 2012).
- [192] Collins, D. J., Neild, A., Liu, A.-Q., Ai, Y. *et al.* The poisson distribution and beyond: methods for microfluidic droplet production and single cell encapsulation. *Lab on a Chip* **15**, 3439–3459 (2015).
- [193] Zerrouki, D., Rotenberg, B., Abramson, S., Baudry, J., Goubault, C., Leal-Calderon, F., Pine, D. J. & Bibette, J. Preparation of doublet, triangular, and tetrahedral colloidal clusters by controlled emulsification. *Langmuir* **22**, 57–62 (2006).
- [194] Yi, G.-R., Manoharan, V. N., Klein, S., Brzezinska, K. R., Pine, D. J., Lange, F. E. & Yang, S.-M. Monodisperse micrometer-scale spherical assemblies of polymer particles. *Advanced Materials* **14**, 1137–1140 (2002).
- [195] Yi, G.-R., Thorsen, T., Manoharan, V. N., Hwang, M.-J., Jeon, S.-J., Pine, D. J., Quake, S. R. & Yang, S.-M. Generation of uniform colloidal assemblies in soft microfluidic devices. *Advanced Materials* **15**, 1300–1304 (2003).
- [196] Kim, S.-H., Lee, S. Y., Yi, G.-R., Pine, D. J., Lange, F. E. & Yang, S.-M. Microwave-assisted self-organization of colloidal particles in confining aqueous droplets. *Journal of the American Chemical Society* **128**, 10897–10904 (2006).
- [197] Levin, Y. Electrostatic correlations: from plasma to biology. *Reports on Progress in Physics* **65**, 1577 (2002).
- [198] Colla, T., Blaak, R. & Likos, C. N. Quenching of fully symmetric mixtures of oppositely charged microgels: the role of soft stiffness. *Soft Matter* **14**, 5106–5120 (2018).
- [199] Go, D., Kodger, T. E., Sprakel, J. & Kuehne, A. J. C. Programmable co-assembly of oppositely charged microgels. *Soft Matter* **10**, 8060–8065 (2014).
- [200] Tagliacucchi, M., Zou, F. & Weiss, E. A. Kinetically controlled self-assembly of latex-microgel core-satellite particles. *The Journal of Physical Chemistry Letters* **5**, 2775–2780 (2014).
- [201] Demirörs, A. F., Stiefelhagen, J. C., Vissers, T., Smalenburg, F., Dijkstra, M., Imhof, A. & van Blaaderen, A. Long-ranged oppositely charged interactions for designing new types of colloidal clusters. *Physical Review X* **5**, 021012 (2015).
- [202] Fischer, E. Einfluss der Konfiguration auf die Wirkung der Enzyme. *Berichte der Deutschen Chemischen Gesellschaft* **27**, 2985–2993 (1894).
- [203] Sacanna, S., Irvine, W. T., Rossi, L. & Pine, D. J. Lock and key colloids through polymerization-induced buckling of monodisperse silicon oil droplets. *Soft Matter* **7**, 1631–1634 (2011).
- [204] Mihut, A. M., Stenqvist, B., Lund, M., Schurtenberger, P. & Crassous, J. J. Assembling oppositely charged lock and key responsive colloids: a mesoscale analog of adaptive chemistry. *Science Advances* **3**, e1700321 (2017).
- [205] McPhee, W., Tam, K. C. & Pelton, R. Poly(*N*-isopropylacrylamide) latices prepared with sodium dodecyl sulfate. *Journal of Colloid and Interface Science* **156**, 24–30 (1993).
- [206] Stieger, M., Richtering, W., Pedersen, J. S. & Lindner, P. Small-angle neutron scattering

- study of structural changes in temperature sensitive microgel colloids. *The Journal of Chemical Physics* **120**, 6197–6206 (2004).
- [207] Acciario, R., Gilanyi, T. & Varga, I. Preparation of monodisperse poly(*N*-isopropylacrylamide) microgel particles with homogenous cross-link density distribution. *Langmuir* **27**, 7917–7925 (2011).
- [208] Tam, K., Ragaram, S. & Pelton, R. Interaction of surfactants with poly(*N*-isopropylacrylamide) microgel latexes. *Langmuir* **10**, 418–422 (1994).
- [209] von Nessen, K., Karg, M. & Hellweg, T. Thermoresponsive poly-(*N*-isopropylmethacrylamide) microgels: tailoring particle size by interfacial tension control. *Polymer* **54**, 5499–5510 (2013).
- [210] Kubota, K., Hamano, K., Kuwahara, N., Fujishige, S. & Ando, I. Characterization of poly(*N*-isopropylmethacrylamide) in water. *Polymer Journal* **22**, 1051 (1990).
- [211] Feeney, P. J., Napper, D. H. & Gilbert, R. G. Coagulative nucleation and particle size distributions in emulsion polymerization. *Macromolecules* **17**, 2520–2529 (1984).
- [212] Hirotsu, S. Phase transition of a polymer gel in pure and mixed solvent media. *Journal of the Physical Society of Japan* **56**, 233–242 (1987).
- [213] Hu, Z. & Huang, G. A new route to crystalline hydrogels, guided by a phase diagram. *Angewandte Chemie* **115**, 4947–4950 (2003).
- [214] Huang, G. & Hu, Z. Phase behavior and stabilization of microgel arrays. *Macromolecules* **40**, 3749–3756 (2007).
- [215] Cho, E. C., Kim, J.-W., Fernández-Nieves, A. & Weitz, D. A. Highly responsive hydrogel scaffolds formed by three-dimensional organization of microgel nanoparticles. *Nano Letters* **8**, 168–172 (2008).
- [216] Shah, R. K., Kim, J.-W. & Weitz, D. A. Monodisperse stimuli-responsive colloidosomes by self-assembly of microgels in droplets. *Langmuir* **26**, 1561–1565 (2009).
- [217] Gelissen, A. P., Schmid, A. J., Plamper, F. A., Pergushov, D. V. & Richtering, W. Quaternized microgels as soft templates for polyelectrolyte layer-by-layer assemblies. *Polymer* **55**, 1991–1999 (2014).
- [218] Conley, G. M., Nöjd, S., Braibanti, M., Schurtenberger, P. & Scheffold, F. Superresolution microscopy of the volume phase transition of pNIPAM microgels. *Colloids and Surfaces A: Physicochemical and Engineering Aspects* **499**, 18–23 (2016).
- [219] Still, T., Chen, K., Alsayed, A. M., Aptowicz, K. B. & Yodh, A. Synthesis of micrometer-size poly(*N*-isopropylacrylamide) microgel particles with homogeneous crosslinker density and diameter control. *Journal of Colloid and Interface Science* **405**, 96–102 (2013).
- [220] Reis, A. V., Fajardo, A. R., Schuquel, I. T., Guilherme, M. R., Vidotti, G. J., Rubira, A. F. & Muniz, E. C. Reaction of glycidyl methacrylate at the hydroxyl and carboxylic groups of poly(vinyl alcohol) and poly(acrylic acid): is this reaction mechanism still unclear? *The Journal of Organic Chemistry* **74**, 3750–3757 (2009).
- [221] Liu, R., Milani, A. H., Freemont, T. J. & Saunders, B. R. Doubly crosslinked pH-responsive microgels prepared by particle inter-penetration: swelling and mechanical properties. *Soft Matter* **7**, 4696–4704 (2011).
- [222] Yuan, Q., Gu, J., Zhao, Y.-n., Yao, L., Guan, Y. & Zhang, Y. Synthesis of a colloidal

- molecule from soft microgel spheres. *ACS Macro Letters* **5**, 565–568 (2016).
- [223] Kim, J., Nayak, S. & Lyon, L. A. Bioresponsive hydrogel microlenses. *Journal of the American Chemical Society* **127**, 9588–9592 (2005).
- [224] Ali, M. M., Su, S., Filipe, C. D., Pelton, R. & Li, Y. Enzymatic manipulations of DNA oligonucleotides on microgel: towards development of dna–microgel bioassays. *Chemical Communications* 4459–4461 (2007).
- [225] Staros, J. V., Wright, R. W. & Swingle, D. M. Enhancement by *n*-hydroxysulfosuccinimide of water-soluble carbodiimide-mediated coupling reactions. *Analytical Biochemistry* **156**, 220–222 (1986).
- [226] Debord, J. D. & Lyon, L. A. On the unusual stability of succinimidyl esters in pNIPAm-AAc microgels. *Bioconjugate Chemistry* **18**, 601–604 (2007).
- [227] Meester, V. & Kraft, D. J. Spherical, dimpled, and crumpled hybrid colloids with tunable surface morphology. *Langmuir* **32**, 10668–10677 (2016).
- [228] Blackley, D. C. *Emulsion polymerisation: theory and practice* (Applied Science Publishers London, 1975).
- [229] Crassous, J. J., Dietsch, H., Pfeiderer, P., Malik, V., Diaz, A., Hirshi, L. A., Drechsler, M. & Schurtenberger, P. Preparation and characterization of ellipsoidal-shaped thermo-sensitive microgel colloids with tailored aspect ratios. *Soft Matter* **8**, 3538–3548 (2012).
- [230] Jeong, U., Im, S. H., Camargo, P. H., Kim, J. H. & Xia, Y. Microscale fish bowls: a new class of latex particles with hollow interiors and engineered porous structures in their surfaces. *Langmuir* **23**, 10968–10975 (2007).
- [231] Crassous, J. J., Mihut, A. M., Månsson, L. K. & Schurtenberger, P. Anisotropic responsive microgels with tuneable shape and interactions. *Nanoscale* **7**, 15971–15982 (2015).
- [232] Meijer, J.-M. & Crassous, J. J. Phase behavior of bowl-shaped colloids: order and dynamics in plastic crystals and glasses. *Small* **14**, 1802049 (2018).
- [233] Obey, T. M. & Vincent, B. Novel monodisperse ‘silicone oil’/water emulsions. *Journal of Colloid and Interface Science* **163**, 454–463 (1994).
- [234] Stöber, W., Fink, A. & Bohn, E. Controlled growth of monodisperse silica spheres in the micron size range. *Journal of Colloid and Interface Science* **26**, 62–69 (1968).
- [235] Van Der Wel, C., Bhan, R. K., Verweij, R. W., Frijters, H. C., Gong, Z., Hollingsworth, A. D., Sacanna, S. & Kraft, D. J. Preparation of colloidal organosilica spheres through spontaneous emulsification. *Langmuir* **33**, 8174–8180 (2017).
- [236] Gong, Z., Hueckel, T., Yi, G.-R. & Sacanna, S. Patchy particles made by colloidal fusion. *Nature* **550**, 234 (2017).
- [237] Brinker, C. J. Hydrolysis and condensation of silicates: effects on structure. *Journal of Non-Crystalline Solids* **100**, 31–50 (1988).
- [238] van Blaaderen, A. & Vrij, A. Synthesis and characterization of monodisperse colloidal organo-silica spheres. *Journal of Colloid and Interface Science* **156**, 1–18 (1993).
- [239] Schätzel, K. Suppression of multiple scattering by photon cross-correlation techniques. *Journal of Modern Optics* **38**, 1849–1865 (1991).
- [240] Urban, C. & Schurtenberger, P. Characterization of turbid colloidal suspensions using light scattering techniques combined with cross-correlation methods. *Journal of Colloid*

- and *Interface Science* **207**, 150–158 (1998).
- [241] Block, I. D. & Scheffold, F. Modulated 3D cross-correlation light scattering: improving turbid sample characterization. *Review of Scientific Instruments* **81**, 123107 (2010).
- [242] Zemb, T. & Lindner, P. *Neutrons, X-rays and light: scattering methods applied to soft condensed matter* (North-Holland, 2002).
- [243] Berne, B. J. & Pecora, R. *Dynamic light scattering: with applications to chemistry, biology, and physics* (Dover Publications, 2000).
- [244] Koppel, D. E. Analysis of macromolecular polydispersity in intensity correlation spectroscopy: the method of cumulants. *The Journal of Chemical Physics* **57**, 4814–4820 (1972).
- [245] Yoshida, H., Ito, K. & Ise, N. Localized ordered structure in polymer latex suspensions as studied by a confocal laser scanning microscope. *Physical Review B* **44**, 435 (1991).
- [246] van Blaaderen, A. & Wiltzius, P. Real-space structure of colloidal hard-sphere glasses. *Science* **270**, 1177–1179 (1995).
- [247] Minsky, M. Memoir on inventing the confocal scanning microscope. *Scanning* **10**, 128–138 (1988).
- [248] Crocker, J. C. & Grier, D. G. Methods of digital video microscopy for colloidal studies. *Journal of Colloid and Interface Science* **179**, 298–310 (1996).
- [249] Ohshima, H. Electrokinetics of soft particles. *Colloid and Polymer Science* **285**, 1411–1421 (2007).
- [250] Fleming, I. & Williams, D. H. *Spectroscopic methods in organic chemistry* (McGraw-Hill, 2008).
- [251] Keeler, J. *Understanding NMR spectroscopy* (John Wiley & Sons, 2011).
- [252] Hore, P. J. *Nuclear magnetic resonance* (Oxford University Press, USA, 2015).
- [253] Svedberg, T. & Nichols, J. B. Determination of size and distribution of size of particle by centrifugal methods. *Journal of the American Chemical Society* **45**, 2910–2917 (1923).
- [254] Svedberg, T. & Rinde, H. The ultra-centrifuge, a new instrument for the determination of size and distribution of size of particle in microscopic colloids. *Journal of the American Chemical Society* **46**, 2677–2693 (1924).
- [255] Planken, K. L. & Cölfen, H. Analytical ultracentrifugation of colloids. *Nanoscale* **2**, 1849–1869 (2010).
- [256] Gravesen, P., Branebjerg, J. & Jensen, O. S. Microfluidics-a review. *Journal of Micromechanics and Microengineering* **3**, 168 (1993).
- [257] Stone, H. A., Stroock, A. D. & Ajdari, A. Engineering flows in small devices: microfluidics toward a lab-on-a-chip. *Annual Review of Fluid Mechanics* **36**, 381–411 (2004).
- [258] Squires, T. M. & Quake, S. R. Microfluidics: fluid physics at the nanoliter scale. *Reviews of Modern Physics* **77**, 977 (2005).
- [259] Whitesides, G. M. The origins and the future of microfluidics. *Nature* **442**, 368 (2006).
- [260] Manz, A., Miyahara, Y., Miura, J., Watanabe, Y., Miyagi, H. & Sato, K. Design of an open-tubular column liquid chromatograph using silicon chip technology. *Sensors and Actuators B: Chemical* **1**, 249–255 (1990).
- [261] Hartman, R. L., McMullen, J. P. & Jensen, K. F. Deciding whether to go with the flow:

- evaluating the merits of flow reactors for synthesis. *Angewandte Chemie International Edition* **50**, 7502–7519 (2011).
- [262] Pastre, J. C., Browne, D. L. & Ley, S. V. Flow chemistry syntheses of natural products. *Chemical Society Reviews* **42**, 8849–8869 (2013).
- [263] Khan, S. A., Günther, A., Schmidt, M. A. & Jensen, K. F. Microfluidic synthesis of colloidal silica. *Langmuir* **20**, 8604–8611 (2004).
- [264] Beebe, D. J., Mensing, G. A. & Walker, G. M. Physics and applications of microfluidics in biology. *Annual Review of Biomedical Engineering* **4**, 261–286 (2002).
- [265] Sia, S. K. & Whitesides, G. M. Microfluidic devices fabricated in poly(dimethylsiloxane) for biological studies. *Electrophoresis* **24**, 3563–3576 (2003).
- [266] Dittrich, P. S. & Manz, A. Lab-on-a-chip: microfluidics in drug discovery. *Nature Reviews Drug discovery* **5**, 210 (2006).
- [267] Adamo, A. *et al.* On-demand continuous-flow production of pharmaceuticals in a compact, reconfigurable system. *Science* **352**, 61–67 (2016).
- [268] Sia, S. K. & Kricka, L. J. Microfluidics and point-of-care testing. *Lab on a Chip* **8**, 1982–1983 (2008).
- [269] Chin, C. D., Linder, V. & Sia, S. K. Commercialization of microfluidic point-of-care diagnostic devices. *Lab on a Chip* **12**, 2118–2134 (2012).
- [270] Reynolds, O. XXIX. An experimental investigation of the circumstances which determine whether the motion of water shall be direct or sinuous, and of the law of resistance in parallel channels. *Philosophical Transactions of the Royal Society of London* **174**, 935–982 (1883).
- [271] Xia, Y. & Whitesides, G. M. Soft lithography. *Angewandte Chemie International Edition* **37**, 550–575 (1998).
- [272] Whitesides, G. M., Ostuni, E., Takayama, S., Jiang, X. & Ingber, D. E. Soft lithography in biology and biochemistry. *Annual Review of Biomedical Engineering* **3**, 335–373 (2001).
- [273] Qin, D., Xia, Y. & Whitesides, G. M. Soft lithography for micro-and nanoscale patterning. *Nature Protocols* **5**, 491 (2010).
- [274] Umbanhowar, P., Prasad, V. & Weitz, D. A. Monodisperse emulsion generation via drop break off in a coflowing stream. *Langmuir* **16**, 347–351 (2000).
- [275] Günther, A. & Jensen, K. F. Multiphase microfluidics: from flow characteristics to chemical and materials synthesis. *Lab on a Chip* **6**, 1487–1503 (2006).
- [276] Teh, S.-Y., Lin, R., Hung, L.-H. & Lee, A. P. Droplet microfluidics. *Lab on a Chip* **8**, 198–220 (2008).
- [277] Casadevall i Solvas, X. & deMello, A. Droplet microfluidics: recent developments and future applications. *Chemical Communications* **47**, 1936–1942 (2011).
- [278] Simon, M. G. & Lee, A. P. Microfluidic droplet manipulations and their applications. In *Microdroplet Technology*, 23–50 (Springer, 2012).
- [279] Song, H., Chen, D. L. & Ismagilov, R. F. Reactions in droplets in microfluidic channels. *Angewandte Chemie International Edition* **45**, 7336–7356 (2006).
- [280] Mazutis, L., Gilbert, J., Ung, W. L., Weitz, D. A., Griffiths, A. D. & Heyman, J. A.

- Single-cell analysis and sorting using droplet-based microfluidics. *Nature Protocols* **8**, 870 (2013).
- [281] Nguyen, N.-T., Wereley, S. T. & Wereley, S. T. *Fundamentals and applications of microfluidics* (Artech House, 2002).
- [282] Zhu, P. & Wang, L. Passive and active droplet generation with microfluidics: a review. *Lab on a Chip* **17**, 34–75 (2017).
- [283] Baroud, C. N., Gallaire, F. & Dangla, R. Dynamics of microfluidic droplets. *Lab on a Chip* **10**, 2032–2045 (2010).
- [284] Christopher, G. F. & Anna, S. L. Microfluidic methods for generating continuous droplet streams. *Journal of Physics D: Applied Physics* **40**, R319 (2007).
- [285] Seemann, R., Brinkmann, M., Pfohl, T. & Herminghaus, S. Droplet based microfluidics. *Reports on Progress in Physics* **75**, 016601 (2011).
- [286] Zhao, C.-X. & Middelberg, A. P. Two-phase microfluidic flows. *Chemical Engineering Science* **66**, 1394–1411 (2011).
- [287] Anna, S. L. Droplets and bubbles in microfluidic devices. *Annual Review of Fluid Mechanics* **48**, 285–309 (2016).
- [288] Ganán-Calvo, A. M. & Gordillo, J. M. Perfectly monodisperse microbubbling by capillary flow focusing. *Physical Review Letters* **87**, 274501 (2001).
- [289] Anna, S. L., Bontoux, N. & Stone, H. A. Formation of dispersions using ‘flow focusing’ in microchannels. *Applied Physics Letters* **82**, 364–366 (2003).
- [290] Dreyfus, R., Tabeling, P. & Willaime, H. Ordered and disordered patterns in two-phase flows in microchannels. *Physical Review Letters* **90**, 144505 (2003).
- [291] Garstecki, P., Gitlin, I., DiLuzio, W., Whitesides, G. M., Kumacheva, E. & Stone, H. A. Formation of monodisperse bubbles in a microfluidic flow-focusing device. *Applied Physics Letters* **85**, 2649–2651 (2004).
- [292] Kersaudy-Kerhoas, M., Dhariwal, R. & Desmulliez, M. Recent advances in micro-particle continuous separation. *IET Nanobiotechnology* **2**, 1–13 (2008).
- [293] Gossett, D. R., Weaver, W. M., Mach, A. J., Hur, S. C., Tse, H. T. K., Lee, W., Amini, H. & Di Carlo, D. Label-free cell separation and sorting in microfluidic systems. *Analytical and Bioanalytical Chemistry* **397**, 3249–3267 (2010).
- [294] Bhagat, A. A. S., Bow, H., Hou, H. W., Tan, S. J., Han, J. & Lim, C. T. Microfluidics for cell separation. *Medical & Biological Engineering & Computing* **48**, 999–1014 (2010).
- [295] Shields IV, C. W., Reyes, C. D. & López, G. P. Microfluidic cell sorting: a review of the advances in the separation of cells from debulking to rare cell isolation. *Lab on a Chip* **15**, 1230–1249 (2015).
- [296] Huang, L. R., Cox, E. C., Austin, R. H. & Sturm, J. C. Continuous particle separation through deterministic lateral displacement. *Science* **304**, 987–990 (2004).
- [297] Petersson, F., Åberg, L., Swärd-Nilsson, A.-M. & Laurell, T. Free flow acoustophoresis: microfluidic-based mode of particle and cell separation. *Analytical Chemistry* **79**, 5117–5123 (2007).
- [298] Hu, X., Bessette, P. H., Qian, J., Meinhardt, C. D., Daugherty, P. S. & Soh, H. T. Marker-specific sorting of rare cells using dielectrophoresis. *Proceedings of the National Academy*

*of Sciences of the United States of America* **102**, 15757–15761 (2005).

- [299] Akagi, T. & Ichiki, T. Cell electrophoresis on a chip: what can we know from the changes in electrophoretic mobility? *Analytical and Bioanalytical Chemistry* **391**, 2433 (2008).
- [300] Xia, N., Hunt, T. P., Mayers, B. T., Alsberg, E., Whitesides, G. M., Westervelt, R. M. & Ingber, D. E. Combined microfluidic-micromagnetic separation of living cells in continuous flow. *Biomedical Microdevices* **8**, 299 (2006).
- [301] Davis, J. A. *Microfluidic separation of blood components through deterministic lateral displacement* (Princeton University, 2008).
- [302] Yao, L., Li, Q., Guan, Y., Zhu, X. & Zhang, Y. Tetrahedral, octahedral, and triangular dipyramidal microgel clusters with thermosensitivity fabricated from binary colloidal crystals template and thiol–ene reaction. *ACS Macro Letters* **7**, 80–84 (2018).
- [303] Kolb, H. C., Finn, M. & Sharpless, K. B. Click chemistry: diverse chemical function from a few good reactions. *Angewandte Chemie International Edition* **40**, 2004–2021 (2001).
- [304] Conway, J. H. & Sloane, N. J. A. *Sphere packings, lattices and groups*, vol. 290 (Springer Science & Business Media, 2013).
- [305] Megias-Alguacil, D. & Gauckler, L. J. Capillary and van der Waals forces between uncharged colloidal particles linked by a liquid bridge. *Colloid and Polymer Science* **288**, 133–139 (2010).
- [306] Zhang, Z. & Glotzer, S. C. Self-assembly of patchy particles. *Nano Letters* **4**, 1407–1413 (2004).
- [307] Pawar, A. B. & Kretzschmar, I. Fabrication, assembly, and application of patchy particles. *Macromolecular Rapid Communications* **31**, 150–168 (2010).
- [308] Chen, Q., Bae, S. C. & Granick, S. Directed self-assembly of a colloidal kagome lattice. *Nature* **469**, 381 (2011).
- [309] Bianchi, E., Blaak, R. & Likos, C. N. Patchy colloids: state of the art and perspectives. *Physical Chemistry Chemical Physics* **13**, 6397–6410 (2011).
- [310] Romano, F. & Sciortino, F. Colloidal self-assembly: patchy from the bottom up. *Nature Materials* **10**, 171 (2011).
- [311] Yi, G.-R., Pine, D. J. & Sacanna, S. Recent progress on patchy colloids and their self-assembly. *Journal of Physics: Condensed Matter* **25**, 193101 (2013).
- [312] Goller, M. I., Obey, T. M., Teare, D. O., Vincent, B. & Wegener, M. R. Inorganic ‘silicone oil’ microgels. *Colloids and Surfaces A: Physicochemical and Engineering Aspects* **123**, 183–193 (1997).
- [313] Wang, W., Milani, A. H., Carney, L., Yan, J., Cui, Z., Thaiboonrod, S. & Saunders, B. R. Doubly crosslinked microgel-colloidosomes: a versatile method for pH-responsive capsule assembly using microgels as macro-crosslinkers. *Chemical Communications* **51**, 3854–3857 (2015).







*#IAmAScientistBecause* of the inspiring role models I was surrounded by during my education. Also, the lab is conveniently located on the way to the gym.

- @ManssonLinda on Twitter



LUND  
UNIVERSITY

ISBN: 978-91-7422-620-1

Physical Chemistry  
Faculty of Science  
Lund University

